UNIVERSITA` DEGLI STUDI DI NAPOLI

"FEDERICO II"

PH.D. IN CHEMISTRY - XXV CYCLE

DEVELOPING METALLOPROTEIN MODELS FOR DIAGNOSTIC AND SENSING APPLICATIONS

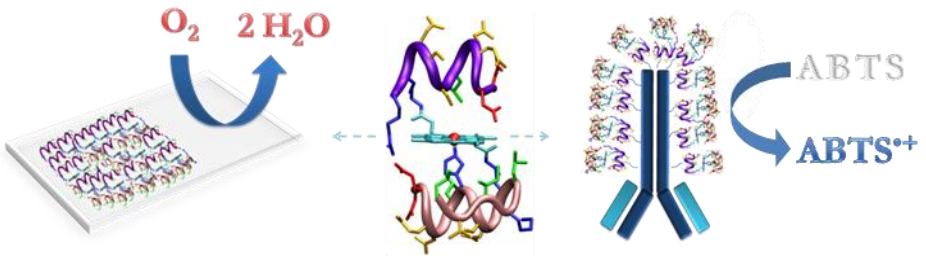

Rosa Vitale

ADVISOR: Prof Angela Lombardi

SUPERVISOR: Prof. Pompea Del Vecchio

COORDINATOR: Prof. Lucio Previtera

Abstract

Metalloproteins were selected by nature to mediate a great and extraordinarily heterogeneous class of processes, which are very important in biology. This class of biomolecules consists of **protein scaffolds** and **prosthetic groups**, which contain one or more metal ions linked to the polypeptide chain by different types of interaction, either covalent or non-covalent.

A mutual relation between metal cofactors and polypeptide chains is estabilished, since (i) metal ions can impart a particular trimensional folding to the protein, thus influencing its function/s, and (ii) the protein matrix is able to modulate the chemical reactivity of metal ions, thus selecting one or few functions among all potential activities.

In this contest, an interesting example is the **heme-protein family**, in which a single prosthetic group, the heme, plays a variety of functions, such as dioxygen storage and transport, electron transfer, hydroxylation and oxidation of organic substrates, disproportionation of hydrogen peroxide, etc..

Through the study of natural proteins and model systems, it is becoming increasingly clear that different proteins are able to optimize the environment surrounding the heme-cofactor for the acquisition of specific functions.

In this respect, this PhD thesis was focused on the study of new models of heme-proteins, belonging to the Mimochrome family, developed by the *Artificial Metallo Enzyme Group* in Naples (Lombardi et. al. 2001). Generally, these complexes are porphyrin-peptide conjugates, containing two peptides, covalently linked to deuteroporphyrin IX, through an amide bond between the propionic groups of the porphyrin and the ε-amino function of a lysine residue. The two peptide chains are in α-helical conformation and cover both planes of the heme, resulting in a helix-heme-helix sandwich.

Through an iterative process of design, synthesis, characterization and re-design, a penta-coordinated model was developed, **Fe(III) MimochromeVI**, which exhibits a peroxidase-like activity (Nastri et al. 2011).

In order to gain deep insight on the role of the peptide chains in modulating the structural and functional properties of Mimochrome VI, some point amino acid substitutions in its peptide chains were introduced.

Here, the rational design, the synthesis and the characterization of five analogs of Mimochrome VI is reported (**figure 1**). These new molecules are characterized by peptide substitutions, which were aimed to evaluate the role of the Glu^2 and Arg^{10} in both peptide chains (decapeptide, or D, and tetradecapeptide, or TD) and the Ser^6 in the decapeptide.

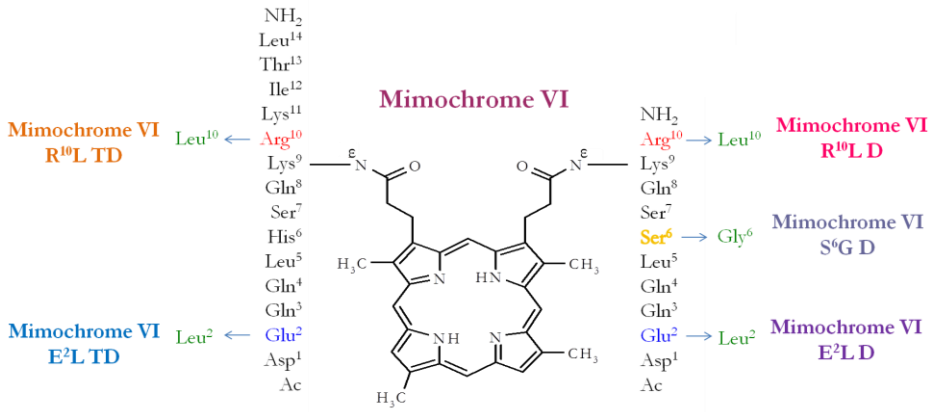

Figure 1 Scheme of the primary structures of Mimochrome VI and the E^2L TD, $R^{10}L$ TD, E^2L D, $R^{10}L$ D, S^6G D analogs.

The newly designed analogues were first screened for their catalytic properties. For this purpose, the oxidation reaction of ABTS (2,2'-azino-bis(3-ethylbenzthiazoline-6-sulphonic acid), through the activation of H_2O_2, was studied. This **bottom-up approach** allowed to select the **Fe(III) Mimochrome VI E^2L TD** analog, whose catalytic efficiency is about three fold higher than the horseradish peroxidase (HRP). Moreover, Fe(III) Mimochrome VI E^2L TD is able to perform about 6000 turn over, without bleaching. These very promising results suggest that the site-specific E^2L amino acid substitution on the tetradecapeptide was beneficial, thus allowing to select a new peptide-based heme protein model with improved catalytic activity.

The important properties of Mimochrome VI and its analogs afforded us in exploring their potentialities in diagnostics and in biosensor technologies.

The spectroelectrochemical characterization of Fe(III)Mimochrome VI immobilized on indium tin oxide (ITO) tridimensional nanoporous films was performed in collaboration with the *Laboratoire d'Electrochimie Moléculaire* (LEM) in Paris, under the supervision of Prof. Véronique Balland and Prof. Benoit Limoges.

Nanoporous films of indium tin oxide (ITO) were used as highly sensitive transparent 3D-electrodes for time-resolved spectroelectrochemistry. This technique was exploited to study the thermodynamics and kinetics of the heterogeneous electron transfer, between Fe(III)-Mimochrome VI adsorbed within such films, and the electrodic surface.

The high film loading, due to the columnar structure of metal oxides in ITO matrix and Fe(III) Mimochrome VI small dimension, combined with the excellent conductivity of this metal oxide film, gave high sensitivity measurements. This allowed the simultaneous characterization of the heterogeneous one-electron transfer dynamics of the Fe(III)/Fe(II) redox couple by cyclic voltammetry and cyclic voltabsorptometry, up to a scan rate of few volts per second, with a satisfactory single-scan signal-to-noise ratio. The spectroelectroanalytical strategy presented here, opens new opportunities for characterizing redox-coupled chemical reactions, within redox biomimetic systems and catalysts. It might also be of great interest for the development and optimization of new spectroelectrochemical sensors and biosensors.

Based on its small dimensions (3.5 kDa) and its highly efficient peroxidase-like catalytic activity, Fe(III)Mimochrome VI is here proposed as reporter enzyme for the functionalization of antibodies usable in

immunochemical assays. Human polyclonal antibodies (h IgG) were functionalized with this synthetic enzyme, by the use of cross-linkers. Conjugates with an enzyme/h IgG ratio up to 13 were prepared. This represents a significant result, when compared to commercial immune-globulins, which are usually linked to 3-4 HRP molecules. The complete characterization of the conjugates is in progress, in order to determine their immunoreactivity and to develop a marketable immunochemical kit.

Introduction

CHAPTER I: ***NATURAL AND ARTIFICIAL METALLOPROTEINS***

CHAPTER II: ***NATURAL AND SYNTHETIC PEROXIDASES IN BIOTECHNOLOGY***

1. Heme and heme-proteins: structures and functions{ XE "1. Heme and heme-proteins\: structures and functions" \t "Vedi" }{ TA \l "1. Heme and heme-proteins: structures and functions" \s "1. Heme and heme-proteins: structures and functions" \c 1 }

Iron-porphyrin complexes, known as hemes, are chemically referred to iron ion, usually in the +2 or +3 oxidation states, enclosed in the center of a large heterocyclic organic ring (the porphyrin), in which four pyrrolic groups are linked together by methine bridges (**figure 2**).

Hemes are the prosthetic groups of a large number of metalloproteins and they are the most diffused and versatile class of cofactors in biology (Chapman et al., 1997).

Through a long process of evolution, nature selected a plethora of heme proteins which are able to carry out such diverse tasks (Holm et al., 1996; Reedy and Gibney, 2004). To date, there are numerous documented different functions in heme-proteins, ranging from **electron transfer** (Dolphin, 1979; Gray and Winkler, 1996), **catalysis** (Dolphin, 1979), **dioxygen transport** and **storage** (Dolphin, 1979), **ligand sensing** (Chan, 2000, 2001), **steroid biosynthesis** (Privalle, 1983), **aerobic respiration**(Yoshikawa, 2002), **photosynthesis** (Schäfer et al., 1996) and even **programmed cell death** (Narula et al., 1999) and **gene expression regulation** (Goldberg et al., 1988; Huang et al., 1997).

This enormous functional diversity is strictly related to the versatility of the heme group and to the protein scaffolds, which creates different heme environments, modulating its chemical reactivity. Hence, the main features of both the heme cofactors and the polypeptide matrix should be examined, when studying heme-proteins.

1.1 Heme properties

The identity of the macrocycle chromophore in each type of natural heme protein is distinguished by its peripheral β-pyrrolic substituents, as shown in **figure 2**.

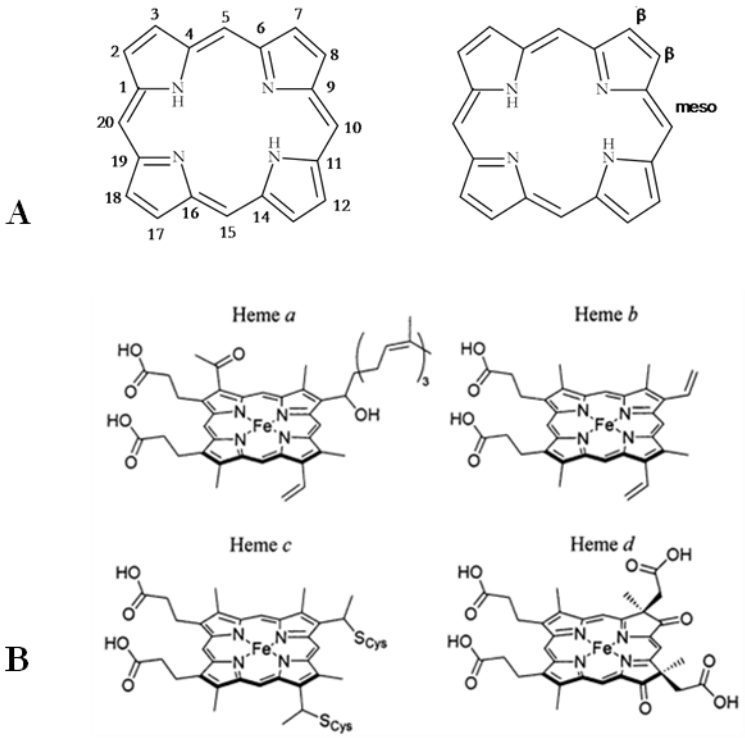

Figure 2. **A**. Basic structure of the porphyrin macrocycle: numbering scheme, according to IUPAC nomenclature, and functionalization sites. **B**. Schematic representation of the main heme structures found in natural heme-proteins (Reedy and Gibney, 2004).

The most common heme tetrapyrrole macrocycle is **heme b**, also called protoporphyrin IX or protoheme. It is found in b-type cytochromes, globins, cytochromes P-450 and hemesensor proteins. Its chemical structure is characterized by methyl groups at positions 3, 7, 12, and 17, vinyl groups at positions 13 and 8, and propionates at positions 2 and 18, on the macrocycle.

Generally, the protein scaffolds bind hemes via the combination of the axial coordination positions available on the iron, hydrophobic interactions with the heme macrocycle, and polar interactions with the propionic acids (Hargrove and Olson, 1996; Hargrove et al., 1996; Reedy and Gibney, 2004).

Heme c is structurally similar to heme b, except that thioether bonds to cysteine residues replace one or both of the vinyl groups and covalently link the heme macrocycle, to the protein scaffold. Cytochromes c and cytochrome f, in which the above mentioned prosthetic group is located, typically contain a CXXCH sequence motif, in which the two cysteines link to the porphyrin macrocycle and the histidine binds to the encapsulated iron (Reedy and Gibney, 2004).

Heme a is biosynthesized from heme b, but it is more hydrophobic and more electron-withdrawing to the iron ion than its precursor. In fact,

heme a is obtained through the conversion of the vinyl group at position 8 into a hydroxyethylfarnesyl side chain, followed by subsequent oxidation of the methyl at position 3 to a formyl group. Heme a is found only in terminal oxidases, such as mammalian cytochrome c oxidase (Reedy and Gibney, 2004).

Other less common heme architectures include heme d (Vainshtein et al., 1986), siroheme (Crane et al., 1995) and chlorocruoroheme (Lemberg and Falk, 1951).

1.2 Protein scaffold in heme-proteins

How different proteins are able to finely tune the environment of the heme cofactor, thus producing different chemistries, has become increasingly clear through the study of natural and artificial model systems. An increasing number of heme-protein structures was solved through high-resolution X-ray crystallography, as well nuclear magnetic resonance spectroscopy, contributing to deeply understand their reactivity and their structural and electronic properties (Bertini and Luchinat, 1999; Perutz et al., 1998; Peterson and Graham, 1998).

It is now well ascertained that the protein matrix, surrounding the heme active site, controls the intrinsic reactivity of the prosthetic group, by selecting one reaction as the only or predominant one. The amino acid composition and the structural organization of the peptide chain governs the properties of the primary (metal coordination geometry, number, type,

donor properties of the axial ligands) and the secondary (local dielectric constant, hydrophobicity, hydrogen bonding interactions near the active site coordination sphere) coordination shells.

The primary coordination sphere plays important roles in modulating the redox potentials, electronic structures, spin states, electron-transfer rates, and catalytic properties. Beyond the primary shell, the peptide matrix still plays a role in modulating the heme chemical properties. In particular, the polarity of the heme micro-environment, which ranges from polar (peroxidases) to non-polar (cytochrome P-450), is strictly connected to the function of the heme-protein, by controlling the chemistry of the heme. Recently, the amino acidic composition at the heme interface was investigated and rationalized through bioinformatics (Li et al., 2011). Considering a non-redundant data set of 125 heme-proteins, it was highlighted that five different amino acids (H, M, C, Y, K) are found to serve as axial ligands to the heme iron with histidine as the dominant residue (~80%) in both heme b and heme c types (**figure 3**).

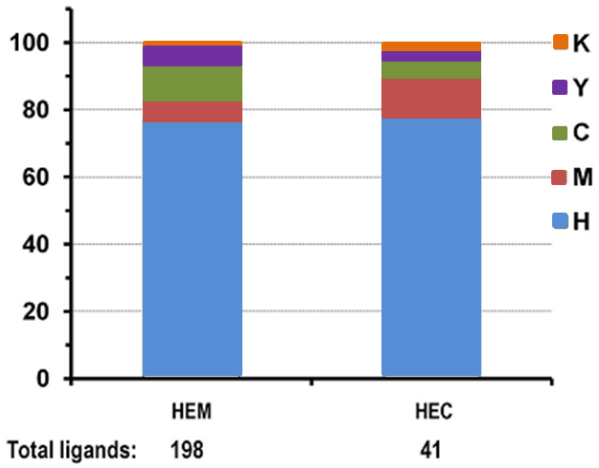

Figure 3 Distribution of the axial ligands for heme b (HEM) and heme c (HEC) (Li et al., 2011).

It was elucidated that there is a natural trend of recreating a hydrophobic pocket around the heme. **Figure 4** reports the relative frequency of the 20 amino acids in heme environment. The top five residues with high relative frequencies are cysteine (C), histidine (H), phenylalanine (F), methionine (M), and tyrosine (Y). Four of the top five (C, H, M, and Y) can serve as axial ligands, while the aromatic residues (F,Y and W) play important roles in the protein-heme interface, through the stacking interactions with the porphyrin. Leucine, isoleucine, and valine, which make hydrophobic interactions with the heme ring structure, are also slightly increased over the background frequencies. The residues with the fewest occurrences are charged residues (D, E and K), suggesting again that the heme binding pocket is mainly a hydrophobic environment.

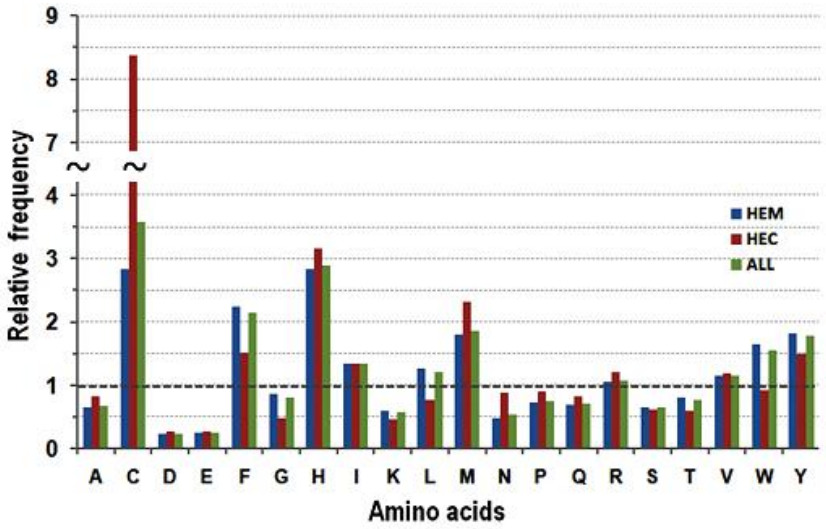

Figure 4 Relative frequency of amino acid residues in heme b (HEM), heme c (HEC), and heme b plus c (ALL) (Li et al., 2011).

Moreover, heme-proteins feature a fascinating range of different folding architectures. Reedy and Gibney have studied the main structural motifs found in heme-proteins in the CATH database (Class, Architecture, Topology and Homologous superfamily) and they have hierarchically categorized the indentified protein structures by bioinformatics' tools (**figure 5**). Even if β-sheets (green, 13%) or mixed α/β structures (yellow, 10%) are not uncommon, the graph clearly shows the current dominance of the mainly α-helical (red, 77%) secondary structures in heme proteins of known structure (Reedy and Gibney, 2004).

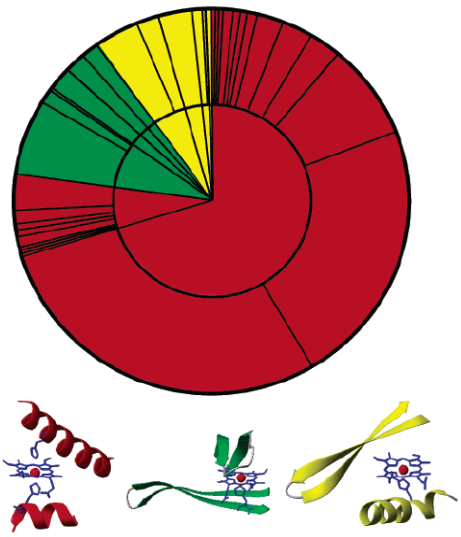

Figure 5 Structural classification of natural heme proteins and reference to mainly α-helical (myoglobin in red), mainly β-sheet (nitrophorin in green) and mixed α/β (FixL kinase in yellow) secondary structure binding sites for heme (Reedy and Gibney, 2004).

It is important to conclude by highlighting that the control of the functional specificity by the primary coordination sphere is well understood, on the basis of the selection of such coordinating and, eventually, catalysis-involved amino acid residues. However, the contribution of medium- and long-range interactions is still not completely rationalized. Hence, research activity is still needed, in order to deepen the knowledge about the structural and functional properties of this key class of natural proteins.

1.3 Heme-protein models: from porphyrin to peptide-porphyrin systems

The function, the structure and their mutual correlation in natural heme-proteins was widely studied in literature. However, these protein complexity continues to obscure the full description of the factors governing the heme properties.

A large number of artificial model systems are being developed, in an attempt to (i) provide further insights for structure-activity relationships, (ii) understand the minimal requirements for a specific function, (iii) reproduce the properties of the parent natural proteins in smaller molecules, and, most importantly, (iv) construct new and tailor-made molecules, which can be useful for biomedical, pharmaceutical, biological, and environmental applications (Lombardi et al., 2001; Nastri et al., 1998a).

The development of low molecular weight heme-protein models started in the early 1970s and it was based on the construction around the heme of bulky moieties by covalently linking aromatic or aliphatic substituents to the porphyrin ring (Collman et al., 1993; Lombardi et al., 2001; Mansuy, 1993; Meunier, 1992).

The promising works of Traylor, Collman, Momenteau, and Reed have notably contributed to this research area, and they are mainly focused on the construction of a penta-coordinated heme-model for the development of **dioxygen binding molecules** (Collman, 1997; Momenteau and Reed,

1994; Traylor, 1981; Traylor et al., 1979). In these systems, chelated hemes are characterized by a histidine or pyridine ligand covalently bound to the propionic group of pyrro-, proto-, meso- and deuteroheme. Some representative examples are constituted by the **picnic basket**, **picket fence** and **capped porphyrin** systems, where the coordination state of the iron (II) is achieved by using hindered substituents on the meso or the pyrrole positions of a tetraphenyl porphyrin (TPP) (**figure 6**).

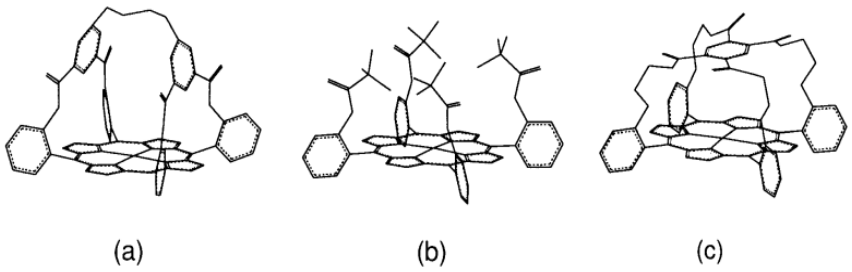

Figure 6 Schematic representation of (a) picnic-basket porphyrin, (b) picket-fence porphyrin, and (c) capped porphyrin as dioxygen binding model compounds (Nastri et al., 1998a).

These model systems have enabled the comprehension of many structural properties of the natural heme-proteins. Despite the important scientific contribution deriving from the study of these molecules, they did not display any interesting functionality and, hence, they did not find widespread practical applications.

Several metallo-porphyrins, which are soluble in polar organic solvents or in water, were developed for applications in catalysis (**figure 7**).

For example, some systems were evolved to mimic the **oxygenation reaction** performed by the **cytochrome P450** (Collman et al., 1993; Mansuy, 1990; Meunier, 1992). However, these systems show two compromising drawbacks, mostly linked to their instability and the impossibility of modulating the structure and the function of the synthetic molecules.

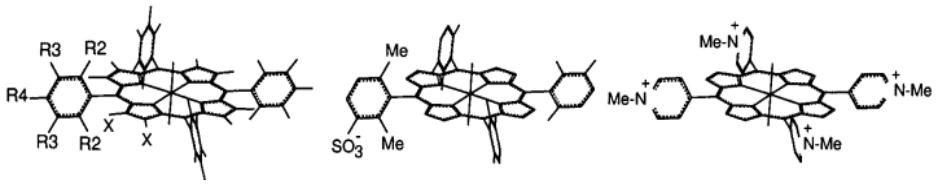

Figure 7 Schematic representation of substituted porphyrins as cytochrome P450 models (Nastri et al., 1998a).

Peptide-based models have gained enormous importance for the identification of the factors governing the heme properties, as they seem to better mimic both the structural characteristic sand reactivity of the natural systems. Peptide architecture around the heme can serve for substrate recognition and to reproduce the chemio-, regio-, and stereoselectivity of natural heme-proteins. They display both sufficient size and chemical diversity to allow the construction of functional binding and catalytic sites (Baltzer, 1999; Baltzer et al., 2001; DeGrado et al., 1999; Hellinga, 1996, 1998; Lu and Valentine, 1997; Regan, 1995). Moreover, the use of α-helical peptides able to cage the heme group, was and still remains the focus of the majority of this research are, because the α-helix motif is a recurring structural motif that surround the heme cofactor in

numerous natural heme-proteins. Over the years, a large number of helical peptide- based heme-protein models have appeared in the literature. They differ in structural complexity, and can be grouped into two classes, according to the nature of the interactions between the heme and the helical peptides: 1) models in which peptide chains incorporate one or more heme groups, by non-covalent self-assembling around the heme; 2) models in which peptide chains are covalently linked to the heme. Excellent examples of non-covalent heme-peptide adducts were reported by the groups of DeGrado, Dutton and Haenhel, who used the four-helix bundles as protein cages for mono-heme and multi-heme binding (Choma et al., 1994; Koder and Dutton, 2006; Koder et al., 2006, 2009; Monien et al., 2007; Rau and Haehnel, 1998; Rau et al., 2000, 1998; Robertson et al., 1994).

DeGrado, Dutton and co-workers first described *de novo* designed four-helix bundle proteins that spontaneously fold in aqueous solution and assemble with one or more hemes (Choma et al., 1994; Robertson et al., 1994). Subsequently, Dutton and co-workers reached impressive results in the design of protein structures, which assemble arrays of cofactors and reproduce native-like functions. They used the terms **maquettes**, French word for scale model of something, to refer to these molecular models (Koder and Dutton, 2006). The maquettes are based on a sequence with high α-helix forming propensities, with residues arranged in the heptad repeat pattern, typical of left-handed coiled coils. Such a sequence spontaneously assembles into a four helix bundle scaffold, with glutamate

and lysine exposed to the solvent, and leucine buried into the interior (Koder et al., 2006, 2009).

An alternative strategy for the design of four-helix bundle with controlled topology and housing the heme cofactor, is the chemical synthesis of template-assembled synthetic proteins (TASP), first introduced by Mutter and co-workers (Mutter and Vuilleumier, 1989). In this strategy, four α-helices are covalently connected to a cyclic decapeptide template to afford a self-assembled four-helix bundle, housing a specific cofactor. This offers the advantages that the engineering of anti-parallel four-helix bundle is easily accomplished through the covalent attachment of different peptide chains onto the template. Haenhel and co-workers used this approach for the development of modular organized proteins (named MOP), designed to provide a suitable scaffold for the incorporation of a variety of cofactors (Rau and Haehnel, 1998; Rau et al., 2000, 1998).

This section will mainly focus on covalent heme-peptide adducts, which are composed by a heme cofactor linked to one or more peptide chains, in order to promote stable and geometrically defined structures. Different strategies were used for developing covalent peptide porphyrin systems. In literature there are both examples of small **natural** and **artificial heme-protein models**. Here, some examples of each class will be reported.

Microperoxidases (**figure 8**) are obtained by proteolytic digestion of cytochromes c and they are important examples of **natural covalent peptide porphyrin systems** (Aron et al., 1986; Low et al., 1997; Marques,

2007; Paléus et al., 1955; Tuppy et al., 1955). Their peptide moiety contains the **Cys-(Xaa)$_2$-Cys** motif and they are covalently linked to the heme c via tioether linkages. To date no crystal structure of any micro-peroxidase was reported. Based on molecular dynamics, it was suggested that the peptide retains a conformation very similar to that of the amino acid residues of the parent protein (Bushnell et al., 1990; Harbury and Loach, 1959). In horse heart cytochrome c the N-terminal residues up to Cys-14 are part of an α-helix that terminates with a type III β-turn between Cys-14 and Cys-17 (Bushnell et al., 1990). It was proposed that MP8 and MP11 suggest that the peptide chain shield the proximal face of the porphyrin and the distal face is completely open to solvent. MP8 in aqueous solution has its amino acids largely arranged as a torus in a plane parallel to the porphyrin (Marques, 2007). Microperoxidases (MP8, MP11 and other analogs) were shown to be effective catalysts in oxidation and oxygenation reactions. However, these mini-enzymes are significantly limited by their tendency to aggregate and their low stability under catalytic conditions. It is quite important to underline the protective role of the peptide matrix of the catalyst, considering that the nude protoporphyrin is even less stable than Microperoxidases (Lombardi et al., 2001; Marques, 2007).

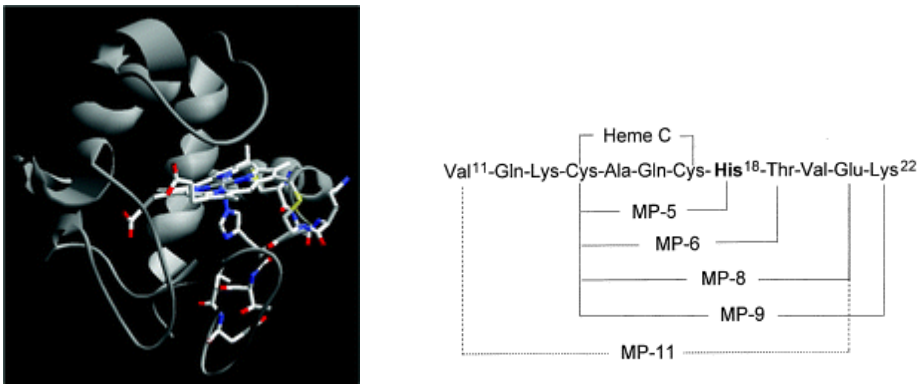

Figure 8 Model structure and sequence of Microperoxidases (Marques, 2007).

The development of the peptide synthesis and design techniques has pushed scientists in exploring new possibilities of mimicking the natural heme-proteins active site, by developing completely synthetic porphyrin peptides systems.

Benson and co-workers prepared a series of peptide-sandwiched mesoheme complexes, indicated as **PSM**s (Arnold et al., 1997; Benson et al., 1995; Liu et al., 1999a; Marques, 2007; Wang et al., 1997; Williamson and Benson, 1998). In PSMs the mesoheme II or IX is covalently linked to one or two peptide chains via an amide linkage between the propionate heme function and the N-ε nitrogen of lysine residues. A His residue in each peptide coordinates the heme iron, thus allowing the peptide chains to fold above and below the porphyrin ring, giving rise to a sandwich structure. The work on PSM molecules clearly confirms that in order to build a peptide-based heme protein model with a well-defined three-dimensional structure, many factors should be taken into account. The

covalent attachment of the peptide chains to the porphyrin ring may not result in the stabilization of the desired structure. The peptide sequences should be accurately designed in order to encompass all the essential elements for metal coordination and folding. Benson and co-worker have also developed interesting heme-protein models whose structure was supported by *de novo* design approach (Liu et al., 1999b). Through a combination of Fe–His coordination, an N-terminal helix capping motif, and macrocyclization *via* disulfide bond formation between two peptide chains, they succeeded in selecting peptide-based heme models with extra-ordinarily high helix content and notable structure stability (**figure 9**). Benson contribution showed that a combination of motifs commonly encountered in protein structures can provide considerable structural stabilization to heme-protein models built from short peptides.

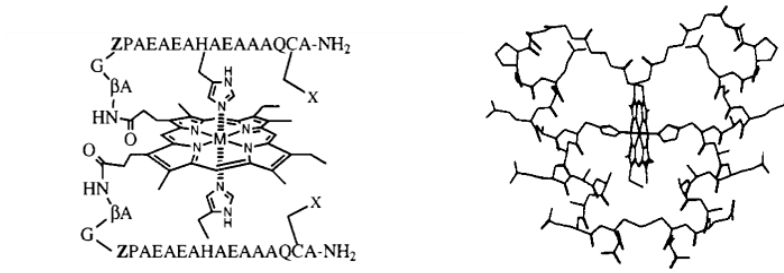

Figure 9 Peptide sequence and model structureof one diasteromer of the PMS peptide-mediated macrocycle (Liu et al., 1999b).

The *Artificial Metallo Enzymes Group* (AMEG) in Naples, where this work was carried out, has a long experience in mimicking metalloproteins in small peptide-based molecules for the selection of new advanced catalysts.

A whole family of synthetic heme-protein models, named **Mimochromes**, was developed and fully characterized (D'Auria et al., 1997; Lombardi et al., 1998a, 1998a, 2001, 2003; Nastri et al., 1997, 1998a, 1998a, 2011; Ranieri et al., 2010).

Mimochromes are peptide sandwiched deuteroheme systems, which were obtained by miniaturizing natural heme-proteins, in order to partially reproduce their structural and functional properties in small and artificial compounds. Through a detailed structural investigation, it emerged that some natural proteins, like hemoglobin, myoglobin, cytochrome c' and cytochrome b562, were characterized by a heme group almost completely embedded between two relatively small α-helical peptide segments (**figure 10**).

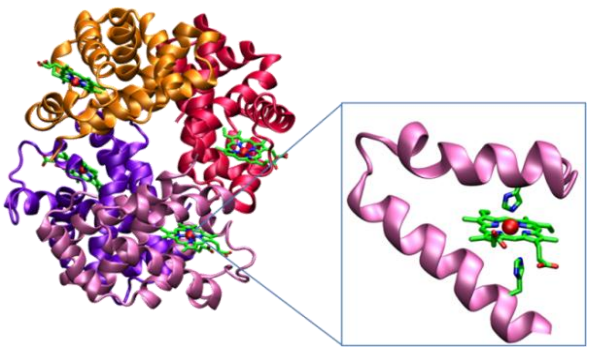

Figure 10 Crystal structure of the Deoxyhemoglobin. Inset: the L88-L96 fragment of the F-helix in the β-chain, which was used to construct the Mimochrome I peptide scaffold (PDB entry ID: 2DN3) (Park et al., 2006).

This structural motif was hence used as template to construct the prototype of the family, named Mimochrome I. The smallest sequence,

required for a complete coating of one face of the heme, was identified in a nine-residue peptide, which contains a central His residue to ligate the heme iron. Hydrophobic residues were placed to surround the axial coordinating residue and to directly face the heme, while the remaining five/six helical residues point outward from the heme. Finally, deuteroporphyrin was preferred to the more common protoporphyrin IX to avoid the possibility of degradation of the sensitive vinyl substituents during the synthesis (Nastri et al., 1997).

Table 1 Peptide sequence of Mimochromes.

MIMCHROME	R, R_1	
I	**R=R_1**	**Ac-L-A-Q-L-H-A-N-K-L-NH_2**
II	**R=R_1**	**Ac-D-L-S-D-L-H-S-K-K-L-K-I-T-L-NH_2**
IV	**R=R_1**	**Ac-E-S-Q-L-H-S-N-K-R-NH_2**
III, V	**R**	**Ac-D-E-H-K-L-H-S-K-K-R-K-I-T-L-NH_2**
	R_1	**Ac-D-E-H-K-L-Y-S-K-K-R-K-I-T-L-NH_2**
VI	**R**	**Ac-D-E-Q-Q-L-H-S-Q-K-R-K-I-T-L-NH_2**
	R_1	**Ac-D-E-Q-Q-L-S-S-Q-K-R-NH_2**

K= Lysine bound to the deuteroporphyrin
H= Histidine coordinating the metal centre Y= Glycine or Serine

Over the time, numerous compounds were evolved in order to (i) improve the water solubility and to favor the formation of a unique and well defined structure (Mimochrome II and Mimochrome IV) and (II) to introduce a structural asymmetry and to stabilize a penta-coordinated

metal ion, thus introducing catalytic activity (Mimochrome III and Mimochrome VI) (**table 1**). The modulation of the structural and, hence, the functional properties of the different analogs was achieved by rationally modifying the peptide sequences. Through reiterated cycles of (i) design, (ii) synthesis and characterization, (iii) re-design of these molecules, it was possible to better and better the properties of the examined compounds. This research activity led to the first asymmetric and penta-coordinated model with a peroxidase-like activity, named Mimochrome VI. It will be described in more detail below, being the main object of study of the present thesis work.

1.4 Mimochrome VI: a heme-protein model with a peroxidase-like activity

The challenge faced up by the project of the molecule Fe (III) Mimochrome VI was to create a proximal and a distal site around the heme. This compound was re-designed on the basis of the information acquired from parent Mimochromes. In particular, the NMR-derived solution structure of Co(III) Mimochrome IV (Lombardi et al., 2003) and the model structure of Co(III) Mimochrome II (Lombardi et al., 1998a) were used to configure the peptide scaffold of the new molecule (**figure 11**). The sequences of Mimochrome II and IV were combined to construct an unsymmetrical five-coordinate mono-histidine model.

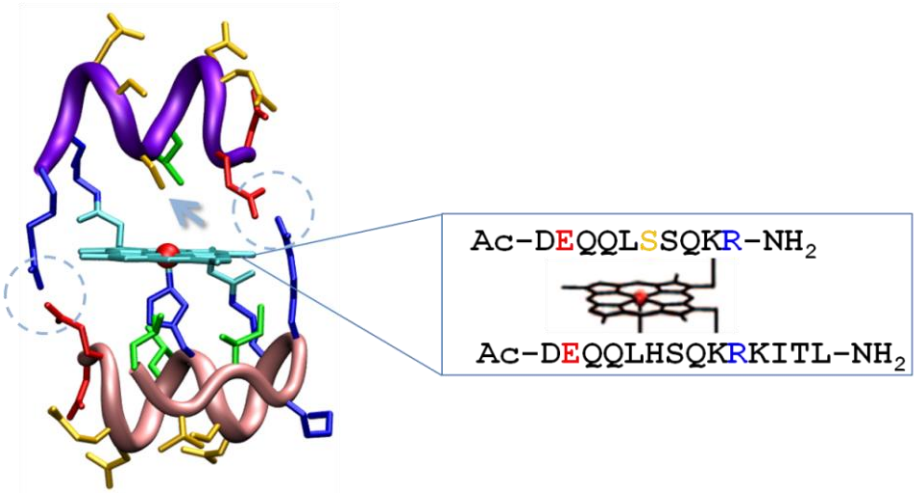

Figure 11 Fe(III)-Mimochrome VI model structure and amino acid sequence (Nastri et al., 2011).

The asymmetry in both primary and secondary coordination shells was realized by combining two peptide chains, different both in length and in their amino acid composition. The tetradecapeptide chain, derived from the sequence of Mimochrome II, contains a histidine (His^{6}) as a potential axial ligand to the metal in the proximal face. The decapeptide chain, derived from the sequence of Mimochrome IV, displays a serine (Ser^{6}) to create a cavity near the metal site, on the distal face of the heme. In analogy with the other Mimochromes, both peptide chains are covalently linked to the deuteroporphyrin propionate, through the Lys^{9} side chains. Some substitutions from the sequences of Mimochrome II and IV were introduced to further stabilize the secondary and tertiary structures. Inter-chain ion pairs, between glutamate (Glu^{2}) on one helix and arginine (Arg^{10}) on the other helix, were introduced in both peptide chains to stabilize the tertiary structure. The positively charged Arg^{10} and the negatively charged Glu^{2} at the C-terminal and N-terminal ends, respectively, with the opposite sign relative to the helix dipole, may also provide stabilization of the secondary structure of the two helices. Finally, several glutamines ($Gln^{3,4,8}$) and a serine (Ser^{7}) were introduced in the solvent exposed positions to promote water solubility.

The secondary structure of the tetradecapeptide was designed to adopt a short helical conformation (residues 1–9), a loop γβD (residues 10 and 11) and a short β-strand (residues 12–14) that folds back (through the loop) to interact with the helical part.

The decapeptide chain was designed to adopt a helical conformation from residue 1 to residue 8.

The tertiary structure can be described as a the sandwich, characteristic of all Mimochromes, in which:

- the two peptide chains embrace the metalloporphyrin;
- the helical segments are antiparallel to each other
- the helix axes are about parallel to the porphyrin plane.

All the spectroscopic and functional properties, deriving from its characterrization, describe Fe(III) Mimochrome VI as a very promising heme–protein model and an efficient biocatalyst. In fact, it displays a typical peroxidase-like catalytic activity towards different reducing substrates. Fe(III) Mimochrome VI shows a catalytic efficiency in the oxidation of ABTS (2,2'-azino-di(3-ethyl-benzothiazoline-6-sulfonic acid) and guaiacol, which is comparable to that of native horseradish peroxidase (**table 2Table 3**). Moreover, Fe(III) Mimochrome VI converts phenol to 4- and 2-nitrophenol in the presence of NO_2 and H_2O_2 in high yields.

Concerning the catalytic properties, it was demonstrated the important role of both the peptide chains, in modulating the Fe(III) Mimochrome VI properties. In fact, the so-called mono-adduct, which lacks the distal decapeptide chain, has showed a higher k_{cat} than the value displayed by the full Fe(III) Mimochrome VI, in the same experimental conditions (**table 2**). This can be interpreted in terms of a faster access of the substrate and

co-substrate to the iron site when the decapeptide chain is missing. At the same time, Fe(III) Mimochrome VI mono-adduct shows lower apparent affinity towards the substrate and co-substrate. This indicates that the decapeptide chain in Fe (III) Mimochrome VI may assists their binding. Most interestingly, the mono-adduct is more susceptible to oxidative degradation, as shown by the much lower number of turnovers that is able to perform, with respect to Fe(III) Mimochrome VI. This is a clear evidence of the protective effect to degradation exerted by the decapeptide chain, which represents a very interesting property of this kind of molecule.

Table 2 Catalytic parameters in the oxidation of ABTS (AH_2) through H_2O_2 activation.

Enzyme	K_m H_2O_2 mM	K_m AH_2 mM (10^2)	k_{cat} s^{-1} (10^{-2})	k_{cat}/K_m H_2O_2 $mM^{-1}s^{-1}$	k_{cat}/K_m AH_2 $mM^{-1}s^{-1}$ (10^{-3})
M-VI	44	8.4	3.7	8.4	4.4
Mono-adduct	80	13	6.9	8.6	0.053
HRP	0.85	107	62	7.310^3	5.8

Table 3 Catalytic parameters in the oxidation of guaiacol (AH_2) through H_2O_2 activation.

Enzyme	K_m H_2O_2 mM	K_m AH_2 mM (10^2)	k_{cat} s^{-1} (10^{-2})	k_{cat}/K_m H_2O_2 $mM^{-1}s^{-1}$	k_{cat}/K_m AH_2 $mM^{-1}s^{-1}$ (10^{-2})
M-VI	8.7	$9.2\ 10^{-3}$	8.0	0.91	8.7
HRP	$11\ 10^{-2}$	0.8	**4.0** 10^{-2}	$3.8\ 10^3$	5.0

Finally, the efficient binding of small ligands, such as carbon monoxide, imidazole and nitric oxide can be easily detected by discrete spectroscopic modifications of the Fe(III) and Fe(II) Mimochrome VI species, respectively.

These results demonstrate that small synthetic peptides can impart high enzyme activities to metal cofactors, and anticipate the possibility of constructing new biocatalysts tailored to specific functions (Nastri et al., 2011).

2. The horseradish peroxidase: a versatile tool for biotechnology

Peroxidases have a considerable potential for application in many different areas. Their commercial application is especially well established in analytical diagnostics (e.g. biosensors and immunodetection technologies). Due to its characteristics, the horseradish peroxidase (HRP) is quite adapt to successful use in analytical systems (e.g. flexibility, stability, sensitivity in range of analyte detection and availability in pure form at reasonable cost) (Azevedo et al., 2003)

2.1 HRP: overview on functional and structural main features

Horseradish peroxidase (HRP) was discovered in 1810 by Planche, who observed that soaking a piece of horseradish roots into a tincture of guaiacum, resin led to the development of a strong color (Planche, L. A. 1810). The molecule responsible of that phenomenon was precisely HRP, which would have become the most widely studied of all peroxidases (Johannes Everse et al., 1991).

It is now accepted that peroxidases occur as a large family of isoenzymes. Horseradish peroxidase isoenzyme C, the most diffused and studied of the family, comprises a single polypeptide of 308 amino acid residues, the sequence of which was determined by Welinder in 1976 (**figure 12**) (Azevedo et al., 2003; Welinder, 1976).

Figure 12 The amino acid sequence of HRP C (Welinder, 1976).

The N- terminal residue is blocked by pyroglutamate and the C- terminus is heterogenous, with some molecules lacking the terminal residue, Ser^{308}. There are 4 disulphide bridges between 11–91, 44–49, 97–301 and 177–209 cysteine residues. Nine N-glycosylation sites can be recognized in the primary sequence from the motif **Asn-X-Ser/Thr**. The HRP C carbohydrate profile is heterogeneous, and it is mainly constituted by branched hepta-saccharides, many minor glycans, *N*-Acetylglucosamines and several mannose residues. The total carbohydrate content of HRP C is usually 18-22% and it depends on the source of the enzyme (Veitch, 2004; Yang et al., 1996).

HRP C contains two types of metal center, Fe(III) protoporphyrin IX and two calcium atoms (**figure 13**). Both are essential for the structural and functional integrity of the enzyme.

At the proximal side, the heme group is attached to the enzyme at His^{170} by a coordinate bond. The second axial position (on the distal side of the heme plane) is unoccupied in the resting state of the enzyme, but available to hydrogen peroxide during the enzyme turnover. Small molecules, such as carbon monoxide, cyanide, fluoride and azide, are able to bind to the heme iron atom at this distal site.

The two calcium ions are located at the heme distal and proximal positions and they are both hepta-coordinated by a combination of amino acids side chains (Asp carboxylates, Ser and Thr hydroxyl groups), backbone carbonyls and water (Veitch, 2004).

The structure of the enzyme is largely α-helical, although there is also a small region of β-sheet, in purple and yellow, respectively in **figure 13**. There are two domains, the distal and the proximal, between which the heme group is located. (Gajhede et al., 1997; Veitch, 2004).

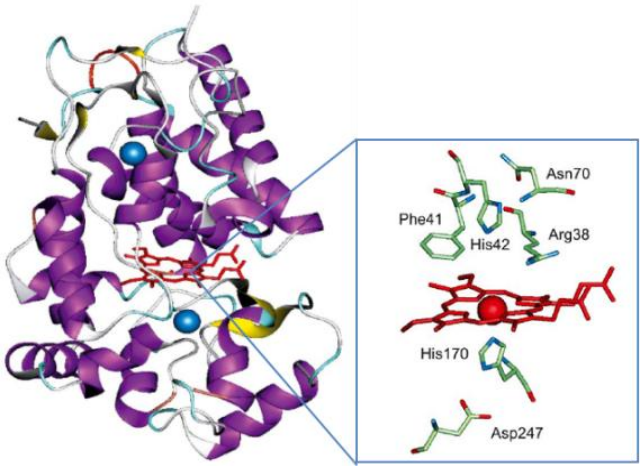

Figure 13 Three-dimensional representation of the X-ray crystal structure of horseradish peroxidase isoenzyme C (PDB entry ID: 1H5A). Inset: Key amino acid residues in the heme-binding region (Veitch, 2004).

Most reactions catalyzed by HRP C and other horseradish peroxidase isoenzymes can be expressed by the $H_2O_2 + 2AH_2 \rightarrow 2H_2O + 2AH^{\cdot}$ **Equation 1**, in which AH_2 and $AH^{\cdot}$ represent a reducing substrate and its radical product, respectively. Typical reducing substrates include aromatic phenols, phenolic acids, indoles, amines and sulfonates.

$$H_2O_2 + 2AH_2 \rightarrow 2H_2O + 2AH^{\cdot} \qquad \textbf{Equation 1}$$

The mechanism of catalysis was extensively investigated (Berglund et al., 2002; Poulos and Kraut, 1980; Veitch and Smith, 2000) and is schematically described in **figure 14.**

The first step in the catalytic cycle is the reaction between H_2O_2 and the Fe(III) resting state of the enzyme to generate compound I, a high oxidation state intermediate, comprising Fe(IV) oxo-ferryl center and a porphyrin-based cation radical. A transient intermediate (compound 0) formed prior to compound I was detected in reactions between HRP C and H_2O_2 at low temperatures and described as Fe(III)-hydroperoxy complex (Poulos and Kraut, 1980).

In formal terms, compound I is two oxidizing equivalents above the resting state. The first one-electron reduction step requires the participation of a reducing substrate and leads to the generation of compound II, Fe(IV) oxo-ferryl species that is one oxidizing equivalent above the resting state. Both compound I and compound II are powerful oxidants, with redox potentials estimated to be close to +1V. The second one-electron reduction step returns compound II to the resting state of the enzyme (Veitch, 2004).

The formation of a third species, named compound III, was reviewed. This intermediate is best described as a resonance hybrid of iron(III)-superoxide and iron(II)-dioxygen complexes. A high-resolution crystal structure of 95% pure compound III published recently shows dioxygen bound to heme iron in a bent conformation (Berglund et al., 2002).

A mechanism for the reduction of bonded dioxygen species to two molecules of water was proposed. This mechanism involved four successive, one-electron, reductions with the concomitant uptake of a proton, from

Compound III to the ferrous HRP, via the intermediate forms of Compound I, Compound II and ferric HRP.

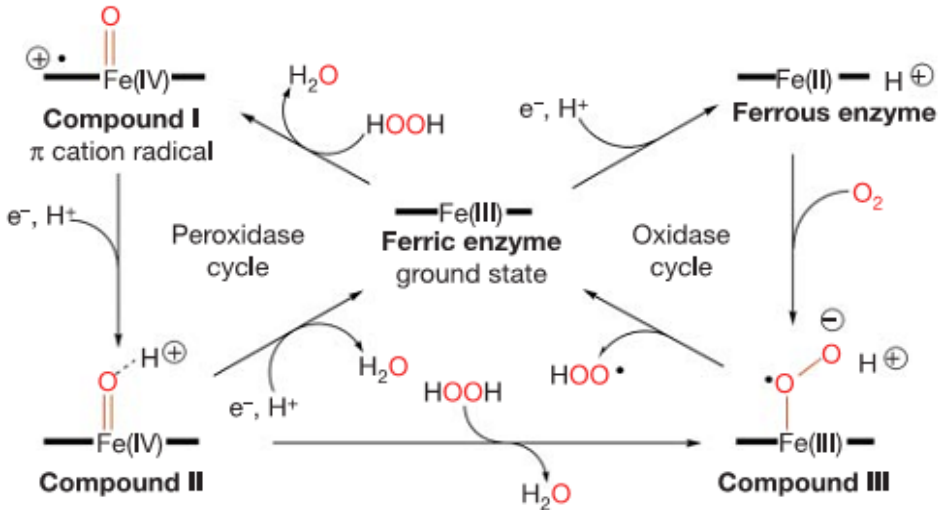

Figure 14 The five oxidation states of HRP during the catalytic cycle (Berglund et al., 2002).

2.2 HRP in biosensors development

Biosensors are becoming more and more important tools in medicine, quality control, food and environmental monitoring, and research (Chaubey and Malhotra, 2002). IUPAC defines chemical and biological sensors as a "*device that uses specific biochemical reactions, mediated by isolated enzymes, immunosystems, tissues, organelles or whole cells, to detect chemical compounds usually by chemical, optical or thermal signals*" (Thévenot et al., 1999, 2001)

As indicated in **figure 15**, biosensors usually contain two basic components, connected in series:

- a **bioreceptor**, which is a biomolecule, or a bio-inspired molecule, able to specifically recognize the analyte;
- a physicochemical **transducer**, which transforms the physicochemical signal, deriving from the recognition event, into a easily measurable signal (Thévenot et al., 2001).

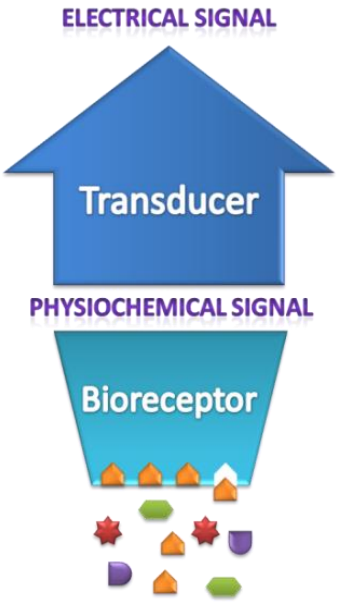

Figure 15 Scheme of a general biosensor arrangement.

Both elements act in concert and let to detect and quantify specific molecules in a complex samples, thanks to the high recognition specificity of the bio-molecules and the sensitivity of the transduction mechanism (Collings and Caruso, 1997).

According to the measuring principle of the transducer, biosensors are divided into **electrochemical**, **optical**, **calorimetric**, **acoustic**, **evanescent wave**, **surface plasmon resonance** and **piezoelectric** (Collings and Caruso, 1997; Mello and Kubota, 2002).

Electrochemical biosensors, the most widely used, are based on the generation of an electrochemical signal during the interaction of the biological component with the analyte. Depending upon the electrochemical property measured, they can be further divided into **amperometric** (in which redox processes provide current flow at constant potential), **potentiometric** (potential changes at constant current, using generally ion-selective electrodes) and **conductimetric** (conductance changes in the ionic environment) biosensors (Azevedo et al., 2003; Chaubey and Malhotra, 2002; Griffiths, 1993).

Redox-active metalloproteins are usually components of electro-chemical biosensors. When using an enzymatic recognition element, the transduction and the recognition elements match in the same molecular mechanisms, often providing an important amplification of the signal, due to the enzyme turn over.

Since HRP is capable of reducing H_2O_2 and also some organic peroxides, HRP-based biosensors can be used to control and monitor these peroxides, in pharmaceutical, environmental and dairy industries (Somasundrum et al., 1996), in bleaching operations in the textile and paper industries (Gündoğan-Paul et al., 2002), in air and water ozonisation processes and in food products(Mulchandani and Rudolph, 1995). The principle of detection is rather simple and it is schematically represented in **figure 16 A**. The peroxide oxidizes the enzyme and the electrode reduces it back to its native form. It is possible to measure a reduction current, which is proportional to the peroxide concentration (Chaubey and Malhotra, 2002).

If HRP is coupled with a hydrogen peroxide producing oxidase (**figure 16 B**), then the system becomes sensitive to the oxidase substrate, enabling the control and monitoring of a wide range of analytes such as glucose (Yabuki et al., 2001), ethanol (Azevedo et al., 2005), cholesterol (Bon-giovanni et al., 2001; Peña et al., 2001), lactate (Serra et al., 1999), amino acids (Domínguez et al., 2001), and many others.

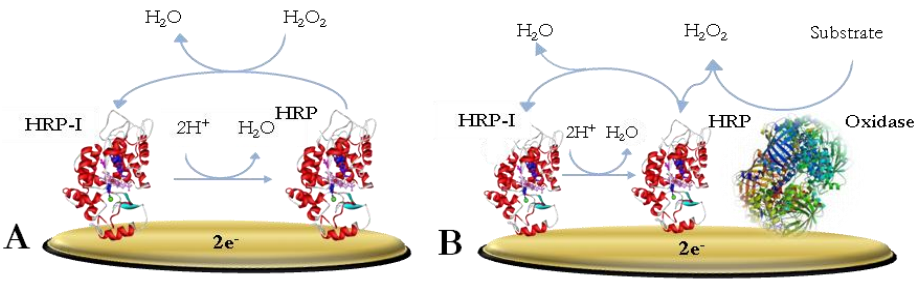

Figure 16 Schematic representation of HRP-based biosensors. A. HRP modified electrode for the detection of H_2O_2. B. bi-enzymatic system, incorporating HRP and Oxidase.

Hydrogen peroxide is not the only possible substrate, whose processing can be electrochemically detected. Recently, an amperometric flow biosensors for cyanide was developed by using HRP-adsorbed carbon-felt (CF)(Wang and Hasebe, 2011). Hu and Li reported the bio-electrocatalytic activity of HRP-electrodes for the O_2 reduction (Liu et al., 2006; Zhang et al., 2004). The produced compound III is directly reduced to the ferrous-HRP via ferric-HRP (**figure 14Figure** 17). As a result, the dissolved O_2 is reduced to H_2O, which leads to a bio-electrocatalytic cathodic current appearance.

Cyanide is well known inhibitor of peroxidase activity, and binds to the sixth coordination position of heme-iron. Since this binding-site is same of O_2, the cyanide competitively inhibits the formation of compound I. Wang and Hasebe demonstrated the reversible inhibition of the HRP electrocatalytic activity, which was easily detected by electrochemistry. This represented a promising perspective for the set-up of a new biosensor for the quantitative analysis of cyanide in wastewater, alternative to the conventional and more expensive and time-consuming methods (e.g. colorimetric, potentiometric and chromatographic).

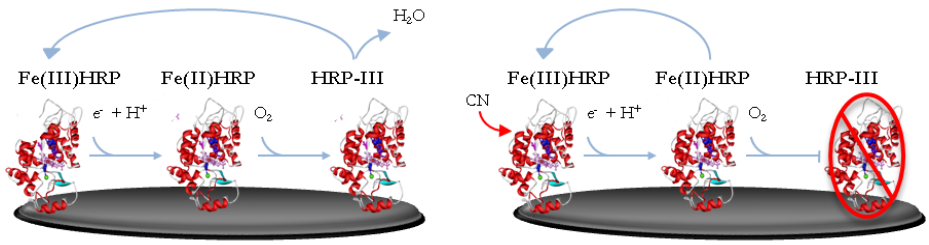

Figure 17 Schematic representation of HRP-based biosensor for cyanide detection.

2.3 HRP as reporter enzyme in immunodetection

HRP is widely used as an enzyme label in medical diagnostics and research applications. Covalent conjugates of proteins, antibodies and other molecules with HRP are useful and versatile tools for ultra-sensitive detection in immunoassays, such as enzyme-linked immunosorbent assays (**ELISA**) and immuno-histochemistry (**IHC**) (Azevedo et al., 2003).

The term immunoassay describes a wide range of tests used to specifically detect and quantify analytes. They are based on the formation of immunocomplexes, between an antigen and a specific antibody. The detector system is usually an enzyme (e.g. HRP), which is covalently bound to the antibodies. Immunocomplexes are quantified by measuring a colorimetric, fluorescent or chemiluminescent signal, deriving from the enzymatic reaction. The immunological component brings the detection specificity, while the enzyme component gives the analytical sensitivity (Ashley et al., 2008).

Even though ELISA and IHC techniques are quite similar for the immunodetection approach, they differ for several aspects.

The first difference between ELISA and IHC is the origin of the sample. Usually ELISA are realized on liquid samples (e.g. biological fluids, but even water or food samples), while IHC is realized on histological samples (e.g. biopsies). Consequently, the specimen preparation before the immunodetection is quite different.

A typical **ELISA** immunoassay involves:

- the immobilization of an antigen onto a solid support (e.g. multi-well polystyrene plate, bead, membrane):this step can be realized directly by **chemical adsorption** (**figure 18 C**) or *via* a **capture antibody** (**figure 18 D,E**)
- the recognition of the analyte with a specific antibody: the antigen can be detected **directly**, by a primary enzyme-conjugated antibody (**figure 18 C,D**), or **indirectly**, by a primary recognition antibody and a secondary enzyme-conjugated antibody (**figure 18 E**)

IHC requires proper tissue collection, fixation and sectioning, in order to preserve cell and tissue morphology and the antigenicity of target epitopes. After fixation, usually in paraformaldehyde, samples are sectioned and slices are mounted on microscope slides. Even in this case the detection can be **direct** (**figure 18 A**) or **indirect** (**figure 18 B**)

HRP is well suited for the preparation of enzyme-conjugated antibodies and antigens, due to its relatively good stability and medium molecular size, but especially for its ability to yield chromomeric products with high turnover number (Azevedo et al., 2003). One survey of HRP use stated that this enzyme is incorporated in about 80% of all antibody conjugates for different purposes (Hermanson, 2008). Moreover, the availability of substrates for colorimetric, fluorimetric and chemiluminescent assays provide numerous

detection options (Duffy and Murphy, 2001; Huy et al., 2005; Kuroda et al., 2001; McInvale et al., 2000; Roda et al., 2002; Yavo et al., 2001)..

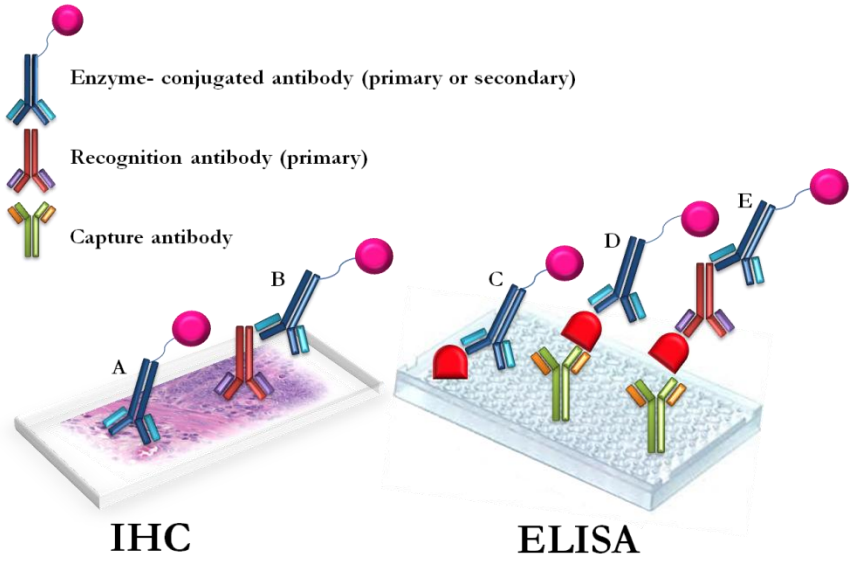

Figure 18 Schematic representation of ELISA and IHC techniques

2.4 Limits of HRP in biosensors and immunoassays

As previously discussed HRP, and other natural enzymes were widely used in biosensors and immuno-conjugate development. However, the relatively high dimensions of HRP (and generally of natural proteins) can cause a series of disadvantages in both fields of biotechnological applications.

Concerning **biosensor** development, the main problems that can be encountered with the use of natural enzymes and metalloproteins are:

- the variable orientation of the redox centers and the denaturation of the proteins, upon the immobilization on the sensor surface,
- the lack of efficiency of electron transfer pathways (ET), due to the polypeptide extended moiety, that can shield or slow down the ET,
- the limited density of redox-active centers per surface unit.

In order to promote a well-organized arrangement of the redox centers and to limit the proteins denaturation, several self-assembled monolayers (SAM) were developed, aimed to mediate the indirect binding on the sensor surface (Samanta and Sarkar, 2011). Briefly, SAMs are organic molecules (thiols, sulphides, cyanides, alkylphosphonates and alkane-thiols), which are able to form spontaneously organized layers by chemisorptions (Nuzzo and Allara, 1983). They were widely investigated in literature, as they provide a facile means of defining the chemical composition and structure of a functionalized surface. Through proper selection of terminal functional group, specific surface/solution interactions (covalent, electrostatic or hydrophobic) can be exploited to immobilize molecules at an interface. SAMs can be prepared and characterized using various methods (Arya et al., 2009).

Concerning the ET pathways, a better electrochemical biosensor performance was obtained in **second generation biosensors**, by introducing a **mediator** in the analytical system. These are small artificial electron transferring agents, that shuttle electrons between the redox centers and participate in the reaction with the biological component, thus speeding the ET (Cass et al., 1984; Chaubey and Malhotra, 2002, 2002; Parra et al., 2006).

Subsequently, **third generation biosensors** were developed, in order to construct electrochemical systems with superior selectivity, stability and durability. These devices exploit the unmediated direct electron transfer (DET) between redox-active metalloproteins and the transducer. An attractive feature of systems based on direct electron transfer is the possibility of modulating the properties of the analytical device, by using protein modification with genetic or chemical engineering techniques.

Efficient direct electron transfer reactions were reported for a restricted number of redox enzymes, mostly. Nevertheless, several studies, based on heme-proteins adsorbed or immobilized on various electrodes, still showed that high-molecular weight enzymes are not amenable to direct electrical communication with the electrode. In fact, the heterogeneous ET between the electrode and the redox-active center may be not favored, due to unavailability of efficient ET routes, also due to partial or full protein unfolding/denaturation on the electrode surface.

Concerning the **immunoconjugate** production, it is important to underline that commercially available HRP-conjugates are limited to one to three HRP molecules per antibody (Ab). This value is mainly due to the steric hindrance of HRP during the conjugation reactions and represents the limit for maintaining the functionality of the conjugate. This molar ratio of conjugation is effective in routine experiments, but it may lack the sensitivity required for detecting targets present in low picogram to femtogram amounts. In conventional ELISA kits, this limit is often solved by using

additional steps to amplify the signal: these methods increase the cost of the assay and the number of steps, that must be optimized each time.

Several approaches to increase ELISA sensitivity are reported in literature, involving the use of biotin-streptavidin HRP-Ab (Nara et al., 2008) and bionanocapsule-based HRP-Ab systems (Iijima et al., 2010), HRP-Ab functionalized nanoparticles (Zhou et al., 2011) and HRP-Ab functionalized carbon nanotubes (Chunglok et al., 2011). Generally, these different approaches share the same target: to increase the number of enzyme molecules per molecule of antibody, in order to create a probe for the analytes detection with better performances and measurements with higher sensitivity.

On the basis of the previous considerations, it emerges that increasing the sensitivity of the measurements achievable by electrochemical biosensors and immunochemical techniques represents still now a very challenging scientific field, to whom we have referred during the realization of this research project.

Aim of the project

The goal of this PhD project is the development of new biomimetic catalysts, based on heme-enzymes, for applications in diagnostic and biosensor technology.

As outlined in the previous paragraph, the technology used to date still suffers of several problems, mainly derived from the high dimension and quite low stability of natural metalloenzymes.

Therefore, this project aims to exploit the remarkable catalytic activity of Mimochrome VI (see **1.4 Mimochrome VI: a heme –protein model with a peroxidase-like activity**) as starting point for the development of new bio-inspired devices.

The project, which lays at the interface between chemistry, biochemistry and biology, takes advantages from the use of different methodologies and techniques, such as **metalloprotein design**, **chemical synthesis**, **spectroscopic**, **structural** and **catalytic characterization**, **immobilization procedures** on solid surfaces and **cross-linking** with biomolecules (**figure 19**).

All these methodologies have contributed to accomplish the two main objectives of the project.

- ✓ **Improve the catalytic performance of Mimochrome VI.**

  Through a re-design procedure and computational techniques, it is possible to introduce some point amino acid substitutions, in order to verify their role in the modulation of the heme-model properties. In particular, five Mimochrome VI analogs were designed, synthesized and characterized during the research activity, here reported. Trough this re-design/characterization approach it was possible to select new catalysts, with improved functional properties.

- ✓ **Evaluate the potential of Mimochrome VI for the development of bio-inspired devices.**

  The use of Mimochrome VI is here proposed for the development of new and advanced biosensors and immunochemical assay. By exploiting the small dimensions and its high catalytic efficiency, it was possible to increase both biosensors surface coverage and antibodies conjugation ratio. This approach will be crucial for a considerable signal amplification and hence, for the development of more sensitive immunochemical assays and biosensors.

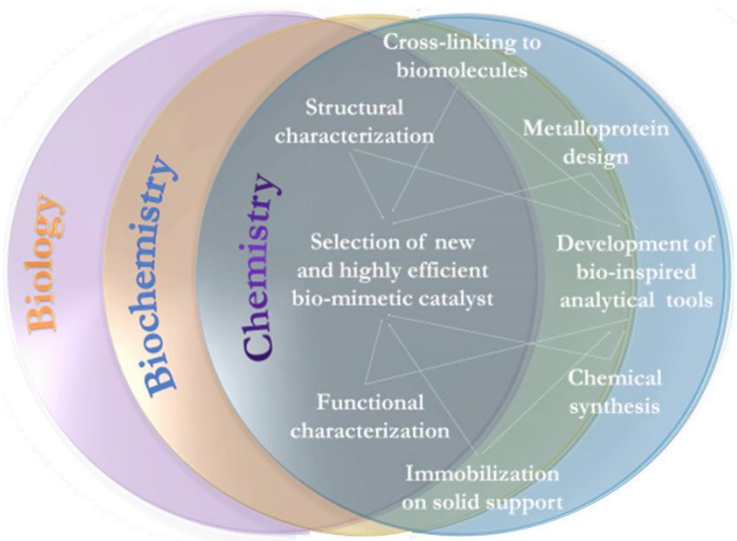

Figure 19 Representation of how basic and applied research, taking advantages of several techniques and methodologies, at the interface of biology, biochemistry and chemistry, are applied in this PhD project.

Results and discussion

CHAPTER III: ***DEVELOPING NEW HEME-PETIDE CATALYSTS***

3. Mimochrome VI and its analogs: design and synthesis of new catalysts

Fe(III) Mimochrome VI is an asymmetric and penta-coordinated heme-protein model with a peroxidase-like catalytic activity. As previously described, this peptide-deuterporphirin adduct was designed on the basis of the information acquired from the structural and functional characterization of the previous models. Based on the results obtained through the analysis of several Mimochromes, the central role of the peptide moiety in their structure/function relations progressively emerged. In fact, the amino acid composition of the peptide sequences can be designed in order to:

- impart typical secondary (α-helical) and tertiary (sandwich helix-heme-helix) structures (D'Auria et al., 1997; Lombardi et al., 1998b; Nastri et al., 1997, 1998b);
- stabilize a symmetric and hexa-coordinated chemical environment to the heme (Lombardi et al., 2003; Nastri et al., 1998b);
- select a stereochemically stable structure (Lombardi et al., 2003);
- modulate the redox properties of the heme (Del Gatto, 2007; Lombardi et al., 2003; Ringhieri, 2010);
- improve the water solubility and stabilize an asymmetric and penta-coordinated peptide-based heme-model (Nastri et al., 2011).

Concerning the role of the peptide moiety in Fe(III)Mimochrome VI, its implication in the structural and functional properties of the molecule was described in the introduction (see **1.4 Mimochrome VI: a heme-protein model with a peroxidase-like activity**). Here, it is important to focus on

the R^{10} and E^{2} residues, which are placed in both tetradecapeptide and decapeptide chains, and the Ser^{6} on the decapeptide chain (**figure 20**).

In the model structure, the R and E residues are involved in the stabilization of the α-helix, *via* charge-dipole interactions, and in the tertiary sandwiched structure, by the formation of inter-chain ion pair.

The S^{6} is placed in the decapeptide chain to create a micro cavity in the proximal site of the deuteroheme. The serine residue was selected in order to facilitate the access of small ligands and substrates, thanks to its small and space-saving side chain. This residue, unable to interact with the metal ion, was placed in the middle of the decapeptide chain, thus stabilizing a penta-coordinated state of the heme. Further, the hydroxyl group in the side chain is supposed to interact *via* hydrogen bonds with H_2O_2 during the first step of the catalytic cycle, and hence it can improve the affinity towards this substrate.

In order to verify the role these five amino acid residues (E^{2}, S^{6} an R^{10} in the decapeptide and E^{2} and R^{10} in the tetradecapeptide) in the structural and functional properties of Fe(III) Mimochrome VI, it was decided to introduce single point substitutions and to verify their effect on the catalysis. Five analogs of Fe(III) Mimochrome VI were designed, synthesized and characterized for this purpose (**figure 21**).

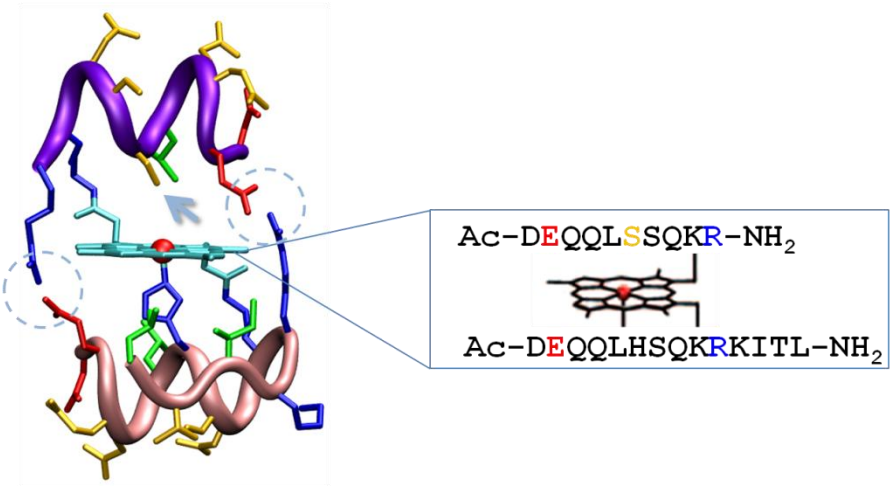

Figure 20 Model structure and sequence of Fe(III) Mimochrome VI molecule: in evidence the inter-chain ion pair between E^2-R^{10} (circle) and the S^6 on the distal side of the heme (arrow).

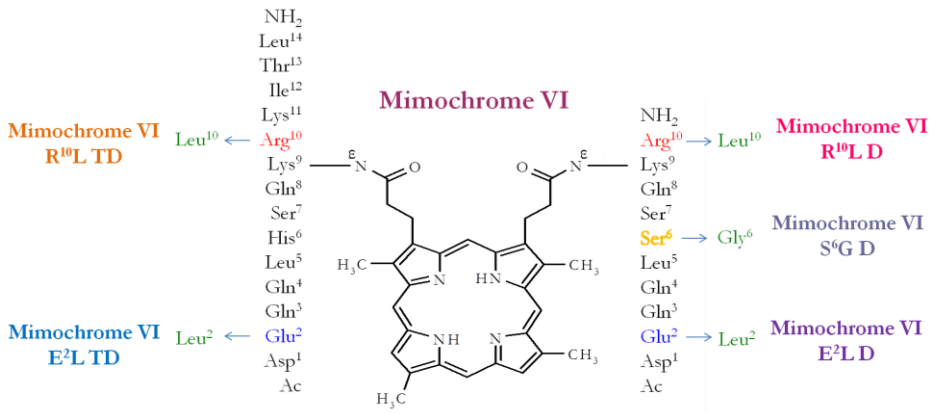

Figure 21 Scheme of peptide sequences of Mimochrome VI analogs. The amino acid substitution on the tetradecapeptide (TD) and decapeptide chain (D) are pointed out.

The charged residues (E^2 and R^{10}) were substituted with the hydrophobic leucine (L), in order to eliminate their ion-pair interactions. These substitutions feature the **E^2L TD**, **E^2L D** and **R^{10}L TD**, **R^{10}L D** analogs of Mimochrome VI. The S^6 was replaced by a glycine (G), which has still a small and non-coordinating side chain and lacks the hydroxyl group,

which is supposed to mediate the H_2O_2 delivery to the active site of the mini enzyme. This substitution characterizes the **S^{6}G** analog.

Fe(III) Mimochrome VI and its five analogs were prepared, following the same synthetic strategy used for the other Mimochromes (Nastri et al., 2011). Peptide chains were synthesized in solid phase, by using 9-fluorenylmethoxycarbonyl (Fmoc) protection strategy. The selective deprotection from (4-methoxyphenyl)diphenylmethyl group (Mmt) of Lys^9 residues on the two chains is required before their cleavage from the resin. In this way, it is possible to obtain the peptides with the free Lys^9 and all other residue side-chains still protected (**figure 22**).

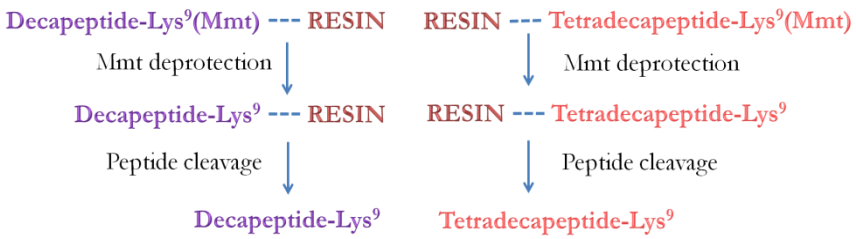

Figure 22 Selective deprotection of Lys^9 side chain of decapeptide and tetradecapeptide side chain

This aspect is important for the selective coupling to the deuteroporphyrin IX, which was carried out in solution. In order to optimize the hetero-dimer formation (TD-deuteroporphyrin IX-D) and to avoid undesired byproducts (TD-deuteroporphyrin IX-TD or D-deuteroporphyrin IX-D), the synthesis was continued, by coupling first one peptide to the deuteroporhyrin IX and subsequently, the so-called monoadduct was bound to the other peptide chain. In particular, to limit coupling of the first peptide to both propionate groups, it was slowly added to the solution containing the porphyrin. In such way, the

porphyrin is in excess and reacts with all peptide molecules in solution, thus favoring monoadduct formation.

Once obtained the di-substituted product, the remaining protecting groups were removed from both peptide chains by treating with trifluoro-acetic acid. Thus, the iron ion was inserted in the free base porphyrins, by following the acetate method (Buchler, 1979). The products were finally purified by reverse-phase HPLC and their identity is confirmed by LC-MS analysis. For more detailed description of protocols and synthetic results, please refer to materials and methods section.

3.1 Mimochrome VI and its analogs: functional characterization

The functional properties of the five analogs of Fe(III) Mimochrome VI were investigated in order to understand the effects of the peptide amino acid composition on the catalytic properties.

In particular, the experiments here presented were carried out in order to assess the ability of these compounds to activate H_2O_2 for the oxidation of a reducing substrate: ABTS or 2,2'-azino-bis(3-ethylbenzothiazoline-6-sulphonic acid) (**figure 23**).

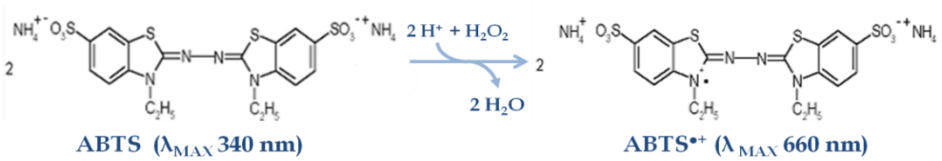

Figure 23 Chemical structure of ABTS and oxidation reaction with H_2O_2.

ABTS is commonly used as a substrate with hydrogen peroxide for the kinetic study of peroxidase enzymes, since it can be efficiently oxidized in a mono cationic radical form ($ABTS^{+\bullet}$) (Childs and Bardsley, 1975; Savenkova et al., 1998). In fact, the formal reduction potential of ABTS is high enough let it to act as an electron donor for the reduction of oxo and peroxo species (Bourbonnais et al., 1998) The product of the reaction exhibits a green color and a λ_{MAX} at 660 nm and its formation can be easily detected by spectrophotometric measurements.

The analysis of the kinetic data by Michaelis-Menten fitting of the experimental points provides the following catalytic parameters:

- v_{max}, which is the reaction rate at saturating concentration of substrate: at low substrate concentrations, the initial rate increases almost linearly, while at saturating substrate concentrations, v_0 achieves the maximum value (v_{max});
- K_m is the Michaelis-Menten constant, representing the substrate concentration at which the half of the v_{max} is reached. It represents the enzyme apparent affinity for substrates;
- $k_{cat} = {v_{max}}/{[enzyme]}$ which is the catalytic constant (or turnover number) and is defined as the maximum number of molecules of the substrate that an enzyme can convert to product, per catalytic cycle, per unit of time;
- ${k_{cat}}/{K_m}$, which is the catalytic efficiency and gives information on the catalytic activity at low substrate concentration.

The kinetic parameters can be determined by studying the dependence towards both substrates and by analyzing the experimental data with a two substrate Michaelis-Menten kinetic model (**equation 2**):

$$v = \frac{[E]_0}{\frac{1}{k_{cat}} + \frac{K_{m\,A}}{k_{cat}[A]} + \frac{K_{m\,B}}{k_{cat}[B]}}$$

Equation 2

where:

- $[E]_0$ is the enzyme concentration, which is supposed to be constant and not inactivated at the initial time (t_0);
- k_{cat} is the catalytic constant;
- $K_{m\,A}$ and $K_{m\,B}$ are the Michaelis-Menten constants for ABTS and H_2O_2, respectively;
- $[A]$ and $[B]$ are the ABTS and H_2O_2 concentrations, respectively.

In order to perform a first screening of the functional properties of the afore mentioned molecules, their catalytic activity was studied in the same conditions used for Fe(III) Mimochrome VI (100 mM phosphate buffer pH 6.5, 50% (v/v) TFE, at fixed catalyst concentration and variable substrates concentration). Experimental data were compared to those obtained for the kinetic characterization of HRP(100 mM citrate buffer pH 4.6 and 7) and two other peptide-based heme-protein models (MP-8 and MP-11).

3.1.a Catalytic characterization of Mimochrome VI analogs: effects of tetradecapeptide modifications

In order to determine the kinetic properties of Fe(III) Mimochrome VI E^2L TD, R^{10}L TD analogs, the dependence towards both substrates (ABTS and H_2O_2) was analyzed (**figure 24**). The concentration of the catalyst was fixed at $2.0 \cdot 10^{-8}$ M. For the analysis of the dependence towards the oxidizing substrate, ABTS concentration was fixed ($1.0 \cdot 10^{-1}$ M), while different H_2O_2 concentration, in the range of $1.0 \cdot 10^{-4}$-$2.0 \cdot 10^{-2}$ M were explored. When studying the dependence towards the reducing substrate, H_2O_2 concentration was fixed ($2.0 \cdot 10^{-2}$ M for E^2L TD and $1.0 \cdot 10^{-2}$ M for R^{10}L TD), while ABTS was varied ($5.0 \cdot 10^{-6}$-$1.0 \cdot 10^{-4}$ M). The kinetic parameters obtained by fitting the experimental data with the **equation 2** are summarized in

table 4.

3.1.b Catalytic characterization of Mimochrome VI analogs: effects of decapeptide modifications

The effects of the decapeptide substitutions (E^2L D, R^{10}L D and S^6G D) were studied by the same approach (**figure 25**). The concentration of the catalyst was fixed at $2.0 \cdot 10^{-7}$ M, because of their lower catalytic activity. Experiments were carried out (i) at steady ABTS ($1.0 \cdot 10^{-1}$M) and variable H_2O_2 concentrations ($1.0 \cdot 10^{-4}$-$2.0 \cdot 10^{-2}$ M) and, *vice versa*, (ii) at constant H_2O_2 (50 mM for M6 E^2L D, 20 mM for R^{10}L D, 50 mM for S^6G D) and different ABTS concentrations ($5.0 \cdot 10^{-6}$-$1.0 \cdot 10^{-4}$M). The kinetic parameters obtained by fitting the experimental data with the **equation 2** are summarized in

table 4.

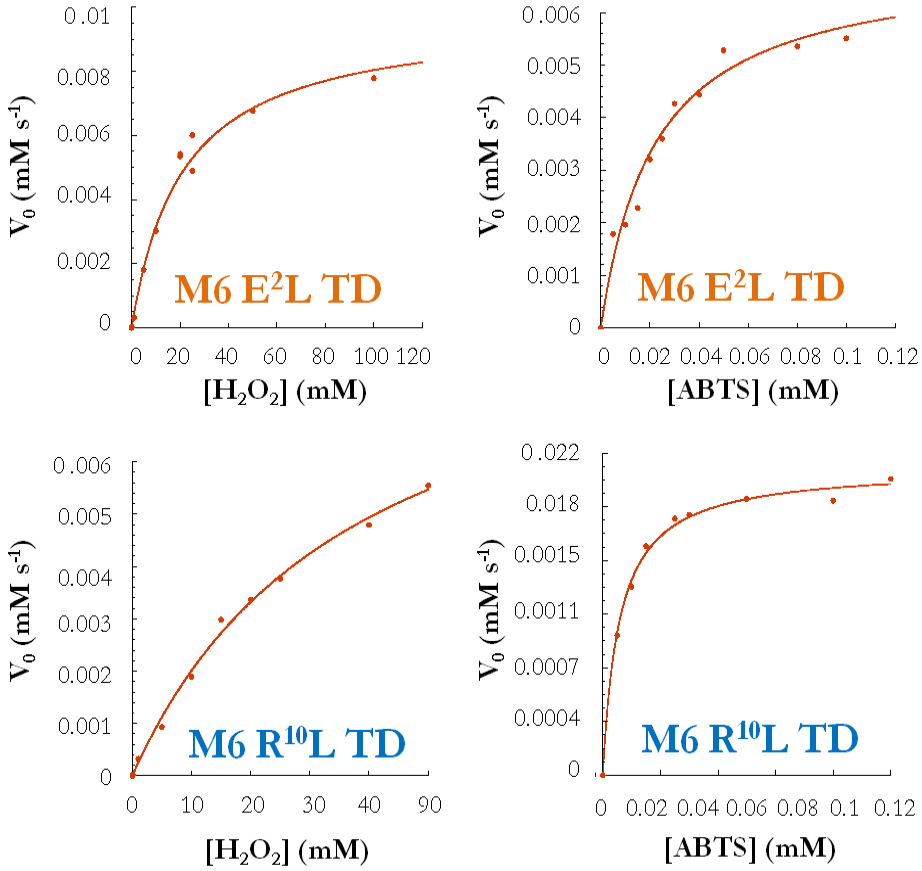

Figure 24 Kinetic study of tetradecapeptide-modified Mimochrome VI analogs. Initial rates of ABTS oxidation at various H_2O_2 concentrations and *vice versa*. The data were fitted according to **equation 2** for a two substrates Michaelis-Menten model.

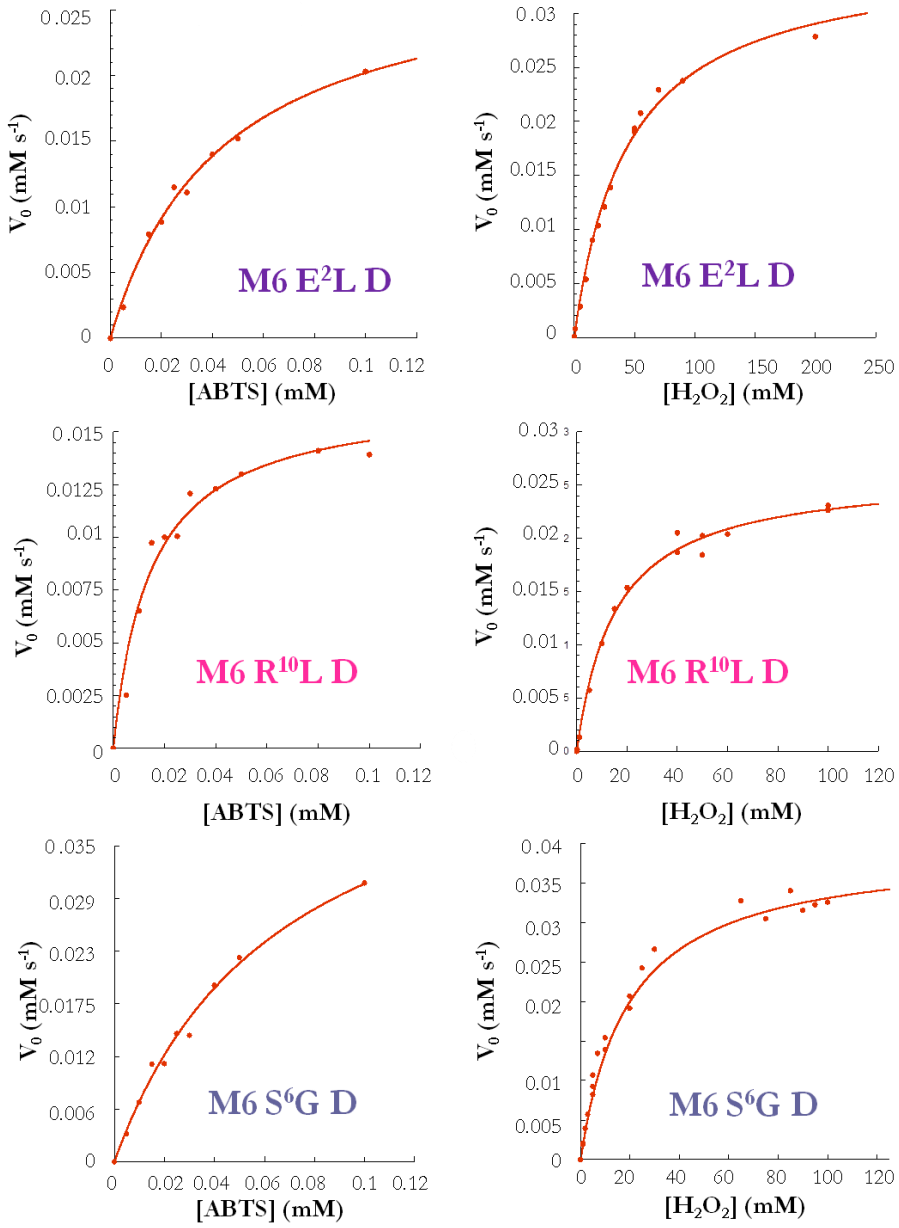

Figure 25 Kinetic study of decapeptide-modified Mimochrome VI analogs. Initial rates of ABTS oxidation at various H_2O_2 concentrations and *vice versa*. The data were fitted according to **equation 2** for a two substrates Michaelis-Menten model.

3.1.c Catalytic characterization of Mimochrome VI analogs: analysis of the turnover numbers

One important parameter to focus, in order to gain more insight in the functional properties of these molecules, is the comparison of their turnover numbers (TON). TON are considered as the number of moles of substrate that a mole of catalyst can convert, before inactivation. In order to assess the turnover number, the enzymatic activity was studied at fixed ABTS ($1.0 \cdot 10^{-4}$M) and H_2O_2 ($3.0 \cdot 10^{-3}$M) concentrations and at different enzyme concentration, in the range from $2.0 \cdot 10^{-8}$ to $1.0 \cdot 10^{-8}$M (**figure 26**). The red kinetic curves reported in the figure represent the minimum enzyme concentration at which it is still possible to oxidize all the ABTS present in solution, which can be deduced by the achievement of the plateau of the $ABTS^{\bullet+}$ absorbance (Abs_{660}=1.1). These concentration values were used to calculate the TONs of the analogues, which are reported in

table 4.

3.1.d Catalytic characterization of Mimochrome VI analogs: pH dependence

The role of the of pH on the activity was also examined.. The pH profile of the v_0 for the $ABTS^{+\bullet}$ formation is characterized by curves with a maximum activity at pH 6.5 (**figure 27**). It seems that the amino acid substitutions do not affect the optimum pH of the oxidizing reaction towards ABTS.

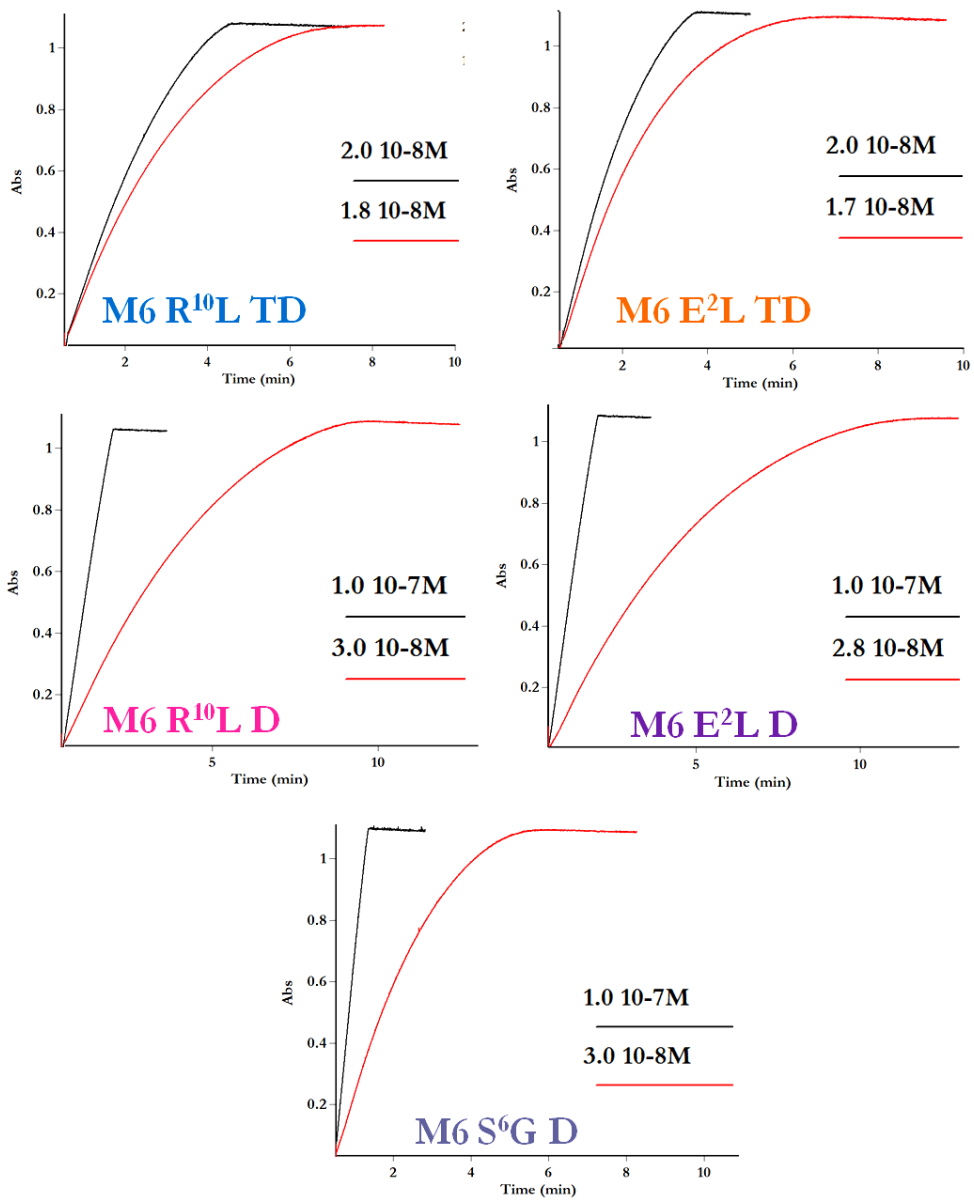

Figure 26 Kinetic experiments at varying enzyme concentration to determine the TON values for the five Fe(III) Mimochrome VI analogs.

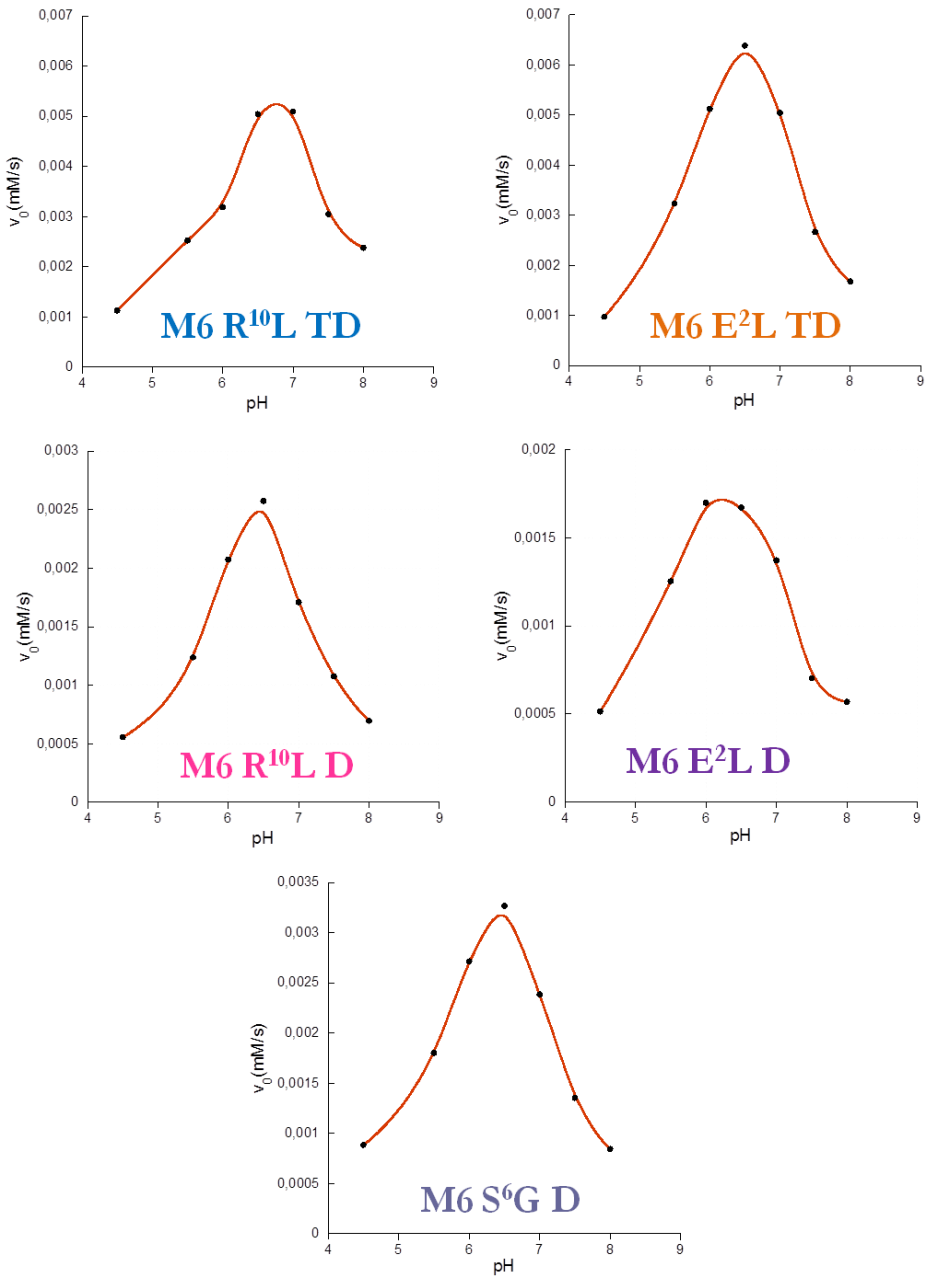

Figure 27 Kinetic characterization of Fe(III) Mimochrome VI analogs: dependence of the initial rate (v_0) versus pH . experiments were carried out in100 mM phosphate solutions in the pH range 4.5-8, 50 % TFE(v/v).

Table 4 Steady state kinetic parameters for H_2O_2 oxidation of ABTS catalyzed by Fe(III)-Mimochrome VI(a: Nastri et al., 2011), its analogs, MP-11 and MP-8(b: Adams and Goold, 1990) and natural HRP(b: Nastri et al., 2011).

Enzyme	pH	$K_m^{H_2O_2}$ (mM)	$K_m^{AH_2}$ (mM)	k_{cat} (s^{-1})	$k_{cat}/K_m^{H_2O_2}$ ($mM^{-1}\ s^{-1}$)	$k_{cat}/K_m^{AH_2}$	Mw(E) (Da)	Specific Activity (mmol $g^{-1}\ s^{-1}$)	TON·1e^{-3} [ABTS]/[E_0]
E^2L TD	6.5	31.3	0.0500	785	25.1	15704	3538	222	5.88
R^{10}L TD	6.5	54.0	0.0380	685	12.7	18026	3508	195	5.56
S^6G D	6.5	45.6	0.125	468	10.3	3743	3520	133	3.33
R^{10}L D	6.5	19.7	0.0290	169	8.58	5828	3508	48.2	3.33
E^2L D	6.5	95.6	0.115	381	3.99	3316	3538	108	3.57
Mimochrome VI [a]	6.5	44.0	0.0840	371	8.43	4417	3551	104	4.00
MP-8 [b]	7.0			$2.6\cdot10^{-3}$	1.73				
MP11 [b]	7.0			$13\cdot10^{-3}$	6.87				
HRP [a]	4.6	0.854	1.07	6209	7270	5803	44174	141	50.0
	7.0	0.0115	5.10	52.5	4565	10.3	44174	1.19	0.33

3.2 Mimochrome VI E^2L TD: structural characterization

In order to gain more insight about the effects of the amino acid substitutions on the catalytic properties of the molecules here described, a preliminary structural characterization of the Fe(III) Mimochrome VI E^2L TD analog was performed. This molecule was selected on the basis of its highest k_{cat}, which makes it the most promising catalyst of the new generation of Mimochrome VI.

3.3 Mimochrome VI E^2L TD: analysis of the secondary structure

The first structural feature, which was investigated through circular dichroism spectroscopy, was the secondary structure content and its dependence towards the co-solvent trifluoroethanol (TFE) (**figure 28**).

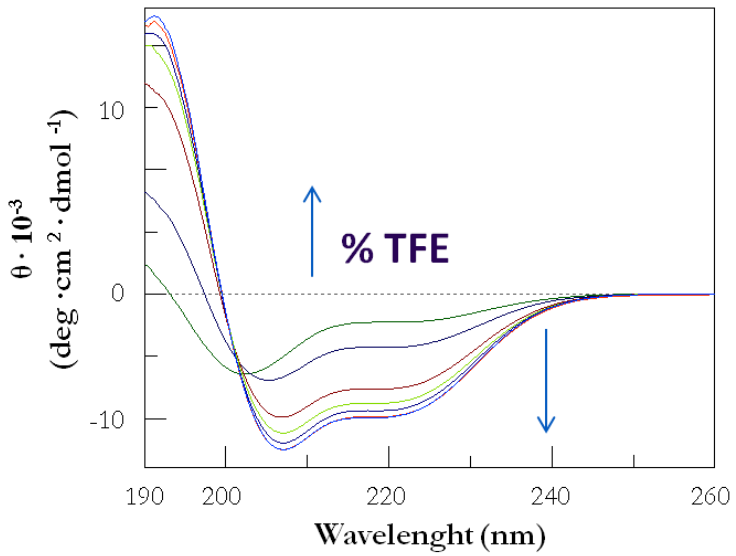

Figure 28 Secondary structure of Fe(III) Mimochrome VI E^2L TD. CD spectra of Fe(III) Mimochrome VI E^2L TD ($7.15 \cdot 10^{-6}$ M) in phosphate buffer (10 mM, pH 6.5) at various TFE percentages (v/v), recorded in 1 cm path length cuvette.

All spectra are characterized by a negative band around 220-222 nm (amide transition n-π*), a negative band between 202-207 nm (amide transition π-π*) and a positive band around 190 nm (amide transition π-π*, perpendicular coupling). These band position indicative of peptide chains in α-helical conformation.

In particular, some parameters can be more clearly indicative of this type of conformation. These parameters, whose values in the present spectral characterization are summarized in **table 5**, are:

- the ratio between the ellipticity of the minimum at 222 nm and the minimum at shorter wavelength (θ_{ratio}),
- the position of the minimum to the lowest wavelength (λ_{min}),
- the wavelength value at the zero point of ellipticity (λ_0)

Generally, the intensification of the mean residue molar ellipticity at 222 nm (θ_{222}), joined to an increase of θ_{ratio} to a value close to unity, a shift towards 207 nm of the λ_{min} and a shift of the λ_0 value towards higher wavelengths, are indicative of stabilization of helical structures (Fasman, 1996; Vuilleumier and Mutter, 1993).

As it can be observed by the modifications of the CD spectra shapes (**figure 28**), the trend of θ_{222} versus TFE percentage (**figure 29** and **table 5)**, TFE addition induces the stabilization of the α-helical structure. In fact, when adding the co-solvent, it can be observed:

- the shift of the λ_{min} from 202 nm to 207 nm;
- the enhancement of the θ_{222}, from -2200 to -9700 deg $cm^{-1}dmol^{-1}res^{-1}$;
- the increase of the θ_{ratio} from 0.36 to 0.77;
- the shift of λ_0 from 193 nm to 200 nm.

The presence of a isodichroic point at 202 nm suggests a transition between a random coil and a helical conformation induced by TFE, as reported in literature (Jasanoff and Fersht, 1994). It can be deduced that the maximum α-helical stabilization is reached at 30% TFE (v/v) and that at 50 % TFE (v/v) there are no more structural transitions.

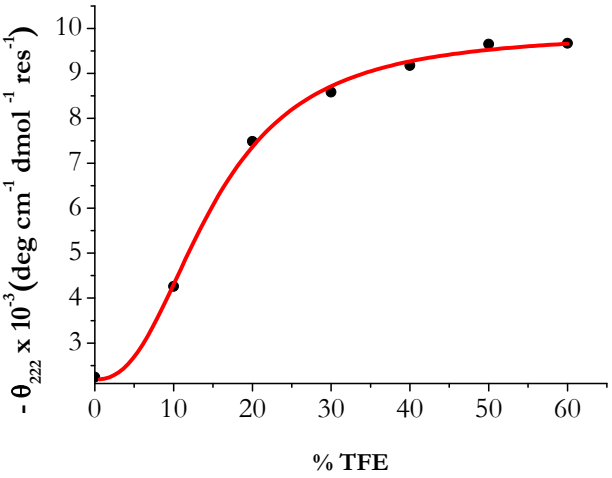

Figure 29 Mean residue ellipticity as function of TFE for Fe(III) E²L TD Mimochrome VI.

Table 5 CD parameters for Mimochrome VI E²L TD secondary structure.

		% TFE						
		0	**10**	**20**	**30**	**40**	**50**	**60**
α- helical propensity	**$\theta_{222} \cdot 10^{-3}$ (deg cm^{-1}dmol^{-1}res^{-1})**	-2.2	-4.3	-7.5	-8.6	-9.2	-9.6	-9.7
	$\theta_{min} \cdot 10^{-3}$ (deg cm^{-1}dmol^{-1}res^{-1})	-6.1	-6.9	-9.9	-11.2	-12.0	-12.5	-12.6
	θ_{ratio}	0.36	0.62	0.76	0.77	0.77	0.77	0.77
	λ_0 (nm)	193	198	199	200	200	200	200

3.4 UV-vis spectroscopy of porphyrins: an overview

UV-visible spectroscopy has been widely applied for the characterization of peptide-based heme-protein models, because it is one of the most powerful techniques for the analysis of the heme properties. Useful information on artificial porphyrin containing systems can be obtained by comparing their spectral properties with those of natural heme-proteins, and *vice versa*.

The porphyrins and their various metal complexes show very distinct spectra and UV-visible spectroscopy can be conveniently applied for ascertain: (i) the insertion of the metal into the porphyrin ring, (ii) the oxidation and spin state of the metal, (iii) the nature of the axial ligands. The highly conjugated p-electron system of the porphyrin ring is responsible for its intense color. Two $\pi \rightarrow \pi^*$ electronic transitions are responsible for the absorption bands, typically found in the porphyrin spectra (Adar, F., 1978; Buchler, J.W.,, 1979; Eaton, W.A., 1981; Gouterman, 1961). An intense band is detected around 400 nm, and it is referred to as B band, or Soret band or γ band; much weaker bands are observed in the 500-600 nm visible region (**table 6**).

Table 6 Scheme of porphyrins electronic transitions.

	Transition	ε ($M^{-1}c^{-1}$)
Soret	$a_{1u} \rightarrow e_g$	$\approx 10^5$
Q_0, Q_v	$a_{2u} \rightarrow e_g$	$\approx 10^4$

These weaker bands are referred to as Q bands or β-α bands. The α band corresponds to the lowest porphyrin π → π* singlet transition Q_0, and the β and to the vibronic envelope Q_v (Dolphin, 1979; Gouterman, 1961). The visible bands are very sensitive to the metal inserted into the porphyrin ring, and to peripheral substituent groups.

The Q_0 and Q_v transitions are polarized in the x, y plane of the porphyrin: for a metal porphyrin, with D_{4h} symmetry, the dipole transitions in the x and y directions are equivalent and both the Q_0 and Q_v transitions are doubly degenerate. Thus, the spectrum of a metal porphyrin usually shows two bands in the visible region. In free base porphyrins, two protons are linked to two opposite inner nitrogens. In this case, the porphyrin plane no longer possess the four fold symmetry and β and α bands splits. In fact, the degenerate Q_0 transition is replaced by transitions polarized along each of the non-equivalent x and y axis, Q_0^x and Q_0^y. Each transition has its vibronic envelope (Q_v^x and Q_v^y), and, as a consequence, four distinct bands characterize the spectrum of free base porphyrins in the visible region (Adar, F., 1978; Buchler, J.W.,, 1979; Eaton, W.A., 1981; Gouterman, 1961).

The positions of the Soret, β and α bands depend on the metal electron configuration, and the energy of the transitions varies as a consequence of the coupling between the metal and the porphyrin orbitals.

The absorption spectra of metalloporphyrins are thus classified into three types, normal, hypso and hyper (Buchler, J.W.,, 1979).

Normal-type spectra are observed for a majority of metalloporphyrins with closed shell metal ions, where the relevant porphyrin π orbitals do

not significantly interact with the metal orbitals. The Soret, α and β bands are often found around 400 nm, 570 and 530 nm, respectively.

Hypso-type spectra follow the normal absorption pattern, but all bands are blue-shifted, due to filled metal d orbital to porphyrin π* back donation. Metal ions that cause hypso-type spectra are limited to those of d^6-d^9electron configuration.

Finally, hyper-type spectra consist of more-or-less shifted α-, β-,and Soret bands and one or more additional bands. They are difficult to analyze because the number of extra-bands varies from one metal ion to another, and the positions of all bands are far more dependent on the axial ligands than in the other types (Buchler, J.W.,, 1979). Metal ions with d^1-d^5 electron configuration show these hyper type spectra. Most of them can be easily found in lower oxidation states within the porphyrin, causing normal- or hypso-type spectra. Mn(III)- and Fe(III)-porphyrins are the best known examples in this respect.

The UV-visible spectra of heme-proteins show absorption patterns quite similar to those observed in simple metalloporphyrins. They are very sensitive to the oxidation and spin state of the iron, which are modulated by the protein environment. In addition to the Soret, β and α bands, four extra-bands are found in the lower energy of the visible region, and they are usually referred to as IV, III, II and I (Bullock and Myer, 1978).

3.5 UV-vis characterization of Mimochrome VI E²L TD: free base and metal complex

In order to verify that the porphyrin ring was not subjected to chemical modification during the synthesis, and to analyze the spectroscopic modification of Mimochrome VI E²L TD upon Fe(III) ion insertion, the UV-Vis spectra of both free base and metal complex were analyzed (**figure 30Figure 31**).

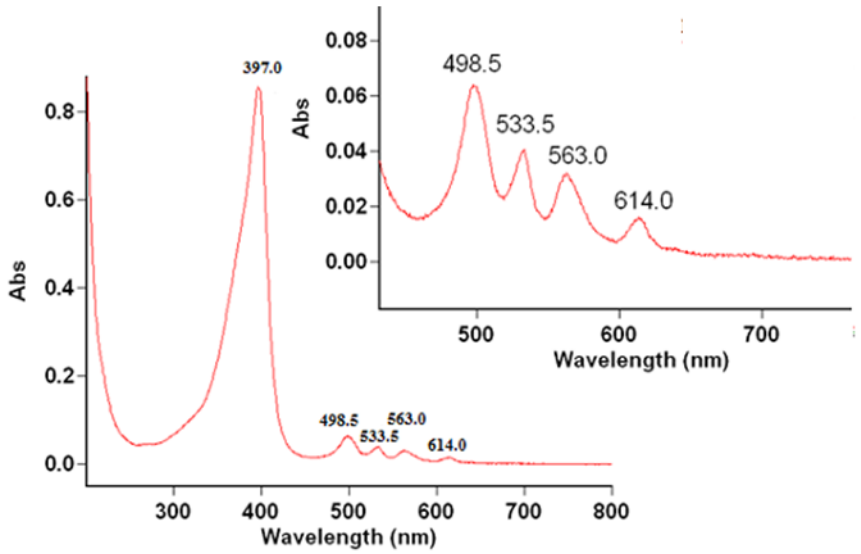

Figure 30 UV-vis spectrum of Mimochrome VI E²L TD free base. Spectrum recorded in H_2O/ TFE 50% (v/v) at pH 6.5. Free base concentration 1.0·10-⁵M.

The free base spectrum in the visible region is characterized by the presence of four distinct bands, localized at 498 nm, 533nm, 563 nm and 614 nm, and by a much more intense band at 397 nm (Soret band).

The number of the bands in the visible region is in agreement with the four not equivalent transitions, expected on the basis of an asymmetrical

system, due to the presence of two protons on two nitrogen atoms in the porphyrin ring.

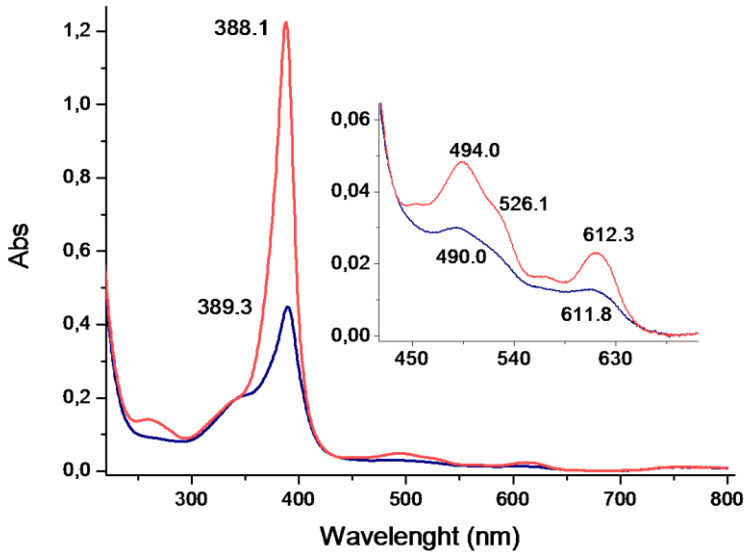

Figure 31 UV-vis spectra of Fe(II) Mimochrome VI E^2L TD at pH 2.0 (red line) and 6.5 (blue line). Spectra are recorded in H_2O/ TFE 50% (v/v). Fe(II) Mimochrome VI E^2L TD $1.2 \cdot 10^{-5}$M.

Analysis of the Fe(III)-complex spectrum confirmed the successful insertion of the iron. At pH 2.0, the system exhibits a hypso-type spectrum in which all bands underwent a blue shift (**figure 31**). In particular, the Soret band shifted from 397 nm to 388 nm, while the bands in the visible region are positioned at 494 nm, with a shoulder at 526 nm, and 610 nm. This spectrum is consistent with a hexa-coordinated high-spin compound: the histidine residue, at this pH, is protonated and the iron is coordinated by two weak axial ligands (two water molecules).

The position and intensity of the bands provide useful information on the metal coordination state. Increasing the pH from 2.0 to 6.5 causes a

decrease in the intensity of the Soret band, together with a slight red shift. In fact, in water at pH 6.6, the maximum of the Soret bands hifts from 389 nm to 391 nm, while the bands in the visible region move from 494 nm to 486 nm (β band) and from 610 nm to 601 nm (CT band).Furthermore, the band near 350 nm (N band region) broadens and the its relative intensity to the Soret band changes. These spectral modifications are consistent with changes in the ferric ion axial coordination from H_2O/H_2O to His/H_2O, in the high spin state (Nastri et al., 2011).

This spectral behavior was observed in simple porphyrin systems, such as deuterohemin–histidine (Fe(III)-DP-His) (Casella et al., 1996), and deuterohemin-peptide-histidine adduct (Fe(III)-DP-P11-His) (Casella et al., 1991), as well as in some natural heme-proteins, with reconstituted Fe(III) deuteroporphyrin, as myoglobin (Rossi-Fanelli and Antonini, 1957) and hemoglobin (Antonini et al., 1964), which present an imidazole and a water molecule as axial ligands (**table 7**).

Table 7 Spectroscopic parameters of Fe (III) Mimochrome VI E^2L TD and others iron deuteroporphyrin complexes.

Compound	Solvent	Soret (nm)	β (nm)	CT (nm)
Fe^{III}Mimo VI E^2L TD	H_2O/TFE pH2	388	494	612
Fe^{III}Mimo VI E^2L TD	H_2O/TFE pH6.5	389	490	612
Fe^{III}Mimo VI	H_2O pH 2.0	389	495	611
Fe^{III}Mimo VI	Buffer/TFE pH 6.5	391	490	602
Ac-MP8	pH 7	395	494	622
Ac-MP8	pH1.5	394	494	620
Fe^{III}-DP-His	H_2O/ CH_3OH	390	492	616
Fe^{III}-DP-P11-His	CH_3OH	390	490	590

3.6 UV-vis characterization of Mimochrome VI E^2L TD: study of the coordination properties

In order to study in more details the coordination properties of the complex, a UV/Vis pH titration of Fe (III) Mimochrome VI E^2L TD was performed in the pH range 2.0–10.0 in aqueous solutions and in the presence of 50% TFE (v/v) (**figure 32**). The progressive increase of the pH, causes some modifications of the spectrum, which suggest ligand exchange, in analogy of what it was observed for Fe(III) Mimochrome VI (Nastri et al., 2011). Two transitions, with midpoints at pH 3.4 and 6.3, were observed (**figure 33**). At pH 2.0, the Fe (III) Mimochrome VI E^2L TD spectrum is typical of a predominantly high spin ferric porphyrin (S=5/2), with the Soret band at 387 nm, the Q bands at 494, 525 nm, and then CT (charge-transfer) band at 610 nm. In the range of pH from 2.0 to 5.5, in correspondence of the first transition, the decrease in intensity of the Soret and CT bands, together with a slight red shift of the Soret band, are consistent with changes in the ferric ion axial coordination from H_2O/H_2O to His/H_2O, in the high spin state (Kennedy et al., 2001; Nastri et al., 2011). This behavior was in agreement with the parent molecule Fe(III)Mimochrome VI.

Increasing the pH to about 7.0 causes a further decrease of the Soret band intensity, with a concomitant modification of the bands in the visible region. In fact, Q bands are detected as two main bands at 488 and 605 nm, with two shoulders at 520 and 568 nm.

This spectral changes can be attributed to a second variation of ligand field, which can be related to the deprotonation of an aspartic acid on the proximal site of the porphyrin (D^1 on the tetradecapeptide chain). However, preliminary experiments of pH titration monitored thorough

CD spectroscopy, in the far UV region (secondary structure) and in the visible region (Soret band), let us to hypothesize a phenomenon of pH-dependent oligomerization (data not shown). To gain structural insights of the species involved in the heme coordination at pH 6.5, corresponding to the active form of the molecule, further characterization by Resonance Raman spectroscopy, DOSY NMR and Magnetic circular dichroism are required and in progress.

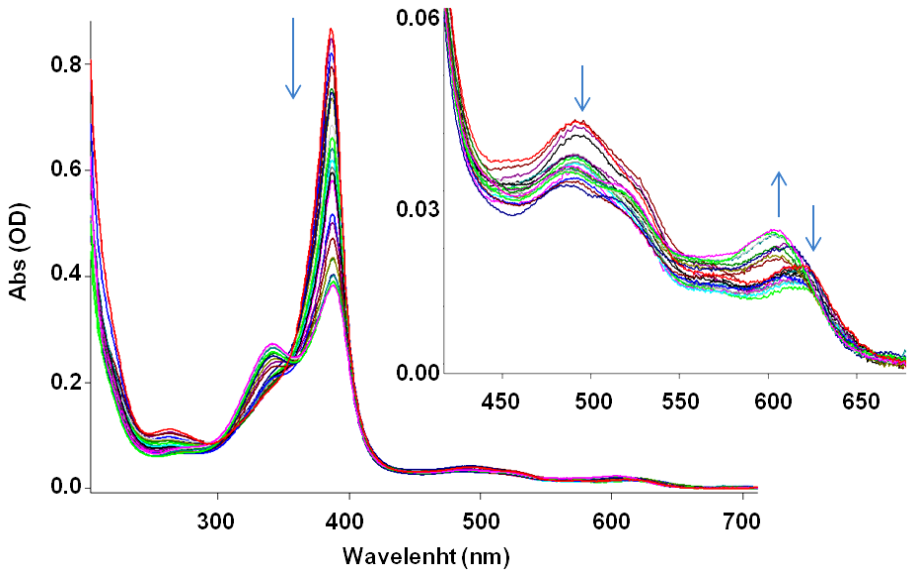

Figure 32 UV/vis spectra of Fe(III) Mimochrome VI (7.21×10^{-6} M) at various pH (2.0–10.0). The spectroscopic titration was performed using TFA and NaOH (at concentrations in the range 0.1–1m), in a 1.0 cm path length cuvette. Arrows indicate the intensity modification of the Soret and Q bands observed by increasing the pH.

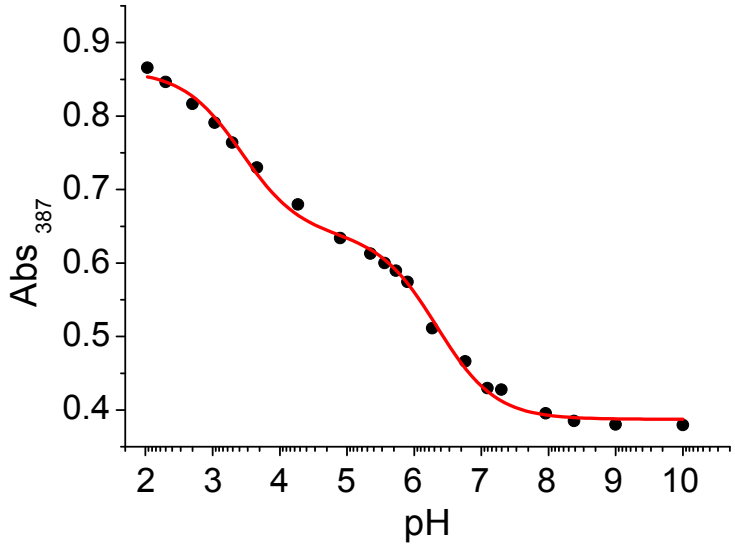

Figure 33 Absorption variation of the Soret band as function of pH. Data points were fitted with a 2 equilibrium model, which describes a first transition at pH 3.4 and a second one at pH 6.3.

Discussion

All the catalytic data demonstrate that all the analogs display a good peroxidase-like activity.

Table 4 reports the comparison of the catalytic parameters for all Mimochome VI analogs, HRP and peptide-based peroxidase models (MP-8 an MP-11).

The data obtained from the functional characterization of Mimochrome VI analogs evidenced the role of each substituted amino acid on catalysis.

Based on the k_{cat} values, it can be concluded that modifications in the decapeptide chain worsened the catalytic properties of the parent molecule. In fact, except the increase of the apparent affinity towards H_2O_2 displayed by the $R^{10}L$ D analog, all the functional properties are lower for these molecules respect to Mimochrome VI.

On the contrary, tetradecapeptide modifications have produced two analogs, whose catalytic efficiency is four times higher than Mimochrome VI, and even higher than HRP.

The first aspect that has to be highlighted is the site-specific effect of the substitution. This suggests that the simple charge modifications, due to the E-L or R-L substitution, is not the main responsible of the catalytic efficiency modification, because the effects are quite different if the modification is in the distal or the proximal side of the deuteroheme (i.e. in the decapeptide or in the tetradecapeptide).

A first hypothesis, to explain this trend can be proposed by analyzing the amino acid composition of the protein chains in proximity of the heme, in natural peroxidases. In this regard, the structures of the horseradish

peroxidase from *A. rusticana* (HRP) (Rodriguez-Lopez et al., 1996; Veitch, 2004) and the chloroperoxidase from *C. fumago* (CPO) (Sundaramoorthy et al., 1995) were considered (**figure 34**).

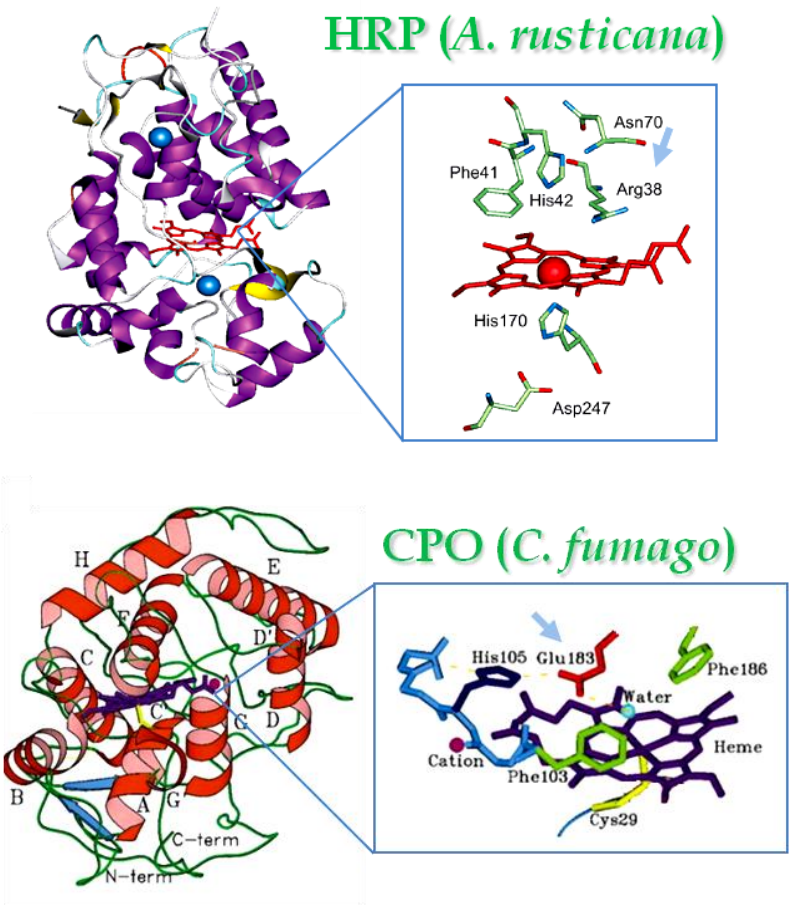

Figure 34 Crystal structure of the HRP (PDB entry ID: 1H5A) and CPO (PDB entry ID: 2CPO). Inset: the heme environment with the function-involved amino acids.

The role of the R^{38} in the catalytic cycle was widely studied, since the elucidation of HRP catalytic mecha-nism (Poulos and Kraut, 1980). Through the combined structural and functional characterization of HRP and R^{38} mutants of HRP, it emerged that this important distal residue is involved in charge stabilization of a precursor enzyme-substrate complex, with relevant effects on the trigger of the cycle (**figure** 35). In fact, R^{38} interacts with compound I and II, *via* hydrogen bonds, and it stabilizes the OH^- group, deriving from the O-O cleavage occurring at compound I forma-tion, *via* electrostatic interactions (Rodriguez-Lopez et al., 1996).

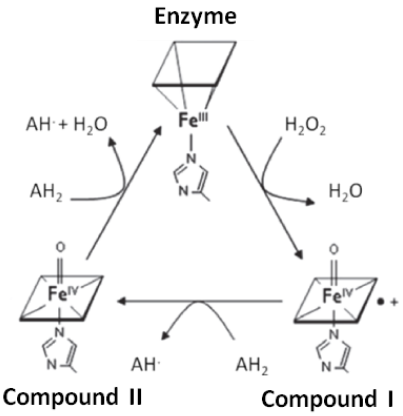

Figure 35 Peroxidase catalytic cycle and compound I and II formation.

Concerning the CPO, its crystal structure reveals that the heme pocket in is typically polar, with an acid-base catalytic group which is not a histidine, as found in HRP (His^{42}) and other peroxidases. In fact, the side chain of Glu^{183} extends from the distal helix F and is positioned directly adjacent to the peroxide-binding site. The catalytic role of E^{183} is probably similar to that of the distal histidine in peroxidases (e.g. H^{42} in HRP): the carboxylate accepts a proton from the incoming peroxide and donates a proton to the leaving hydroxyl group, thus facilitating the heterolithic cleavage of O-O bonds and the consequent formation of the compound I (**figure 35**) (Sundaramoorthy et al., 1995).

Hence, it emerges that a Glu or a Arg residue in the distal site of the heme can be actively involved in the catalytic cycle, thus significantly determining the functional properties of the enzyme.

On the basis of these considerations, it can be hypothesized that, in E^2L and $R^{10}L$ TD analogs, breaking inter-chain ion pair could leave free the corresponding R^{10}or E^2on the distal side of the heme. These residues could undergo to a conformational change, thus pointing directly to the heme and participating to the reaction mechanism, similarly to what observed for the natural peroxidase above described (**figure 36**).

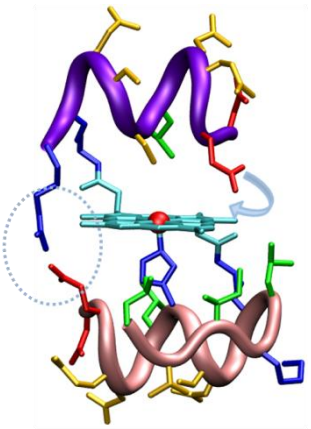

Figure 36 Proposed effect of the E^2L TD substitution.

Based on the preliminary structural characterization of E^2L analog, other considerations can be done. The secondary structure content (**figure 28, figure** 29) and the pH-dependence of the catalytic activity (**figure 27**) seem to be not so far different from Mimochrome VI. However, the UV-vis spectroscopy has revealed a difference in the pH titration for the study of the chemical environment of the heme and its coordination properties (**figure 32**). In fact, in Mimochrome VI two transitions were found at pH 3.4 and 7.4, respectively. The first transition was related to the His^6 deprotonation and its consequent coordination to the heme, while the second one was related the coordination of $-OH^-$ groups, due to the pH increase (Nastri et al., 2011). Concerning the E^2L TD analog, while the coordination of the H^6 seems to occur in the same conditions as in Mimochrome VI, a second transition occurs at pH 6.3. This is not really explainable with the OH^- coordination to the heme, because this hypothesis would be disproven by the maximum of the catalytic activity revealed at that pH value. It is possible that some other amino acids can participate to the coordination properties of the molecule (e.g. D^1 on the

tetradecapeptide chain), thus influencing the structure of this new molecule.

Another possibility is that the amino acid substitution has induced the formation of a dimer, or more generally an oligomer, which could be stabilized at pH 6. Thus, these evidences could be used as starting point to rationalize the structure/function differences between E^2L TD analog and Mimochrome VI. Further structural characterization by resonance raman spectroscopy, magnetic circular dichroism, NMR and DOSY NMR are in progress in order to gain more information about the structural properties of this new minienzyme, which can be related to its notable catalytic efficiency.

It should be highlighted that Fe (III) Mimochrome VI E^2 TD is, to the best of our knowledge, the first artificial heme-enzyme, whose catalytic performance approaches that of HRP. The k_{cat} value observed for this minienzyme is only 7.9 -fold lower than HRP, in the experimental conditions for maximal activity for each enzyme, whereas the k_{cat} value of Fe (III) Mimochrome VI E^2L TD is about 15 -fold higher than HRP at neutral pH.

Moreover, Fe (III) Mimochrome VI E^2L TD shows a significant improvement in the activation of H_2O_2, respect to Fe(III)-Mimochrome VI. In fact, the catalytic efficiency of the new developed heme-enzyme for the reducing substrate is about 3- and 4-fold higher than HRP and Fe(III)-Mimochrome VI, respectively.

The catalytic activity of Fe (III) Mimochrome VI E^2L TD, which is comparable to those of complex proteins, demonstrated that its miniaturized structure holds essential elements for tuning the iron-porphyrin peroxidase activity.

Results and discussion

CHAPTER IV: *SPECTROELECTROCHEMISTRY OF MIMOCHROME VI*

4. Spectroelectrochemistry: combined techniques for the characterization of heme-proteins

Mimochrome VI represents a very interesting heme-protein model, whose electrochemical features can be exploited in order to develop new bio-inspired- analytical tools, such as electrochemical biosensors.

The most diffused approach, for the set up of this kind of biosensors, is to immobilize a redox active molecule (such as heme-proteins and/or heme-enzymes) on the surface of an electrode. This configuration is commonly called in electrochemistry **protein film voltammetry** (PFV). When the immobilized molecule is an enzyme, and the applied electrode potential is appropriate, electrons flow between the substrate and the electrode, via the active site of the enzyme. The magnitude of the detected current is simply proportional to the turnover rate of the enzymatic reaction. Ideally, interfacial electron transfer (ET) may be fast and the electrode may be rotated at high speed to avoid mass transport control, so that the current response directly reports on the intrinsic properties of the enzyme.

Three fundamental reasons make PFV potentially much more informative than other methods, for assaying enzyme properties. First, the potential of the electrode can be continuously swept, to provide whichever driving force is required to elicit catalysis. Hence, each data point along the voltammogram can be thought of as an "initial rate" in solution assay, that can be carried out under precise control of the redox conditions (Cornish-Bowden, 2004). Second, experiments can be carried out over a wide range of accessible timescales, in order to study both transient and steady-state processes. Third, the change in catalytic turnover rate instantly translates

into a variation of current. It is essential, in this respect that the current response is not convoluted and obscured by co-substrate diffusion and intermolecular electron transfers (as is the case for mediated electrochemistry). Together with the precise redox control, this excellent temporal resolution of the activity assay allows to precisely characterize how activity quickly evolves with time, following an instant change in experimental conditions. This was found to be particularly useful for studying the kinetics of inhibition, activation, or inactivation of several enzymes. These processes involve redox and redox-coupled transformations, that occur on short time scales and thus cannot be resolved in normal activity assays (Léger and Bertrand, 2008).

However, PFV also has some drawbacks. First, the limited electroactive coverage of redox-active proteins often corresponds to poorly detectable electrochemical signals from direct oxidation or reduction. Second, the native structure of proteins often undergoes somewhat alterations, thus making necessary the use of other techniques, which provide information about biomolecules in the native state. Third, direct electron transfer does not give any information on the chemical nature of the redox processes, since this technique detects electron flux, without giving accurate information about the chemical species involved. Fourth and final, the measured current may be affected by double layer capacitance and/or by current associated to contaminant species (e.g. in the electrolyte or adsorbed on the electrode surface), which could not be always recognized by conventional electrochemical measurements.

In this context, the afore-mentioned limitations may be overcome by coupling **spectroscopy** techniques to **PFV** (Ash and Vincent, 2012). The

goal of this kind of approach is to detect not only the current signal, but also the optical spectrum, upon electrode polarization.

Different spectroscopic techniques were combined with direct electro-chemistry, to study immobilized redox-proteins, such as **UV-visible** (Dong et al., 1995; Whitehouse et al., 2009; Wu et al., 2011), **fluorescence** (Bernad et al., 2007; Krzemiński et al., 2011; Salverda et al., 2010), **infrared** (Iwaki et al., 2005; Lacey et al., 2008; Marshall et al., 2006), **magnetic circular dichroism** (Marritt et al., 2006) and **resonance raman spectroscopy** (Bernad et al., 2007; Hildebrandt and Stockburger, 1989; Khoa Ly et al., 2011; Kranich et al., 2009).

Typically, spectroscopic techniques are more sensitive than electro-chemical ones and they are not affected by the presence of capacitive current, which usually leads less accurate data by voltammetry (Astuti et al., 2004).

Over the years, spectroelectrochemistry was established as a technique of choice to study immobilized enzymes, by monitoring redox-related current signals and spectral changes. In particular, it was found that cross-correlations between electrochemical and optical data can be very useful in elucidating some thermodynamic and kinetic properties (Renault et al., 2011). The information, that can be achieved by the two techniques synchronized each other, are complementary. For example, a more reliable estimation of the surface coverage of the electrodes can be obtained through the comparison of spectroscopic and electrochemical data. In fact, one of the main limits of PFV is the difficult determination of kinetic properties, such as k_{cat}. This parameter, that is so easily measured in solution assays, cannot always be determined in PFV, because the exact amount of

adsorbed enzyme is not accurately determined or even unknown (Léger and Bertrand, 2008).

For this reason, in the last years intense research activity was devoted to spectroelectrochemistry and time-resolved spectroelectrochemistry (Renault et al., 2012; Venturi, 2012).

The availability of conductive and relatively transparent materials is necessary for this kind of approach. Great interest is focused on the optical and electrochemical characteristics of metal oxides. Durrant and coworkers gave a great contribution to the application of metal oxides (nanocristalline mesoporous SnO_2 and TiO_2 electrodes) for the successful characterization of natural redox proteins (eg. flavodoxin, peroxidases, cytochromes, etc.) (Astuti et al., 2009, 2011; Green et al., 2005, 2005; Kemp et al., 2009; Panicco et al., 2008). However, the semiconductive nature of SnO_2 and TiO_2, limits the potential windows that can be explored, and restricts their use to address the kinetics of fast electron-transfer reactions (Renault et al., 2011). Moreover, the randomly sintered nanoparticles of SnO_2 and TiO_2 that are usually used for these electrode functionalization generally lead to poor accessibility of biomolecules within the porous film (Renault et al., 2011).

Balland, Limoges and coworkers used conductive mesoporous nano-structured films of tin-doped indium oxide (ITO) as practical platform for the immobilization of several heme-proteins (e.g. cytochrome c, neuro-globin and microperoxidase-11) an their spectroelectrochemical chara-cterization (Renault et al., 2012; Schaming et al., 2012). They coupled cyclic voltammetry to time-resolved UV-vis spectroscopy in order to characterize the heterogeneous ET of the immobilized metalloproteins on ITO

electrodes, and they even succeeded in determining the catalytic mechanism of O_2 reduction mediated by microperoxidase -11 (Renault et al., 2012; Schaming et al., 2012).

4.1 Spectroelectrochemical characterization of Mimochrome VI: towards biosensor development

The advantages of using **small peptide-based heme-protein models**, as electroactive molecules in electrochemical analytical systems, are dual.

On one hand, the molecular weight and the relative molecular size of these artificial molecules are much lower than natural heme-proteins. This makes possible to significantly increase the surface coverage of the electrodes and, hence, to considerably increase the number of molecules per electroactive unit area.

On the other hand, the absence of the high dimensions protein matrix allows to avoid the interferences with the electronic pathways during the redox processes, which usually make the direct electron transfers (DET) inefficient or even absent. High surface coverage and efficient DETs together have the effect of notably increasing the intensity of the electrochemical signal, thus considerably bettering the sensitivity and the reliability of these type of analytical measurements.

Moreover, the discrete spectroscopic features of porphyrins and their metal complexes (e.g. the high molar extinction coefficient and the discrete spectral variations related to the oxidation, spin and coordination states of the metal ion) make these molecules, and hence heme proteins and heme

protein models, very interesting object for the characterization of the redox processes by spectroscopic techniques.

The spectroelectrochemical characterization of Fe(III) Mimochrome VI immobilized on ITO electrodes was realized in collaboration with Prof. Véronique Balland and Prof. Benoit Limoges, at the *Laboratories d'électrochimie moléculaire* (LEM) of Paris. The aim of this part of the research activity was focused on the thermodynamic and kinetic characterization of the heterogeneous electron transfer and the study of the catalytic reduction of dioxygen. In addition to fundamental studies the development of Mimochrome functionalized highly transparent and porous 3D electrodes will allow to explore their potentialities in the development of high density biosensors (**figure 37**).

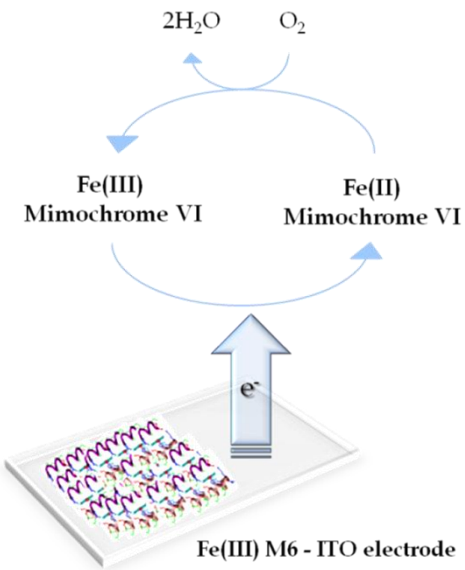

Figure 37 Mimochrome VI immobilized on ITO electrode and catalytic reduction of O_2.

4.2 Mesoporous nanocrystalline 3D ITO electrodes

Tin-doped indium oxide (ITO) is one of the most interesting materials for applications in spectroelectrochemistry, since it combines the optical transparence and a typically metal-like conductivity, and it can be easily deposited as a thin film on solid supports, for practical applications.

The use of this type of metal oxide has two important advantages respect to semiconductive metal oxides (e.g. SnO_2 and TiO_2):

- it is possible to explore wider potential windows;
- the ET are faster, thus providing the possibility of developing time-resolved spectroelectrochemical measurements.

Two different strategies can be used to prepare thin conductive films of doped metal oxide, with controlled porosity and transparency. One is based on hybrid organic-inorganic sol-gel process, which allows to obtain thin films of doped metal oxides with a 3-D mesoporosity (Fattakhova-Rohlfing et al., 2006; Wang et al., 2009) (**figure 38**). This method allows to obtain well-organized nonporous structures, but with restricted film thickness as well as limited porosity (~ 15-20 nm) (Renault et al., 2011).

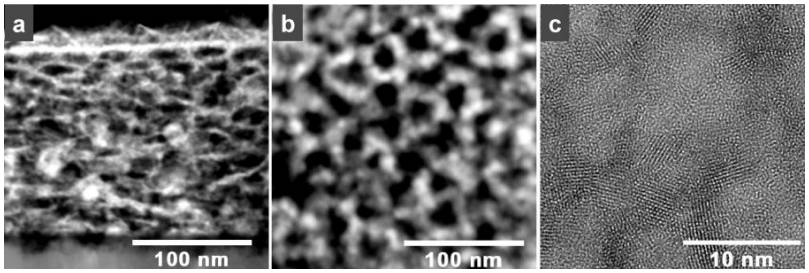

Figure 38 Scanning transmission electron microscopy images in high-angle annular dark-field contrast (STEM-HAADF) of the film in a direction a) perpendicular and b) parallel to the substrate plane show ITO by bright and porosity by dark contrast. c) HRTEM image of a 20 nm side length section of the mesostructure (Fattakhova-Rohlfing et al., 2006).

A second approach is represented by vacuum-based glancing angle deposition (GLAD) (Krause et al., 2010; Robbie, 1998). This technique consists in a single step physical vapor deposition of a metal oxides on solid supports (**figure 39**). Under vacuum atmosphere, the ITO solid block is sublimed by electron bombardment and the so-generated vapor flux is directed on a rotating solid support. Polycrystalline columnar structures are then generated and vertically elongated, thereby forming a porous oxide film. The most important advantage of this technique, respect to the previous one, is the possibility of controlling the morphology of the deposited films, which can be modulated by regulating:

- the deposition angle (α);
- the rate of the incident flux;
- the rotation speed of the support.

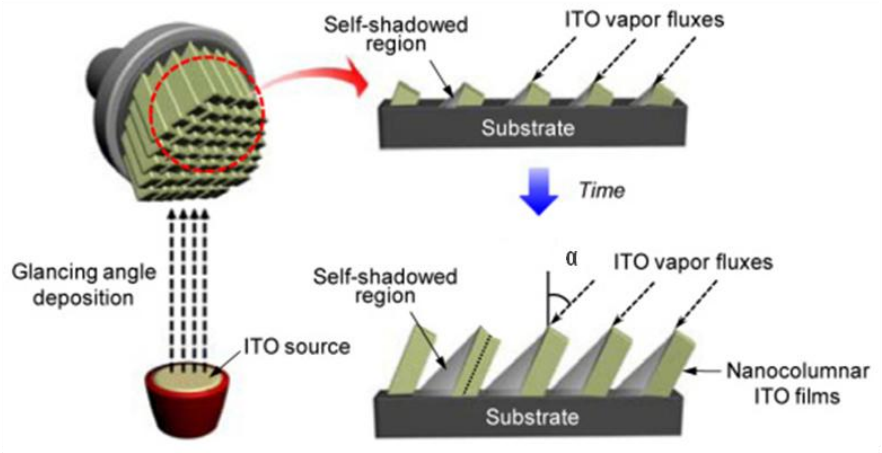

Figure 39 GLAD technique for ITO deposition on solid supports.

The regulation of the morphology of the deposited film is realized in order to adjust the thickness, the surface area, the shape and the porosity of the ITO- nanosized columnar structures. In **figure 40** the top-view and the cross-sectional SEM images of GLAD ITO films are shown, having four film thickness (ranging from 0.25 to 2μm). As it can be observed in these images, as the film thickness is increased, the density of the columns decreases (from ~70 to 8 columns per μm^2), while their diameter increases (~90 to 270 nm). As consequence, the void spacing between the columns increases (~40 to 90 nm). Clearly, even the optical transparency and the conductivity are affected by the film thickness: they decrease and increase, respectively, as the film thickness is raised.

One very interesting aspect of GLAD ITO films is the notable surface are enhancement, due to this columnar architecture. This allows to immobilize

biomolecules as a monolayer, directly communicating with the electrode, thus significantly bettering the DET of these systems.

Clearly, for suitable spectroelectrochemical characterization of adsorbed molecules, it is quite important to select an appropriate GLAD ITO film thickness, which should be a good compromise between transparency and surface enhancement.

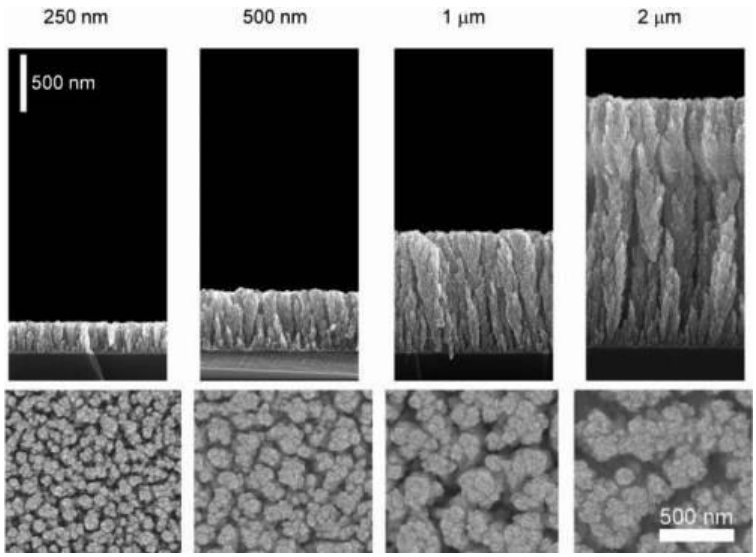

Figure 40 Scanning electron micrograph (SEM) images of different GLAD ITO films prepared with a deposition angle of 80° for different film thickness (side- and top-views) (Renault et al., 2012).

4.3 3D ITO electrode selection and characterization

The first step for Mimochrome VI spectroelectrochemical character-ization was the selection of the most suitable ITO electrode and the characterization of its optical and electrochemical properties.

In analogy to the system developed for microperoxidase 11, 1 μm film thickness of ITO electrode was selected, since for this small peptide-heme adduct, which is very similar to Mimochrome VI molecular structure, this represented a good compromise between optical and electrochemical properties (Renault et al., 2012). In order to determine its optical transparency, the absorbance spectrum of the nude ITO electrode was recorded (**figure 41)**. In the ultraviolet region of the spectrum ($\lambda \leq 350$nm) an intense band is detected, which corresponds to the electron transition from the valence band to the conductive band of the ITO. Nevertheless in the visible region, ITO are mostly transparent, due to the large band-gap value of this materials, exhibiting only small interference fringes, due to the optical scattering caused by the ITO columnar structures.

When increasing the film thickness, the optical transparency of the ITO, in both ultraviolet and infrared regions, considerably increases, thus affecting the spectroscopic detection of the adsorbed molecules (Renault et al., 2012).

Considering that the Soret band position of Fe(III) Mimochrome VI is detected at 389 nm (pH 6.5), this film thickness was confirmed to be a good compromise between conductivity and transparency.

The capacitance of the examined electrodes was determined in oxidative potential window (from 0.4 V to 0.0 V) at different scan rates (0.01-2V/s). The current intensities were normalized for the geometric surface area (0.24 cm^2) and plotted versus the scan rate. The slope of the determined straight line is the capacitance of the electrode. The value of 546 $\mu F/cm^2$ agrees with that typically determined for this film thickness (Renault et al., 2012).

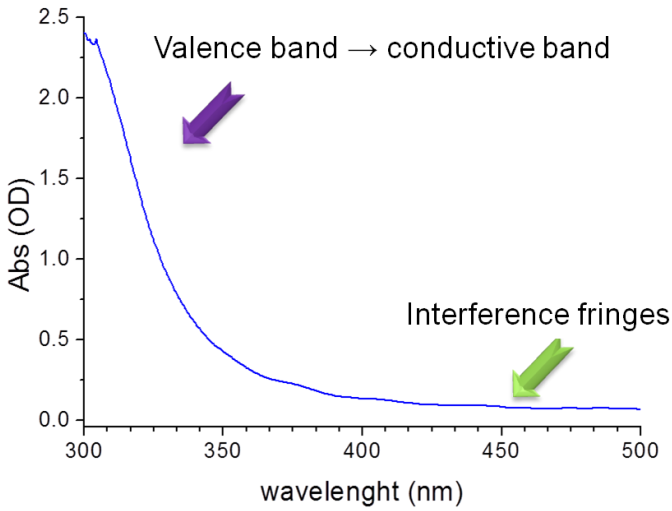

Figure 41 UV-vis absorbance spectrum of GLAD ITO (1 μm film thickness).

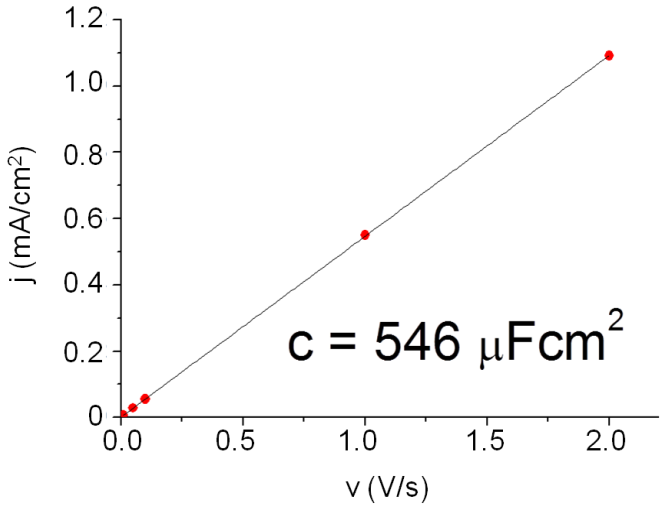

Figure 42 Current density (mA/cm^2) as a function of scan rate (V/s).

4.4 Spectroscopic characterization of Mimochrome VI adsorbed on ITO electrode

Enzymes are often immobilized on surfaces such as particles, films or coated on electrode surfaces for a wide range of applications, from biosensors to biocatalysts. However, the utility of an enzyme in a given process is guided by its structural properties, such as the conformational stability and the coordination state of metal cofactors. Clearly, the immobilization on a support can add, to the original molecular system, numerous potentially disturbing elements, which can depend on the surface nature of the support material, cross linkers, stabilizers, ionic strength, etc (Khan et al., 2011). Usually, the stability of the surface bound enzymes is evaluated from their catalytic activity alone, as it is technically not possible to obtain more structural information. The availability of a transparent

support (ITO electrode) makes possible to compare some spectroscopic characteristics of the adsorbed molecule with those found in solutions, thus allowing to conclude if the structure of the molecule is affected or not by the immobilization process.

For this purpose the UV-vis absorption spectrum of Fe(III) Mimochrome VI in solution was compared to the spectrum of the molecule immobilized on ITO electrode (**figure 43**). It is evident that the two spectra are quite similar, showing the same λ_{MAX} (389 nm) and the same amplitude of the absorption peak of the Soret band. This result suggests that no modifications of the deuteroheme coordination geometry and spin state occurs upon adsorption on ITO electrode.

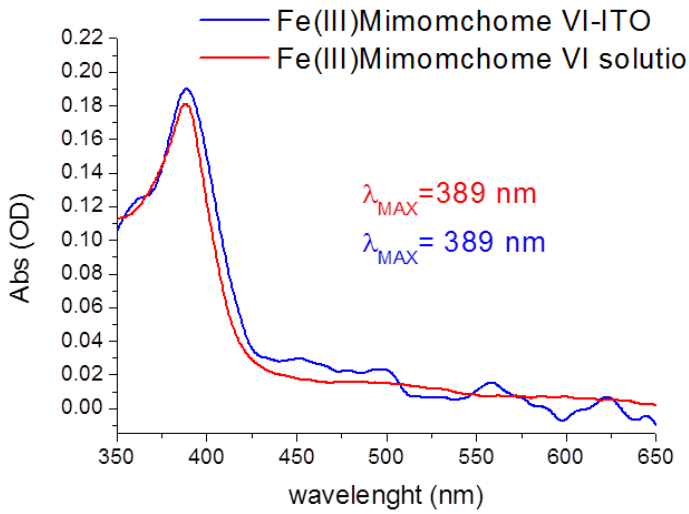

Figure 43 Comparison of UV-vis absorption spectra of Mimochrome VI in solution (red) and adsorbed on ITO electrode (blue).

In order to confirm this hypothesis, the same approach was applied for the comparison of the resonance raman spectra (**figure 44**). This spectroscopic technique allows to obtain information on the vibrational properties of the molecules, and it is powerful in the study of bioinorganic complexes and heme proteins. It is reported that the 1300-1700 cm^{-1} region in the resonance raman (RR) spectra of hemes are characterized by the presence of bands, which are recognized as core-size and spin- state markers (Weiss et al., 2006). The dependence of the position of these marker bands reflects changes in methine- bridge force constants, which are due to the expansion or the contraction of porphyrin, and can be correlated to the porphyrin coordination and spin states. This conclusion derives from the observation that in six-coordinated complexes, iron lies close to the heme mean plane, whereas in five-coordinate complexes iron is displaced from the heme mean plane to the fifth ligand (Weiss et al., 2006). In the first case, expansion of the heme occurs, while in the second case heme is contracted, as a consequence of iron displacement. These skeletal mode frequencies well define the coordination and spin states of the examined compounds and they can be detected by resonance raman spectroscopy.

Even in the case of RR spectra, it is possible to observe that the position of the marker band υ_2, υ_3, υ_4 and υ_{10}, of the molecule in solution and immobilized on ITO electrode, are practically the same. This confirms that the coordination and the spin state of the molecule are not modified upon the adsorption on ITO electrodes.

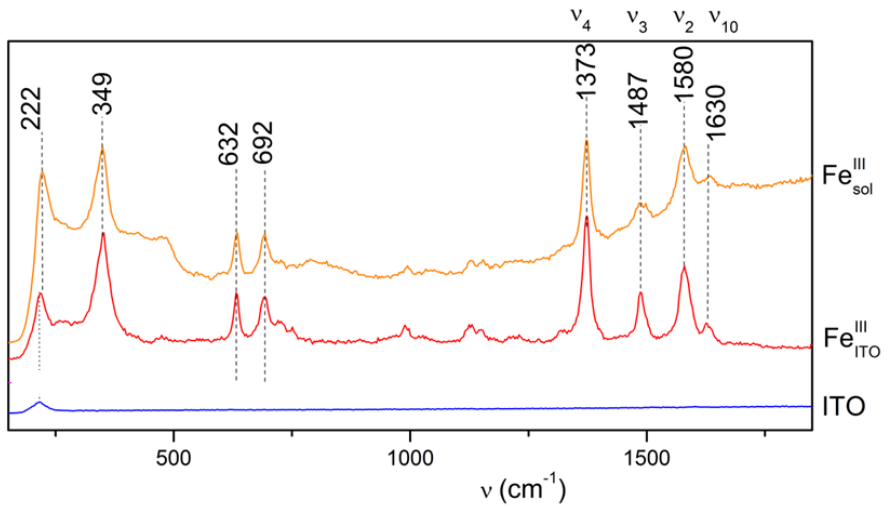

Figure 44 Comparison of resonance raman spectra of Mimochrome VI in solution (50 μM in 10 mM MES buffer pH 6.5) -orange line - and adsorbed on ITO electrode -red line- . As reference the protein-free ITO spectra is also reported -blue line (λ_{ECC}= 405 nm).

The last spectroscopic comparison between Mimochrome VI in solution and adsorbed on ITO was focused on the Fe(III)/Fe(II) forms.

The spectroelectrochemical redox titration, which will be discussed in more details after, was performed in a home-made spectroelectrochemical cell (filled with 90 mM MES buffer, 10 mM KPF6 solution at pH 6.5) by applying reducing potential. The spectrum of the fully reduced was subtracted of the spectrum of the ferric Mimochrome VI-ITO, to obtain the difference spectra reported in **figure 45**. Even in this case, the ferrous and ferric λ_{MAX}, as well as their relative ratio, are un-modified upon adsorption.

In conclusion, the overall results demonstrate that the coordination, the spin state and, more generally, the spectroscopic characteristics of the molecule are not affected by the interaction with the metal oxide film. Therefore, Mimochrome VI represents an interesting example of synthetic and peptide-based heme-protein model, whose redox properties can be conveniently studied by spectroelectrochemistry.

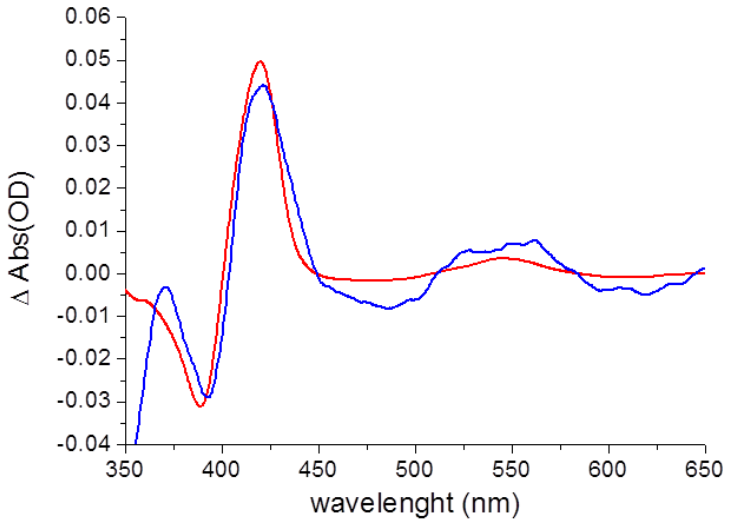

Figure 45 Difference spectra (oxidized minus reduced) in solution (red line) and adsorbed on ITO electrode (blue line). Experiments were conducted in 90 mM MES buffer, 10 mM KPF6, pH 6.5.

4.5 Kinetic of adsorption and desorption of Mimochrome VI on ITO electrode

Generally, molecules can be immobilized on metal oxides surfaces either by **physisorption** and **chemisorption** modes. These materials are rich in hydroxyl groups, thus conferring an acid-base behavior to the film, which is expected to be negatively charged at neutral pH. Hence, **physisorption process** is usually achieved by the formation of hydrogen bandings, van der Waals forces, electrostatic interactions and by physical entrapment within the film porous. Moreover, the metal component of the matrix let possible the establishment of coordination bonds typical of **chemisorption** (e.g. unidentate, bidentate chelating and bidentate bridging). The amino acid composition of Mimochrome VI peptides is characterized by the presence of both positively and negatively charged residues which are supposed to mediate a fast and stable physisorption to the electrode. Moreover, the carboxylate groups of glutamate and aspartate residues could mediate chemisorption processes, further stabilizing the ITO-Mimochrome VI system.

In order to determine the kinetic of the adsorption of Mimochrome VI, the ITO electrode was soaked, at room temperature, in a 50 μM Fe(III) Mimochrome VI solution (in 10 mM MES buffer, pH 6.5), during a determined time. The low ionic strength of this solution was required, since the physisorption and chemisorption processes could be hindered at higher ionic strength, masking charge-mediated interactions. The increment of the absorbance at 389 nm, in the blank-subtracted spectra, was indicative of Mimochrome VI adsorption on the electrode. The experimental point,

which were plotted versus the incubation time, showed a very fast adsorption process with a k_{ads} of 0.17 min^{-1}, reaching the maximum surface coverage in about 30 minutes (**figure 46**).

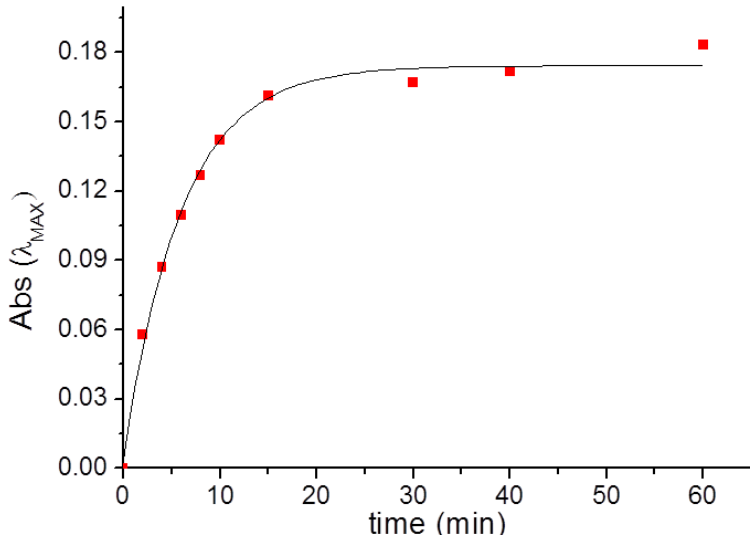

Figure 46 Adsorption kinetic of Mimochrome VI on ITO electrode.

In order to assess the stability of the system at higher ionic strength, which are the typical experimental conditions of electrochemical measurements, the kinetic of desorption was also investigated. For this purpose, the electrode was soaked in a 90 mM MES buffer, 10 mM KPF_6 at pH 6.5. This time the decrease of the Soret band intensity was indicative of Mimochrome VI desorption from the ITO electrode. Absorbance variation at 389 nm was potted versus the incubation time and showed a rapid removal from the film of ~ 10% of Mimochrome molecules initially immobilized, with a k_{des} 0.9 min^{-1} (**figure 47**). This small fraction is reasonably ascribable to a portion of molecules, which are not stably and directly bound to the

electrode, but rather immobilized on it via intermolecular interactions. Desorption experiment were also performed at higher ionic strength, in order to further analyze the stability of the system. In 150 mM MES buffer, 100 mM KPF6 solutions the system is still stable, showing a negligible desorption (data not shown). Hence, the stable interaction of Mimochrome VI with ITO electrodes, which is supposed to be driven by the peptides amino acid composition, was confirmed by these results.

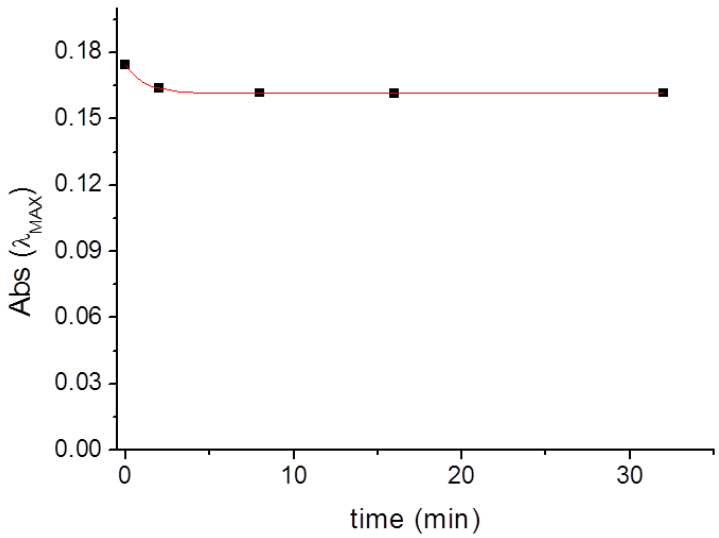

Figure 47 Desorption kinetic of Mimochrome VI on ITO electrode. Experimental points are fitted with a double exponential equation.

4.5 Estimation of the surface coverage

The surface coverage of the ITO electrode with Mimochrome VI was determined by combining both spectroscopic and electrochemical data. On the basis of the spectroscopic characterization of Mimochrome VI adsorbed on ITO electrode, it is possible to assume that the extinction coefficient of the adsorbed mini enzyme is the same as determined in solution (pH 6.5 ε_{389}=63 000 $M^{-1}cm^{-1}$ (Nastri et al., 2011)).

The surface coverage Γ, which is determined by the absolute absorbance (λ = 389 nm) divided by this ε value, and considering 1 μm film thickness, is estimated to be 2-3 $\cdot 10^{-9}$ mol/cm^2. This value was compared to the one obtained by integrating the faradic peak current in the corresponding voltammograms, subtracted of the blank (nude ITO electrode).

The electrochemically-determined Γ was lower than the previously determined (~7 $\cdot 10^{-10}$ mol/cm^2). This discrepancy can be explained on the basis of the important optical contribution of the ITO electrode in the UV region, which could cause a incorrect blank subtraction in the spectroscopic data and an over estimation of the Γ value. This inconvenient was already encountered by Balland and co-workers in previous works on other heme-proteins adsorbed on ITO (Renault et al., 2011, 2012; Schaming et al., 2012).

Time-resolved spectroelectrochemistry allows to overcome this problem. It is possible to monitor the absorbance variation at a specific wavelength, as a

function of time, during the redox cycle, occurring at the polarization of the electrode.

The 421 nm wavelength, indicative of the Fe(II) formation in the film at reducing potential, was selected for this purpose. A stable absorbance variation of 40 mOD was detected at different scan rates, suggesting that the redox process is reversible and that the Γ does not change over the time (e.g. for desorption of Mimochrome VI from the film). This ΔAbs value can be normalized for the Δε, determined in solution to estimate the surface coverage of the electrode. The Γ value obtained by this approach was the same as determined by electrochemistry.

table 8 compares the Γ values of Mimochrome VI and microperoxidase-11, obtained by using the same electrode film thickness (1μm) (Renault et al., 2012). The lower Γ value obtained for Mimochrome VI can be explained considering the slight difference in molecular weights. Moreover, MP-11 is adsorbed as an aggregate and hence it is possible that its molecular diameter is smaller respect to Mimochrome VI, thus explaining the higher surface coverage. However, the columnar architecture of ITO films alllows to adsorb a high number of Mimochrome VI molecules as a monolayer, thus allowing the realization of a complete thermodynamic and kinetic characterization of the system.

Table 8 Saturating surface concentration obtained for Mimochrome VI and mp-11 adsorbed on ITO electrode (1μm).

	MimochromeVI	**MP-11**
Molecular weight	3.5 KDa	1.86 KDa
$\mathbf{K_{ADS}}$	0.17 min^{-1}	0.18 min^{-1}
$\mathbf{\Gamma_{SAT}}$	~ $7 \cdot 10^{-10}$ mol/cm^2	~ $1 \cdot 10^{-9}$ mol/cm^2

4.6 Thermodynamics of Mimochrome VI-ITO electrode ET

The thermodynamic characterization of the Mimochrome VI-ITO system was carried out in order to determine the value of the apparent standard potential E°' and to verify if the Fe(III)/Fe(II) redox interconversion is an equilibrium process, and well described by the Nernst model.

Redox titration of Mimochrome VI was perfomed in a spectroelectrochemical cell, as described in 4.5 paragraph. Redox process was observed to be fully reversible, with well resolved isosbestic points at 403, 450 and 513 nm in the difference absorbance spectra (**figure 48**).

The resulting titration curve was adjusted to the Nernst equation and in the best fit a standard potential E°'=-0.319 vs. Ag/AgCl and a number of transferred electrons n=0.69. The value of the observed E°' is just slightly modified respect to the value measured for the same molecule in solution

and immobilized on a non polar self-assembled monolayer (SAM)-coated gold electrode (Ranieri et al., 2010).

The n value is lower than 1, which will be expected for one-electron Fe(III)/Fe(II) couple. This n value can be attributed to the distribution of Mimochrome VI in various orientations on the surface and in heterogeneous microenvironment, as previously reported (Renault et al., 2012). In order to confirm this hypothesis, the redox titration-relative experimental points were fitted with Nernst equation, assuming a square distribution of potentials and n=1. The best fit gave $E°'^{av}$=-0.319 V and a ΔE of 0.007 V (**figure 49**). The apparent standard potential is the same as determined with classical *nernstian* model, and the discrepancy in the number of electrons involved in the redox process is therefore translated in standard potential dispersion (ΔE).

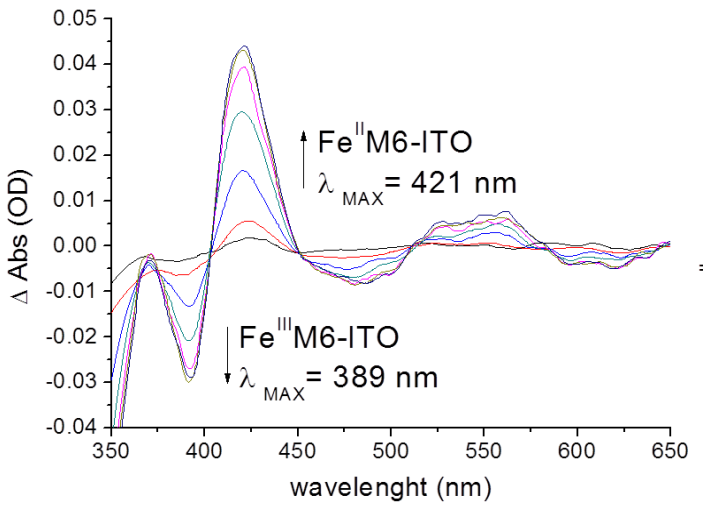

Figure 48 Reductive titration f Mimochrome VI adsorbed on ITO electrode: difference spectra recorded at -0.5 V (black), -0.45 V (red), -0.4 V (blue), -0.35 V (green), -0.3 V (pink), -0.25 (brown), -0.2 V(dark blue). Experiments were carried out in 10 mM MES buffer, 10 mM KPF6, pH 6.5 in Argon saturated atmosphere and at 25 °C.

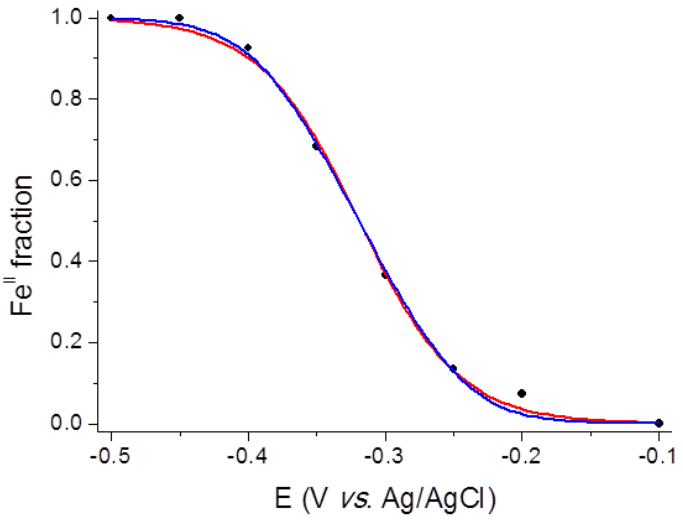

Figure 49 Fraction of reduced Mimochrome VI, determined from the 421 nm absorbance during reducing titration. Nernst fitting using n= 0.69 and E°'=-0.319 V; blue line: fit based on a square distribution of E°' and n=1.

4.7 Cyclic Voltammetry and Voltabsorptometry: study of the heterogeneous electron transfer

The Mimochrome VI-ITO electrode was studied in cyclic voltammetry by monitoring the absorbance changes at the 421 nm (λ_{MAX} of ferrous Soret band). Experiments were performed at various scan rates, ranging from 0.010 to 10 Vs^{-1}, and within the potential window corresponding to the reduction of Fe(III) into Fe(II). Satisfactory absorbance variation signal-to-noise ratios could be reached using integration times as low as 10 milli seconds.

Cyclic voltabsorptograms (CVAs) are diagrams in which the Fe(II) fraction, derived from the absorbance variation at 421 nm, is plotted versus the

potential (E),. Typical CVAs were obtained at different scan rate and they are reported in **figure 50**.

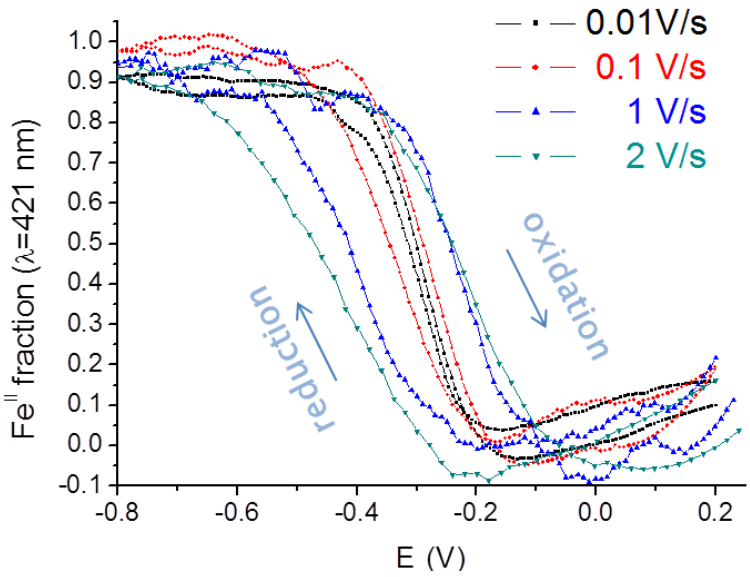

Figure 50 Cyclic voltabsorptograms obtained in the 0.01V/s-2 V/s scan rate range.

The derivative cyclic voltabsorptograms (DCVAs) obtained after time derivation of CVAs are equivalent to cyclic voltammograms (CVs), when both are expressed in flux density ϕ according to the following equation:

$$\phi = \frac{dA_\lambda}{\Delta\varepsilon_\lambda dt} = \frac{\upsilon dA_\lambda}{\Delta\varepsilon_\lambda dE} = \frac{i}{nFS} \qquad \textbf{Equation 3}$$

where :

- A_λ is the absorbance at the wavelength λ,
- $\Delta\varepsilon_\lambda$ is the difference in the extinction coefficients between the reduced and oxidized species, expressed in $mol^{-1}\,cm^2$;

- n is the theoretical number of electrons involved in the redox reaction: n = 1 for the Fe(III)/Fe(II) redox couple;
- F is the Faraday constant (96 500 C mol^{-1}),
- S is the geometric electrode surface area (0.24 cm^2).

The blank subtracted CVs and the DCVAs in the 0.01-2 V/s scan rate range are reported in **figure 51**.

Through the analysis of CVAs, it appears that at low scan rates (0.01V/s), the system is supposed to be in equilibrium, with a well-resolved Fe(III)/Fe(II) transition, centered at E°'= -0.319 V and a good overlapping between the curves describing the reduction and oxidation processes. However, at higher scan rates an increasing hysteresis between the reduction and the oxidation processes is progressively detected. This indicates that the system is no more in equilibrium and that the redox process is under the kinetic control of the interfacial electron transfer. Moreover, the irreversibility of the redox process detected at higher scan rates is also detectable in CVs and DCVA, where the progressive (i) drift of the anodic and cathodic potential peaks and (ii) decrease of the potential peaks current intensities, are observed.

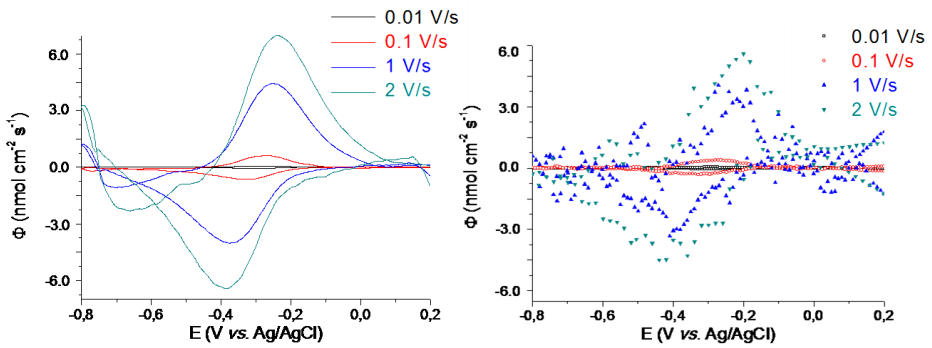

Figure 51 Cyclic voltammogram (left) and derived cyclic voltabsotogramm (right) in the 0.01V/s-2 V/s scan rate range. Intensities of the reversible DCVA waves were almost identical to those obtained with background-subtracted CVs from their large background capacitive current.

As expected for surface-confined electroactive centers, at low scan rates anodic and cathodic peak current flux densities show linear dependencies with the scan rate (**figure 52**). From linear regressions to the experimental data, the slope value of 5.8 V^{-1}, for the reduction process, significantly differs from the value of 9.9 V^{-1}, expected for an ideal one-electron Nernstian redox couple at 20 °C. As a result, the full width at half-maximum (**fwhm**) values of the cathodic and anodic peaks in the DCVA (150 mV) noticeably differ from the theoretical fwhm value of 89 mV for a reversible one-electron electron transfer at 20 °C.

This deviation from an ideal Nernstian behavior can be attributed to a random orientation of absorbed Miimochrome VI molecules on the ITO surface, leading to a distribution of microenvironments around the heme and thus to a distribution of standard potentials (Armstrong et al., 2000). This is in agreement with the apparent value, n_{app}= 0.69, that was obtained

by redox titration experiments, which also deviates from the theoretical value of n= 1 for a Fe(III)/Fe(II) redox couple.

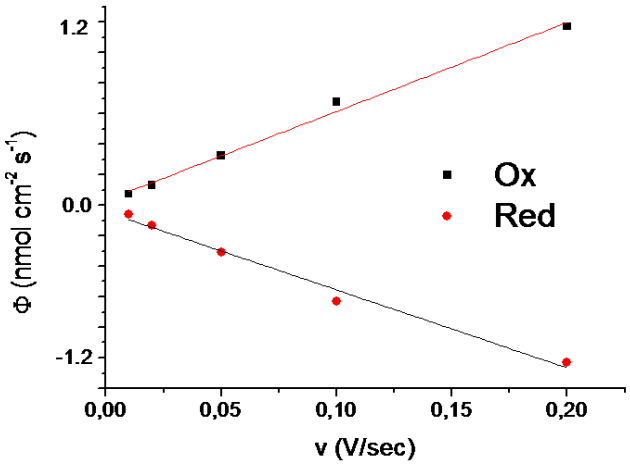

Figure 52 DCVA peak current flux densities of oxidation (black square) and reduction (red circles) as a function of scan rate, with corresponding linear fits with slopes of 5.8 and 5.1 V^{-1}

In order to study and evaluate the characteristics of the heterogeneous electron transfer rate, the dependence of the peak-to-peak potential separation (ΔEP) between the cathodic and anodic waves as a function of the scan rate was investigated (**figure 53**).

At low scan rates, ΔEP were close to nil but nonzero (40 mV). This unusual quasi-reversibility observed at low scan rates, under conditions where the electron transfer is not rate limiting, was previously noticed with immobilized proteins (Armstrong et al., 2000). Upon increasing the scan rate, the peak-to-peak potential separation is increased, reflecting the progressive kinetic control by the rate of electron transfer to the heme

centers. From the shift of the peak potentials as a function of the scan rate, the heterogeneous electron transfer rate constant **ks** was determined by fitting the resulting trumpet plots to the theoretical curves calculated from the classical Butler−Volmer equations, under thin-layer conditions (Léger and Bertrand, 2008). Using a charge-transfer coefficient of α= 0.5, the best fits gave ks=4s^{-1}. This ks value, is significantly lower than the one deduced for MP-11 (ks=10 s^{-1}), thus suggesting a relatively slower heterogeneous electron transfer in Mimochrome-ITO system.

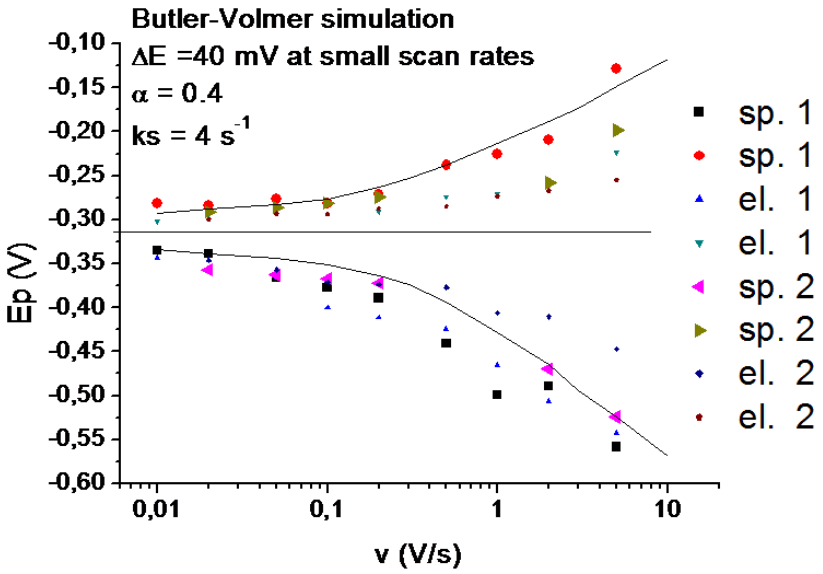

Figure 53 Trumpet plots obtained from the anodic and cathodic peak potentials in DCVAs (sp) and CVs (el) as a function of scan rate. Experimental pints are referred to two different ITO electrodes (1 and 2) functionalized with Mimochrome VI.

4.8 Mimochrome VI-ITO: catalytic reduction of O_2

In order to assess Mimochrome VI-ITO catalytic properties, the reduction of dioxygen molecule was explored (**figure 54**). In the presence of O_2, the shape of cyclic voltammograms is notably changed. In fact, the cathodic reversible wave that was detected in argon saturated solution, is converted into a strongly enhanced irreversible reduction peak, which is positively shifted. Such a behavior is typical of an irreversible process, associated to the reduction of dioxygen, which is consequent to Fe(II) formation in the ITO network. This interesting catalytic property of Mimochrome VI represents a good starting point for the study of the mechanism of this enzymatic reaction, which will allow to elucidate the number of electrons and the type of intermediates involved, as it was reported for MP-11, in the same analytical system (Renault et al., 2012).

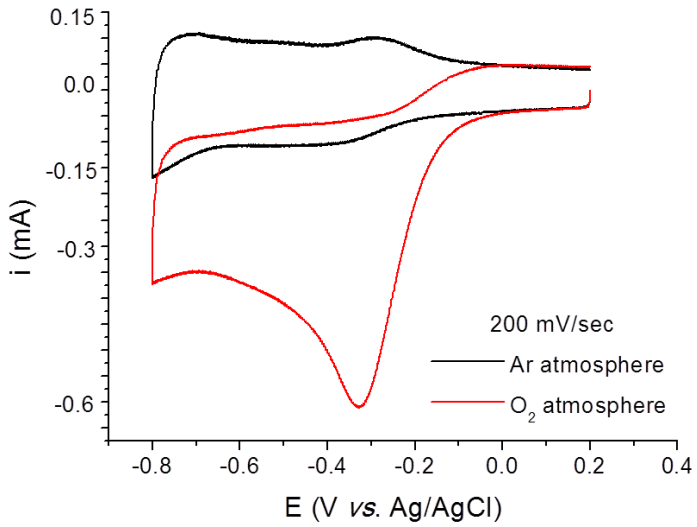

Figure 54 CVs recorded at 200 mV/s for Mimochrome VI-ITO electrode in saturated Ar (black) and O_2 solutions.

Discussion

In this part of the PhD research activity (developed in collaboration with LEM laboratories), the complete spectroelectrochemical characterization of Mimochrome VI, immobilized on ITO electrodes, was performed to elucidate its thermodynamic and kinetic properties.

Regarding the **spectroscopic data**, it was concluded that the spin and coordination states of Mimochrome VI were not affected by the immobilization on ITO electrodes. The unmodified spectroscopic properties are a fundamental point for allowing the spectroelectrochemical characterization of the system. In particular, the resonance raman spectra of Mimochrome VI, that were practically the same for the molecule in solution and immobilized on ITO, were very interesting for the position of the marker bands in the 1300-1700 cm^{-1} region. The detected υ_4 and υ_3 resonance bands are typically ascribed to high spin state (HS) porphyrin, both in heme-protein and in porphyrin models (Weiss et al., 2006). In particular, the frequencies of the spin-state marker υ_3 occur in heme proteins around 1480 cm^{-1} for six- coordinate HS, around 1490 cm^{-1} for five-coordinate HS, and in the range of 1500-1510 cm^{-1} for six-coordinate low spin state (LS) (Reczek et al., 1989).

The interpretation of the position of the υ_2 and υ_{10} skeletal bands is more difficult, since they fall within regions at higher resonance frequencies than those typically found for purely HS heme proteins. This could be reasonably attributed to the structural differences between deuteroporphyrin (which characterizes Mimochrome VI structure) and protoporphyrin (which is typically found in natural heme- proteins). In order to verify if this hybrid

RR spectra is achievable to the heme cofactor chemical differences, a comparison with other deutero-hemin-peptide system is required. Regard this, Fe(III) Mimochrome IV, which is a fully characterized six-coordinated LS model, will be analyzed by RR spectroscopy (Costanzo et al., 2004; Lombardi et al., 2003). Another possibility could be represented by a spin-state admixture (S=3/2, 5/2), according to Maltempo and coworkers quantum mechanical theory (Maltempo, 1976a, 1976b; Weiss et al., 2006). This model was elaborated in order to explain some spectroscopic and magnetic properties of heme proteins and heme models, which were not adequately described by high spin (S=1/2), low spin (S=5/2) or mid spin (S=3/2) states. According to the S=3/2,5/2 quantum mechanical spin state admixture, when the energy separation of the mid-spin and high-spin states approaches the magnitude of the spin orbit coupling parameter, the electronic ground state of the heme is best described as a quantum mechanical admixture of these two spin states. Based on resonance Raman, EPR, NMR, and electronic spectra, several class III peroxidases (Howes et al., 1999, 2001), cytochrome c' (Weiss et al., 2006) and some heme models complexes (Kadish et al., 2000) are well-described by this model.

However, this preliminary discussion about the spin state of Fe(III) Mimochrome VI represents an interesting starting point for a further spectroscopic characterization by resonance raman spectroscopy, in order to deepen the comprehension of its structural and functional features.

Concerning the **spectroelectrochemical characterization of the heterogeneous electron transfer**, it was found that the apparent standard potential of Mimochrome VI immobilized on ITO electrode was

substantially in agreement with that previously observed (Ranieri et al., 2010). This confirms that all the Mimochrome VI properties were not modified by the presence of the metal oxide matrix.

Some deviations from the ideal-system, described by the Nernst model were observed during spectroelectrochemical studies, such as the large fwhm and low n_{app} values. Moreover, a very low value for the heterogeneous electron transfer rate constant (ks) was observed. As previously documented in a comparing study about neuroglobin and cytochrome c immobilized on ITO electrodes, this would suggest a random adsorption of Mimochrome VI in the film network (Schaming et al., 2012). In fact, the heterogeneity of microenvironment around the accessible deuteroheme pocket would lead to a dispersion of the apparent E°', which could be affected by the presence and the number of -OH groups in the network. Moreover, the random orientation of Mimochrome VI could lead to a distribution of distances between the heme center and the conductive surface, thus justifying the observed ks value.

Finally, the ability of Mimochrome VI- ITO to reduce electrocatalitically dioxygen was explored. The preliminary results about the catalysis are encouraging, and will lead to a more detailed study of its mechanism in order to open the way of Mimochrome VI application in electrochemical biosensor development.

Results and discussion

CHAPTER V: *MIMOCHROME VI IN DEVELOPING NEW IMMUNOCHEMICAL ASSAYS*

5. Mimochrome VI as reporter enzyme for antibodies in the development of new ELISA

The research activity of this project was also focused on the biotechnological applications Fe(III) Mimochrome VI. On the basis of its peroxidase-like catalytic activity, this heme-protein model is here proposed as reporter enzyme for the functionalization of antibodies usable in immunochemical assays (e.g. ELISA).

As previously stressed, Mimochrome VI small dimensions (3.5 kDa) and its high catalytic efficiency make it a suitable reporter enzyme for antibodies conjugation. In fact, the reduced steric hindrance during the cross-linking reactions allow to considerably increase the conjugation ratio enzyme/antibody (**figure 55**). This is an important aspect to analyze, since antibodies with a high number of linked enzyme are more powerful probes for the detection of analytes (Chunglok et al., 2011; Iijima et al., 2010; Nara et al., 2008; Zhou et al., 2011). The consequent decrease of the limit of the detection of immunochemical techniques could make possible the easy and reliable detection of analytes and to reduce the costs of these immune-chemical assays. More sensitive assays would make possible to early detect pathologies, which are difficult to diagnose (e.g. celiac disease), to reduce the number of false-positive or false-negative results, and to conduct a reliable follow-up of patients (Vermeersch et al., 2012).

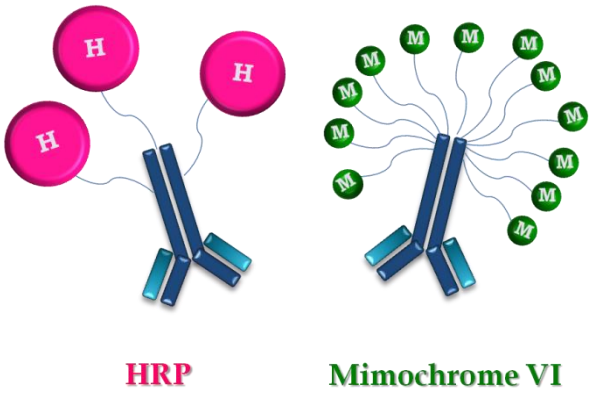

Figure 55 Schematic representation of the enzyme-antibody conjugates obtained by using HRP (≈44 KDa) and Mimochrome VI (3.5 KDa).

5.1 Antibodies: structure and function

Antibodies are immune system-related glicoproteins, which belong to immunoglobulin superfamily. These biomolecules are usually secreted by a type of white blood cell (B plasma cells), in order to specifically interact with foreign organisms (e.g. virus or bacteria) for protecting the host from their invasion.

An **antigen**, or immunogen, is a substance, which is able to elicit this immune response and it is usually recognized and strongly bound by immonoglubilins. Antibodies are typically able to recognize a sequence as small as 5-6 amino acids in length (Mikol et al., 2006). The discrete chemical and structural molecular portion of the antigen, which is involved in this recognition/binding mechanism, is called **epitope**. According to the antigen dimension, a variable number of epitopes can be exposed on its surface.

Each epitope is usually recognized by a single type of antibody. These immunoglobulins are called **monoclonal** and they are selected by immune system for their binding capability, directed against a discrete epitopic target. When a non-self molecule is recognized by immune system, the humoral response is elicited to the production of **polyclonal** antibodies, which hence can recognize and bind different parts of the antigen. Once this first step of immune response is realized, a set of complex effector processes takes place, in order to inactivate the non-self invasion. The complete picture of the immune system is much more complex than described, but its complete description is beyond the aims of this discussion. For more detailed information about immuno-biology, please refer to bibliography (Boehm, 2012; Borghesi and Milcarek, 2006; Janeway, 2005; Litman et al., 1993)

Antibodies can be classified into five subclasses (isotypes): IgG, IgM, IgA, IgE and IgD, which can be monomeric or oligomeric, and which have specific functions in the humoral immune response (**figure 56**) (Chen et al., 2009; Geisberger et al., 2006; Pier and Lyczak, 2004; Underdown and Schiff, 1986).

The IgD, IgE and IgG antibody classes are each made up of a single structural unit, which will be described afterward (**figure 57**). IgDs mainly act as antigen receptors on B cells and they are able to activate basophiles and mast cells to produce antimicrobial factors. IgEs usually bind to allergens and triggers histamine release from mast cells and basophiles, and are involved in allergy. IgGs are the most abundant immunoglobulins, which can be detected in serum, as they provide the majority of antibody-

based immunity, against invading pathogens. Moreover, they are the only antibody isotope capable of crossing the placenta to give passive immunity to the fetus.

IgA antibodies may contain either one or two units, and they are usually found in mucosal areas (e.g. gut, respiratory and urogenital tract) and biological fluids (e.d. saliva, tears, and breast milk) and they prevent pathogens colonization.

IgM antibodies are pentameric made up of five disulfide-linked structural units. These class of immunoglobulins, usually produced as monomers and secreted as pentamers, are involved in the first humoral response, before the other immunoglobulins are sufficient to proceed the immune reaction.

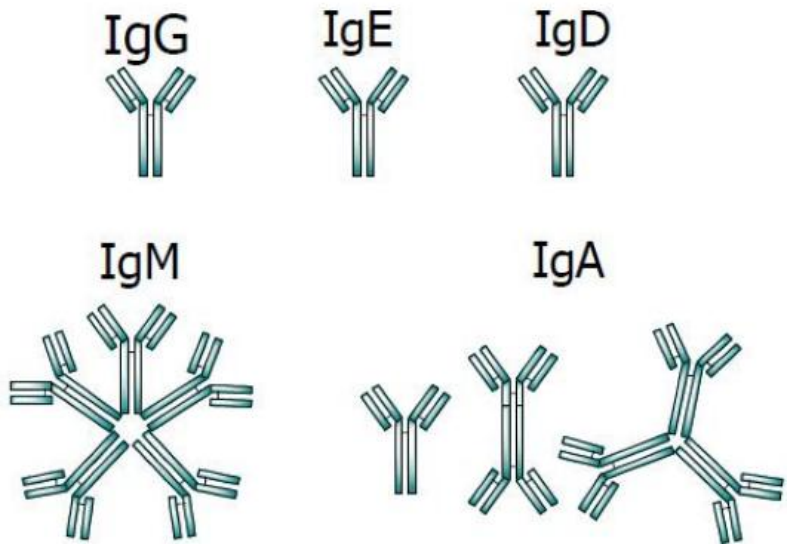

Figure 56 General structures of immunoglobulins isotypes.

The basic structure of these monomers and oligomers is well described by IgGs isotypes (**figure 57**). These immunoglobulins consists of four poly-peptide chains, composed by two identical heavy (H) chains and two identical light (L) chains. H and L chains are joined together by non covalent interaction, as well as disulfide bridges, to form a typically Y-shaped molecule. Depending on the class of immunoglobulin, the molecular weight of the heavy subunits ranges from about 50000 to around 75000 Da. The two light chains of an antibody have a molecular weight of about 25000 Da. For IgG molecules, the intact molecular weight, representing all four subunits, is in the range of 150000-16000 Da (Greg T. Hermanson, 2008).

The N-terminal domain, at the tip of the arms of the "Y", on both the light and the heavy chain, are known to be variable in their amino acid sequence. Thus, they are referred as variable regions (VL and VH). The subdomains of the H chain are made up of three C regions (CH_1, CH_2, CH_3) and one V region (VH). The L-chain, on the other hand, consists of one C region (CL) and one V region (VL). The base of the Y shaped antibodies is called Fc fragment (fragment that crystallizes) and is formed by the association of the two CH_2 and two CH_3 domains. Each arm of the Y shape is referred to as Fab fragment (fragment containing the binding site) and is formed by the association of CH_1 with CL and VH with VL (**figure 57**).

The binding site (**paratope**) of the antibodies is located within the VH and VL domains, each arm containing one binding site. In the variable regions, amino acid sequences can considerably vary from one antibody to another. Certain regions within the V regions have very high amino acid residue variability. These regions are called hypervariable regions, also known as

complementary determining regions (CDRs). Three CDRs are integrated into the L-chain and three into the H-chain resulting in six CDRs for each arm (Al-Lazikani et al., 1997; North et al., 2011; Putnam et al., 1979). The binding site has affinity for the antigen epitopes, resulting to both structural complementary, as well as combination of van der Waals, ionic, hydrophobic and hydrogen forces.

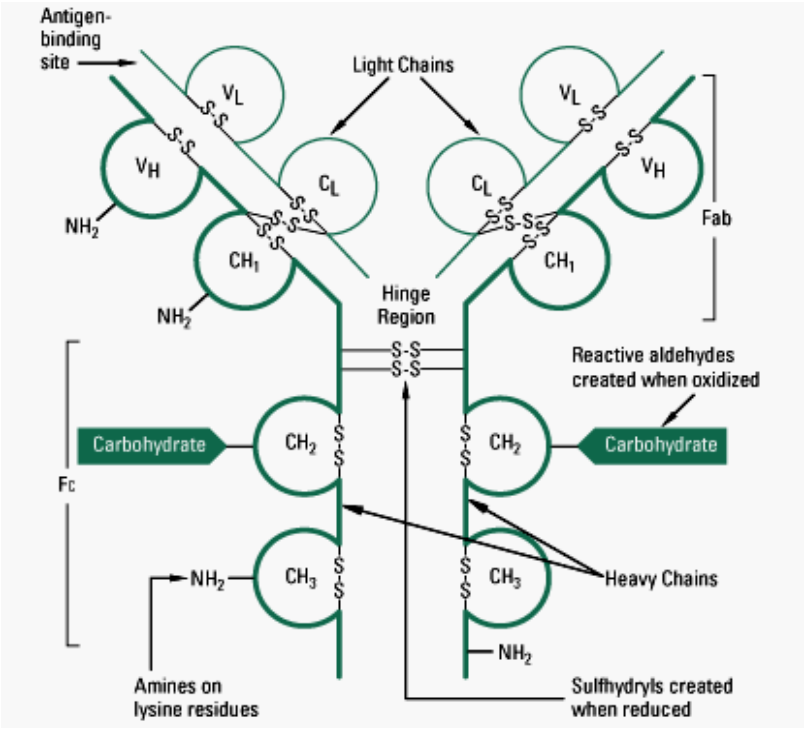

Figure 57 Detailed structure of an IgG antibody molecule.

5.2 Preparation of Antibody-Enzyme conjugates

The unique structural features of antibodies supply a number of choices for modification and conjugation reactions.

IgGs are the most commonly used in immunochemical assays and sensor applications, because of their easy production by immunization of laboratory animals. The chemistry used to effect conjugate formation should be selected in order to retain as much as possible the antigen binding activity (Greg T. Hermanson, 2008).

Antibodies possess a number of functional groups which are suitable for modification and conjugation purposes. Cross-linking reagents may be used to target lysine ε-amine or N-terminal ends, as well as aspartic and glutamic acid residues. In **figure 58 A** the example of a N-hydroxy succini-mide-activated enzyme, for the formation of an amide bond with antibody lysine residues, is showed (details about the chemistry of these reactions will be described after). Lys, Asp an Glu residues are usually targeted in conjugation procedures, since they are quite plentiful, in the antibodies primary structure, as well as uniformly distributed within their three-dimensional structure. This approach is usually adopted when a high conjugation ratio is desired for research purposes.

"Site-directed" methodologies can be applied for milder functionalization, in order to better preserve the native structure of the recognition portion of antibodies. Site-directed chemical modifications schemes makes use of cross-linking reagents that specifically react with some residues, that are

located in precise portion of immunoglobulin surface (Greg T. Hermanson, 2008).

One example of site-directed modification is the one focused on the disulfides in the hinge regions, which hold the heavy chain together and that can be selectively cleaved with reducing agents (e.g. dithionite, etc). In this way, it is possible to create two half antibody molecules, each containing free -SH groups and non-denatured recognition regions. This free sulphydryl groups can be used to cross-link enzymes which exposes groups reactive towards -SH (e.g. maleimide activated enzymes for the formation of tioether bond) (**figure 58 B**) (Sun et al., 2005).

A second method for the site-directed conjugation of antibodies takes advantage of the carbohydrate chains, which are typically attached to the CH_2 domain within the Fc region of the immunoglobulins. Mild oxidation of polysaccharides sugars with sodium periodate ($NaIO_4$) will generate aldheyde groups. Cross-reaction with ammine or hydrazine groups on the enzyme can be used for the coupling (**figure 58 C**). This method usually results in the highest retention of antibodies binding activity within the conjugates. However, it can be not applied for the functionalization of both recombinant antibodies and hybridoma-derived preparations of monoclonal antibodies, since these type of immunoblobulins are usually not glycosilated (Greg T. Hermanson, 2008).

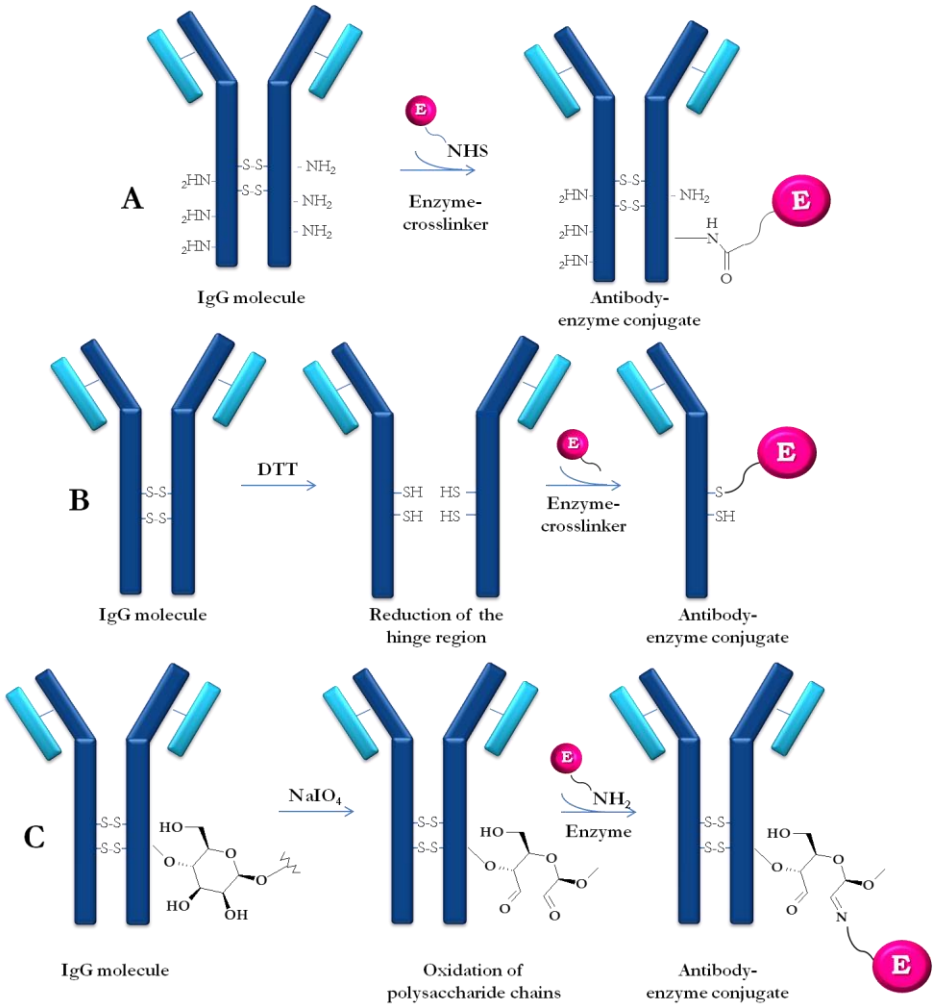

Figure 58 Examples of cross-linking reaction to couple enzymes to antibodies

5.3 Conjugation of Mimochrome VI to Antibodies: heterobifunctional cross-linkers

In order to select the functionalization strategy for coupling Mimochrome VI to IgG, the category of heterobifunctional cross-linkers has been studied. These cross-linkers contain two different reactive groups, which can react with, and hence couple, different targets on proteins and other macromolecules (**figure 59**). The advantage of the use of this type of cross-linking reagents is represented by a better control over the conjugation process, thus limiting polymerizations, often occurring when using homobifunctional linkers. Moreover, the use of heterobifunctional linkers provides the opportunity of multistep procedures, which allows to analyze the products of the reactions, that is an important aspect when protocols are developed.

Figure 59 Scheme of a general crosslinking agent: the two differently reacting groups are separated by an organic cross-bridge, whose molecular structure can be designed in order to introduce spacer arms, which can differ for length and chemical composition.

Reactive groups of this class of reagents are quite heterogeneous and they can be selected on the basis of the structural characteristics of the coupling molecules. The spacer-arm has an important role in conjugates properties,

since it can be selected on the basis of its length, but also for its chemical composition. In fact, it can influence the overall hydrophobicity of the cross-linkers or even their chemical stability. Finally, the spacer arm can contain cleavable groups within their structure, thus allowing the selective disruption of the conjugates and lending flexibility to the experimental design (Greg T. Hermanson, 2008)

5.3 a Conjugation strategy: Antibodies and SATA linker

Polyclonal human IgG were used to develop the cross-link procedures. The selected chemical target for antibodies functionalization was the ε-amine group of lysine residue. As previously stressed, this amino acid is quite represented in the primary structure of antibodies and it is rather exposed on the surface of these glycoprotein, being a good target for functionalization (**figure 60**).

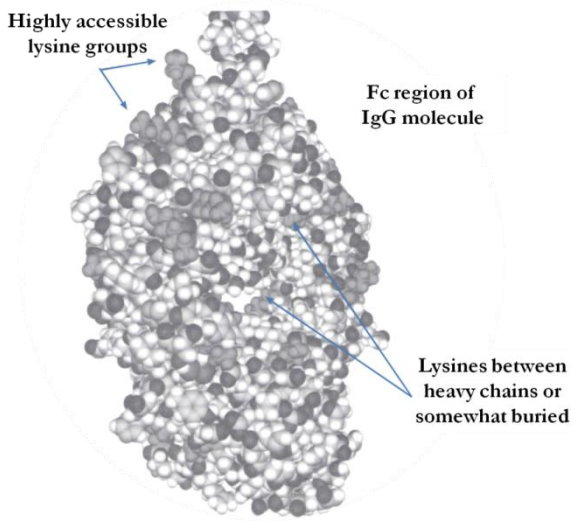

Figure 60 The solvent accessibility of lysine residues in the Fc region of an antibody is illustrated by high lightening Lys groups in solid gray (Greg T. Hermanson, 2008).

In order to introduce a large number of hexogen -SH groups on Lys side chain of IgGs, the *N*-succinimidyl S- acetylthio-acetate (SATA) was selected for the first step of the conjugation (**figure 61)** (Duncan et al., 1983).

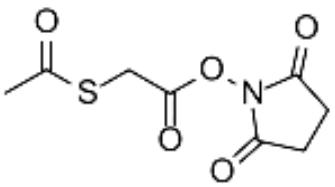

Figure 61 SATA linker molecular structure

The reactive N-hydroxysuccinimide (NHS) ester end of the SATA linker reacts with amino groups in antibodies to form stable amide linkage. The modified antibodies contain protected sulphydryl groups, which can be deprotected, by adding an excess of hydroxylamine (**figure 62**). SATA is often used to form antibody-enzyme conjugates, since the protecting groups of the linker can be removed without adding disulfide reducing agents (e.g. DTT), which could affect indigenous disulfide bridges and, hence, immunoglobulins native structure. In fact, conjugates obtained using SATA have the important advantage to maintain, within conjugates, the bivalent nature of antibodies, which retains both the antigen binding sites. SATA activated immunoglobulins are generally suitable for cross-linking with maleimide-activated proteins.

This first reaction step needs to be performed in slightly basic pH condition (pH 9), in order to maintain Lys amine groups in $-NH_2$ form. By the use of the colorimetric Kaiser test for the free amine groups measurements, it was possible to estimate that about 50 Lys can be functionalized by SATA linker in the used experimental conditions (details in materials and methods).

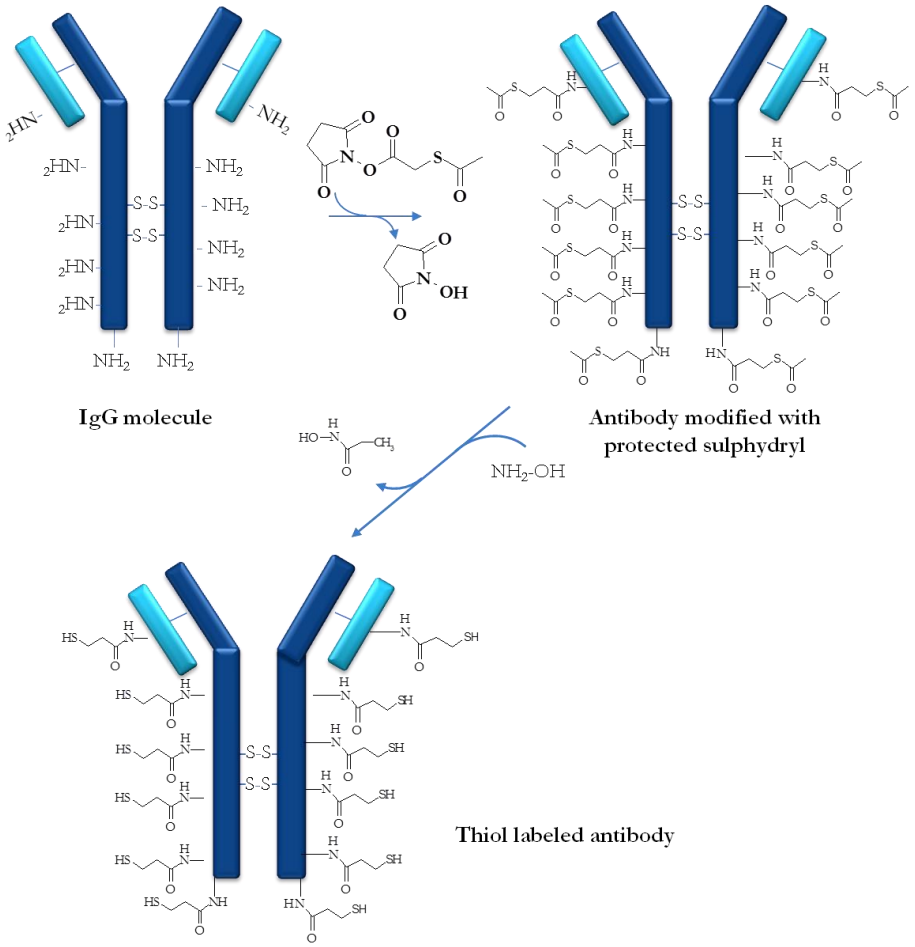

Figure 62 Activation reaction of antibodies with SATA linker.

5.3 b Conjugation strategy: Mimochrome VI and sulfo - SMCC linker

Mimochrome VI has in its primary structure a Lys residue which can be functionalized with a heterobifunctional linker. The sulfo SMCC, succinimidyl-4-(N-Maleimidomethyl)-cyclohexane-1-carboxylate, has been widely used in crosslinking proteins, in particular for the preparation of antibody-enzyme and hapten-carrier conjugates (Dewey et al., 1987; Greg T. Hermanson, 2008; Hashida and Ishikawa, 1985) (**figure 63**).

The NHS ester reacts with primary amine groups, to form stable amide bonds, while the maleimide end is specific for coupling with sulphydryls in the pH range of 6.5-7.5 (Smyth et al., 1964).

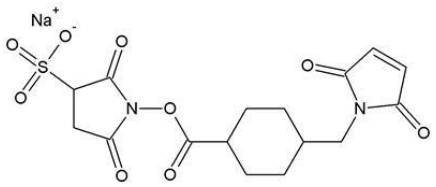

Figure 63 sSMCC linker molecular structure.

Lys^{11} residue on Mimochrome VI tetradecapeptide chain was modified activated with sulfo-SMCC (sSMCC) in the second step of the cross-linking procedure (**figure 64**). The identity of the product has been ascertained by LC-MS analysis (**figure 65**).

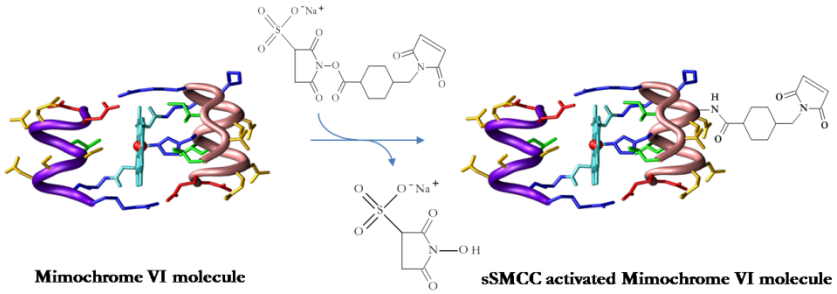

Figure 64 Activation reaction of Mimochrome VI with sSMCC linker.

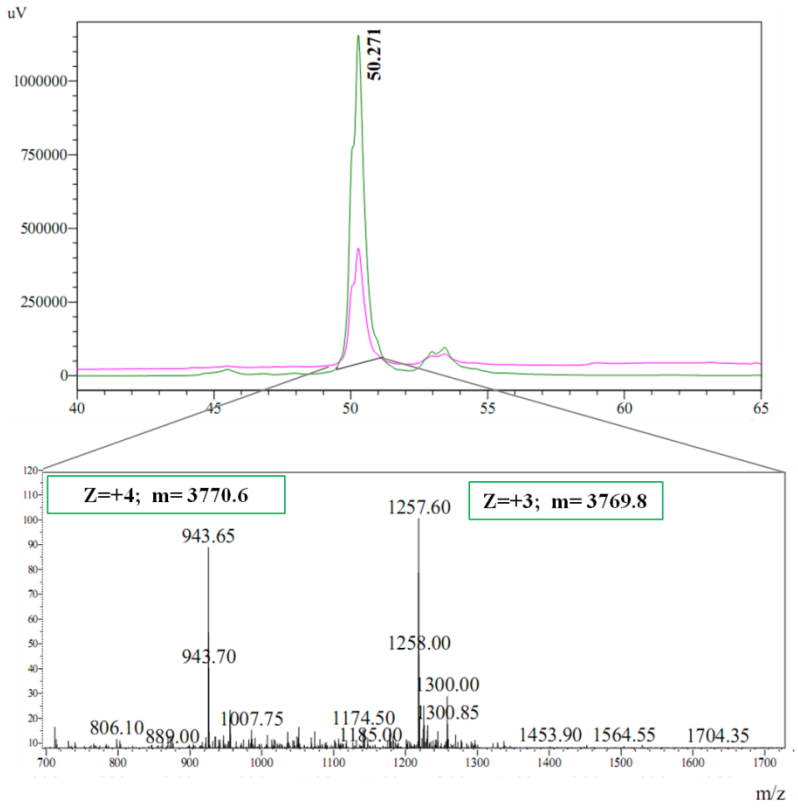

Figure 65 LCMS analysis of SMCC-activated Mimochrome VI. The LC analysis has been realized on a reverse phase HPLC column (Vydac C18- 4.6 mm · 150 mm; 5 µm) by using an elution gradient of acetonitrile from 5% to 40% over 50 min (in 0.1% v/v aqueous TFA). The measured mass of the product (3770.2±0.4 u.m.a.) corresponds to the theoretical one (3771.09 u.m.a).

5.3 c Conjugation strategy: Mimochrome VI-SMCC and IgG SATA cross-linking

The two molecules IgG-SH and SMCC-Mimochrome VI, separately activated, were used in the last step of the conjugation for the synthesis of the IgG-Mimochrome molecules. Conjugate compounds were obtained *via* thioether linkages between the afore-introduced cross-linkers (**figure 66**).

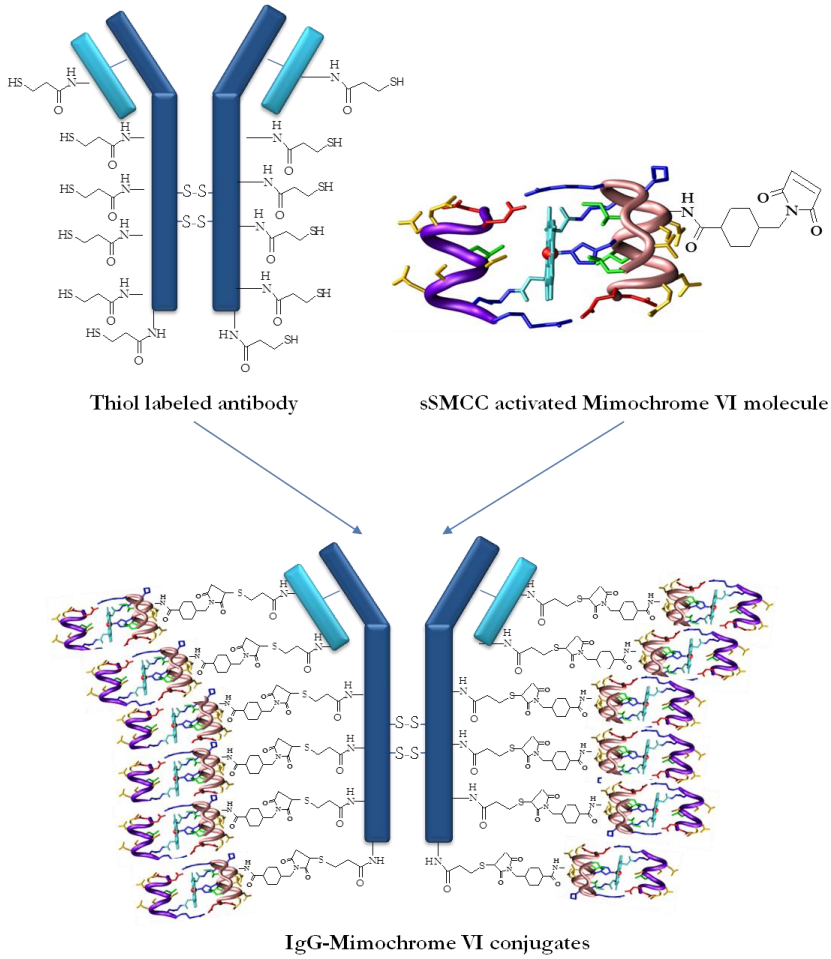

Figure 66 Mimochrome VI- IgG conjugates

In order to obtain a high conjugation ratio, this reaction step has been performed in the presence of a molar excess of sSMCC-Mimochrome (50 equivalents per IgG-SH equivalent). Thus, conjugates were purified through gel-filtration chromatography from the excess of the enzyme, and the analyzed by side exclusion HPLC chromatography, in order to check the absence of unreacted Mimochrome VI in the conjugate preparation (**figure 67**). The absorbance spectrum of the purified conjugates shows a peak at 280 nm (indicative of antibodies) and another one at 394 nm (referring to Mimochrome VI). The conjugation ratio, which has been estimated on the basis of the relative absorbance at these two wavelength, is around 13.

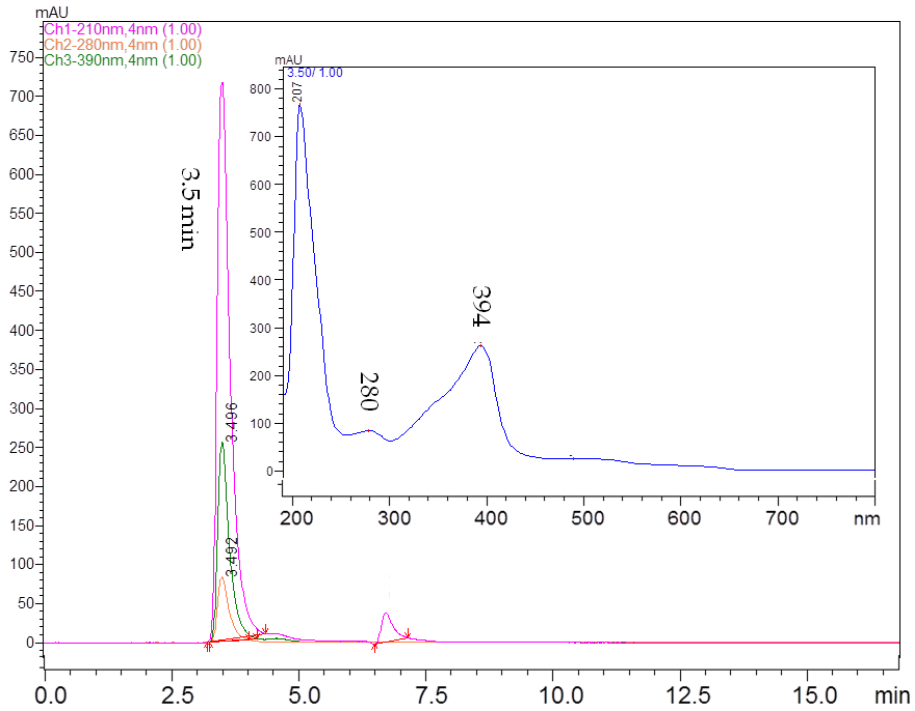

Figure 67 Chromatogram of the purified conjugates (100 mM phosphate buffer pH 6.5). Inset: relative absorbance spectrum

Discussion

On the basis of the presented results, we can conclude that Mimochrome VI is a good example of new synthetic reporter enzyme for the functionalization of antibodies. In fact, it has been successfully conjugated to polyclonal immunoglobulins with a high enzyme/IgG ratio (13 Mimochome VI/IgG). The value obtained by using our heme-protein mimetic in the conjugation to antibodies is a very good result, considering the low enzyme/IgG ratio of commercially available HRP-based preparations, which are obtained by similar procedures (≈3 HRP/IgG).

The purification through gel filtration chromatography allowed us to obtain an homogeneous preparation of IgG-Mimochrome VI conjugates. The absence of free and not covalently-bound Mimochrome VI was an important point, in order to avoid an over estimation of the conjugate catalytic activity in the following steps of the research project.

Mimochrome VI-IgG conjugates retain the ability of oxidizing the ABTS, by using H_2O_2 as co-substrate. Currently, experiments on the immuno-reactivity of these conjugates are in progress, in order to develop a definitive ELISA kit.

Conclusion

The research activity of this thesis project is focused on the rational design, synthesis, and characterization of five Mimochrome VI analogs. These molecules belong to a class of heme-proteins developed by the *Artificial Metallo Enzyme Group* of Naples. The parent compound, Fe(III)-Mimochrome VI, is a penta-coordinated model that catalyzes the oxidation of several substrates by the activation of H_2O_2.

In order to understand the role of the peptide chain and, and in particular of some amino acid residues, in the modulation of the catalytic properties of Mimochrome VI, the following substitutions were introduced:

- ✓ Glu^2L in the tetradecapeptide and decapeptide chain;
- ✓ $Arg^{10}L$ in the tetradecapeptide and decapeptide chain;
- ✓ Ser^6G in the decapeptide chain.

These point substitutions were aimed to:

- ✓ break the inter-chain ion pair between the charged residues, thus allowing to understand the role of these interactions and, as a consequence, of the involved amino acids in the properties of the molecule;
- ✓ verify if the serine residue at the distal site of the heme is involved in the binding of substrates in the heme pocket.

The five analogs were screened for the catalytic activity and the most promising, Fe(III)Mimochrome VI E^2L TD, was selected for its increasing

in catalytic efficiency. Indeed, this new analogue approaches the HRP catalytic performance (see paragraph **3.2 Mimochrome VI and its analogs:functional characterization**). Fe(III)Mimochrome VI E^2L TD displayed a k_{cat} value only 8-fold lower than HRP, in the experimental conditions for maximal activity for each enzyme. Moreover, the kinetic data showed that Fe(III)Mimochrome VI E^2L TD exhibits a catalytic efficiency higher than the reference molecule, Fe(III)Mimochrome VI, and is able to perform about 6000 turnovers, without bleaching.

The characterization of this class of minienzymes demonstrates that their miniaturized structure holds essential elements for finely tuning the iron-porphyrin peroxidase activity. This represents a very important checkpoint for the rational design of new and improved bio-mimetic catalysts.

This class of bio-inspired molecules has important potentialities in biotechnologies, since their properties can be exploited for the construction of highly sensitive diagnostic tools (i.e. biosensors and immochemical assays).

In this context, the spectroelectrochemical characterization of Fe(III)Mimochrome VI immobilized transparent GLAD ITO (indium tin oxide) film was performed in collaboration with the *Laboratoire d'Electrochimie Moléculaire* of Paris. This electrochemical system was characterized by cyclic voltammetry coupled to time resolved UV-visible absorbance spectroscopy. By cross-correlation between UV-visible absorption, spectroelectrochemical data, as well as resonance Raman spectra, it was possible to:

- ✓ conclude that no structural modification of the heme occurred upon adsorption on the metal oxide surface;
- ✓ determine the surface concentration;
- ✓ perform a quantitative analysis of the thermodynamics and kinetics of the direct interfacial electron transfer between the heme and the conductive ITO surface, by monitoring cyclic voltabsorptograms and voltammograms;
- ✓ interpret the heterogeneous electron transfer properties, as a consequence in the orientation of the redox centre in the network.

Fe(III) Mimochrome VI displayed a good electrocatalytic activity in the reduction of dioxygen, which, together with the high surface coverage of the electrode and the good electrochemical properties of the system, could allow to construct a high density electrochemical biosensor.

Finally, Fe (III)-L-Mimochrome VI is here proposed as reporter enzyme for the functionalization of antibodies usable in immunochemical techniques. Considering its low molecular weight(3.5 kDa), it is possible to reduce the steric hindrance during the cross-linking reactions, thus increasing the conjugation ratio enzyme/antibody. By using cross-linkers, it was possible to obtain, to date, polyclonal IgG functionalized with about 13 molecules of this minienzymes. This conjugation enzyme/Ab ratio is significantly higher respect to the commercial immunoglobulins, which are usually linked to 3 or 4 HRP molecules. These conjugates retain the catalytic activity, and immunoreactivity assays are in progress in order to develop a Mimochrome VI-based immunochemical assay, whose technology will be transferred to companies in the field of diagnostic.

In this respect, this project received last October one of the Start Cup Campania prizes, for the foundation of new Start Up Companies.

In conclusion, the work performed during this PhD, is placed at the interface of basic and applied research, and it is based on the application of several techniques and methodologies in the field of chemistry, biochemistry and biology. During the research activity, the important goal of the selection of new synthetic, peptide-based catalysts, with improved properties was reached. Furthermore, on the basis of the results obtained for the functionalization of antibodies and those obtained from the spectroelectrochemical characterization of ITO electrodes, the important potential applications of this class of molecules were confirmed.

Materials and methods

6. Solid phase peptide synthesis: an overview

Since R. B. Merrifield (Nobel prize in 1984) reported on the solid phase chemical synthesis of peptides and small proteins, solid-phase peptide synthesis (SPPS) has become a widely utilized technique for the production of peptides and small proteins (Merrifield, R. B., 1963). The basic idea of the solid-phase approach involves the covalent attachment (anchoring) of the growing peptide chain to an insoluble polymeric support (resin); in this way unreacted soluble reagents can be removed simply by filtration and washing, without losses of the growing peptide chain. Subsequently, the insoluble peptide-resin is elongated by addition of α-amino- and side-chain-protected amino acid residues in a series of addition reactions, which must be performed with high yields. Excess soluble reagents are used to drive sequential coupling and deprotection reactions to completion. The repetitive nature of the coupling and deprotection steps allowed the automation of the main steps of the SPPS methodology.

The acid-labile Boc group or base-labile Fmoc-group are used for the N-α-protection of amino acids. The general scheme of SPPS using Fmoc chemistry is illustrated in **figure 68**. Fmoc- protected amino acids are most popular in SPPS since a mild basic treatment, using piperidine, can be used for the Fmoc-group removal at every stage. The final cleavage and deprotection of the peptidyl resin is accomplished using TFA. An N-α-derivatized amino acid is attached to an insoluble (solid) support, via a flexible linker. The N-α-blocking group is then removed (deprotected) and the amino acid-linker-support is thoroughly washed with solvent. The next

amino acid (which is also N-α-protected) is then coupled to the amino acid-linker-support directly in the presence of coupling reagents. The coupling may also be carried out using peptides instead of single amino acids: this method is referred to as fragment condensation (Simmerman et al., 1982). After the completeness of the coupling reactions, the N-α-dipeptide (or oligopeptide)-linker-support is washed with the solvent.

The deprotection/coupling cycle is repeated until the desired sequence is completed. The peptide-linker-support is cleaved to obtain the peptide as a free acid or amide, depending on the chemical nature of the linker. The cleavage reagent also removes the amino acid side chain protecting groups, which are stable to the deprotection reagent. These steps may be carried out either in batch process, where the support is filtered between each step, or in a continuous flow process, where the support is always solvated during reagent exchange, and the release of the protecting groups is spectrophotometrically monitored.

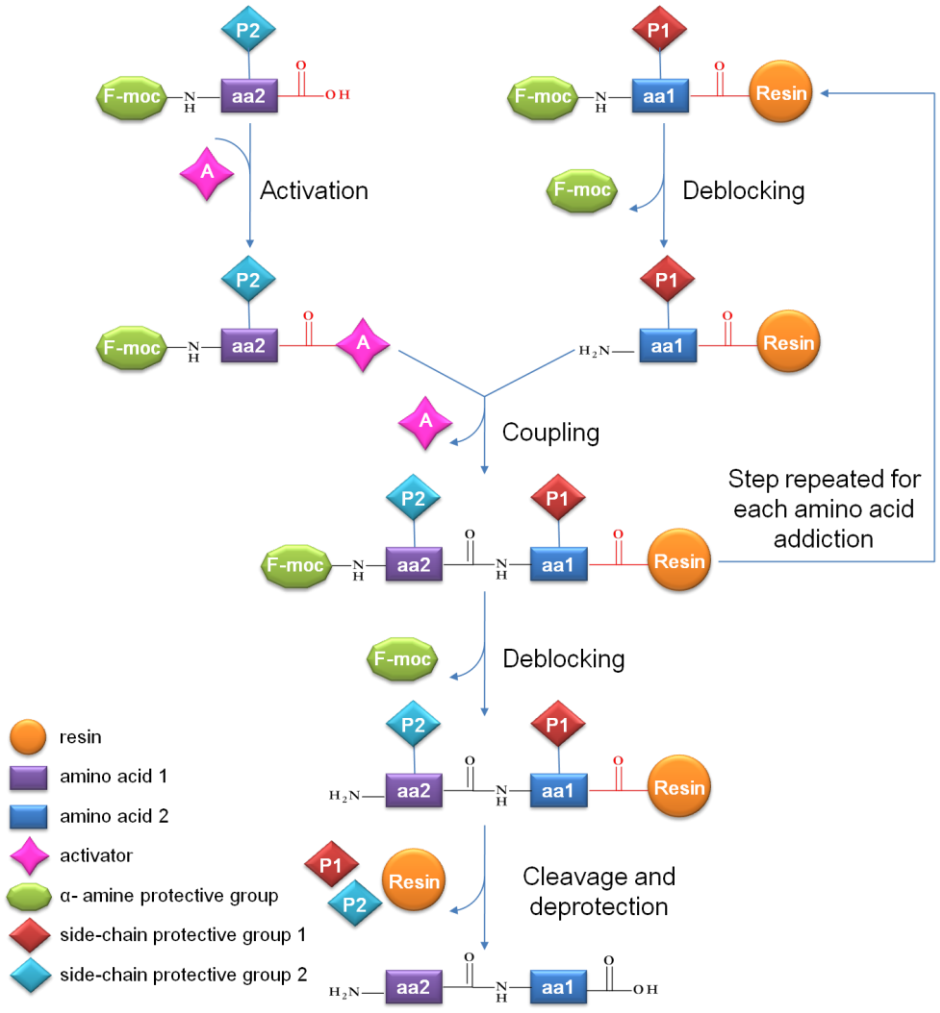

Figure 68 General approach to solid phase peptide synthesis using Fmoc chemistry. Peptides are synthesized from the C-terminus to the N-terminus by stepwise addition of N-α-amino- and side chain-protected amino acid residues to an insoluble polymeric support (resins). Final cleavage of the peptidyl resin and side chain deprotection is achieved using TFA.

6.1 Solid phase synthesis of peptides

All fully protected peptides were synthesized by using a peptide automatic synthesizer (see instrumentations), with Fmoc strategy, on a 0.2 mmol scale. The resin used was the super acid labile Nova Syn TG Sieber, with a substitution level 0.2 mmol/g (**figure 69**).

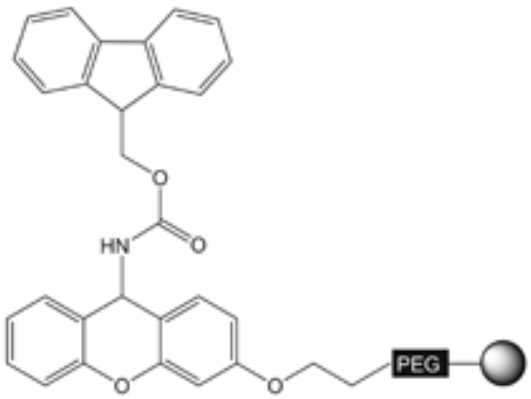

Figure 69 Nova Syn TG Sieber resin for SPPS

For the synthesis of the peptides the following amino acids were used:

- Fmoc-Asp(OtBu)-OH; Fmoc-Glu(OtBu)-OH; Fmoc-Gln(Trt)-OH; Fmoc-Leu-OH; Fmoc-Ser(tBu)-OH; Fmoc-Lys(Mmt)-OH; Fmoc-Arg (Pbf)-OH (**Mimochrome VI decapeptide and its analogs**)
- Fmoc-Asp(OtBu)-OH; Fmoc-Gln(Trt)-OH; Fmoc-Leu-OH; Fmoc-His(Trt)-OH; Fmoc-Ser(tBu)-OH; Fmoc-Lys(Mmt)-OH; Fmoc-Arg(Pbf)-OH; Fmoc-Lys(Boc)-OH; Fmoc-Ile-OH; Thr(tBu)-OH (**Mimochrome VI tetradecapeptide and its analogs**)

The synthetic procedure that was adopted can be schematized as follows:

1. **Deprotection step**: the α- Fmoc group, was removed at the beginning of every cycle with a 20% piperidine solution. After deprotection, the resin is washed several times with NMP.
2. **Coupling**: the activated Fmoc-amino acid (0.5 M HOBt in DMF solution) reacts with the amino-terminal group of the growing peptide chain, to form a peptide bond.
3. **Capping**: this reaction is performed after each coupling step, using Ac_2O/HOBt/DIEA solution in NMP. The aim of this step of the synthetic cycle is to block the amino groups of the growing peptides, which are not efficiently coupled with the last residues, in order to reduce the risks formation of truncated peptides and to drastically reduce the yield of the synthesis.

Deprotection, coupling and capping steps are repeated with each subsequent amino acid, until the chain assembly is completed. Peptides N-terminal amino groups are finally acetylated with Ac_2O/HOBt/DIEA solution in NMP. At the end of the synthesis, the resin is washed several times with NMP and the it is dried. By measuring the resin weight, it is possible to estimate the yield of the synthesis on the basis of the scale used. In all peptides here reported, the yield of the synthesis based on the weight increment was ≥ 85%.

6.2 Mmt deprotection and cleavage of Mimochrome VI peptides

Selective Mmt group cleavage from Lys^9 side chains was needed in order to obtain peptides fully protected, except free Lys residues, for the following coupling reactions with deuteroporphyrin.

After the final assembly on the resin, the N-ε Mmt protecting group of the Lys residue was removed, by repeated treatments with a solution containing 10% acetic acid and 20% trifluoroethanol (TFE) (v/v) in CH_2Cl_2. Each deprotection step was performed by incubating the reaction mixture for 15 min, under gentle agitation; then, the solution was filtered with a vacuum pump. This procedure was repeated until no yellow or red color, indicative of N-methyltrityl cations, were detected in the eluent.

Subsequently, in order to release the fully protected peptide from the resin, 3-4 resin volumes of a freshly prepared cleavage mixture (1% TFA in DCM, v/v) were added. The acidic mixture was incubated for 2 minutes, under mixing. The solution was filtered with a vacuum pump, into an ice-cold flask containing 2 ml of 10% pyridine/methanol (v/v). Finally, the resin was washed with DCM and methanol.

This reaction was followed by Thin Layer Chromatography-TLC, by using as eluent the mix chloroform/methanol/acetic acid (80:18:2); each step was repeated until no product was detected in the collected fractions. The fractions containing the product were pooled and then evaporated under reduced pressure up to 5% of the volume.

Ice-cold water was added and the mixture was cooled on ice to aid precipitation of the protected peptide. The product was washed several times, with fresh cold water and centrifuged at each step (4 min at 4°C, at 3300 g). Therefore, it was dried under vacuum to give the crude C-terminal peptide amide.

The side chain protecting groups were found to be stable in both deprotection and cleavage reactions.

Peptide identity was checked via LC-MS analysis. The mobile phase was made up of H_2O/0.1% trifluoroacetic acid (TFA) (solvent A) and CH_3CN/0.1% TFA (solvent B) linear gradient, from 50% to 90% (solvent B) over 40 min, at a 0.5 $mL \cdot min^{-1}$ flowrate.

A Vydac C8 column (4.6 mm ·150 mm; 5 μm), reverse phase, was used in the LC-MS analysis. Decapeptides and tetradecapeptides chromatograms and the corresponding mass spectra are reported in **figure 70**, **figura** 71, while relative analytical parameters are summarized in **table 9**. This first step of the work-up are allowed to obtain peptides with a satisfactory purity with ≈ 80% yield.

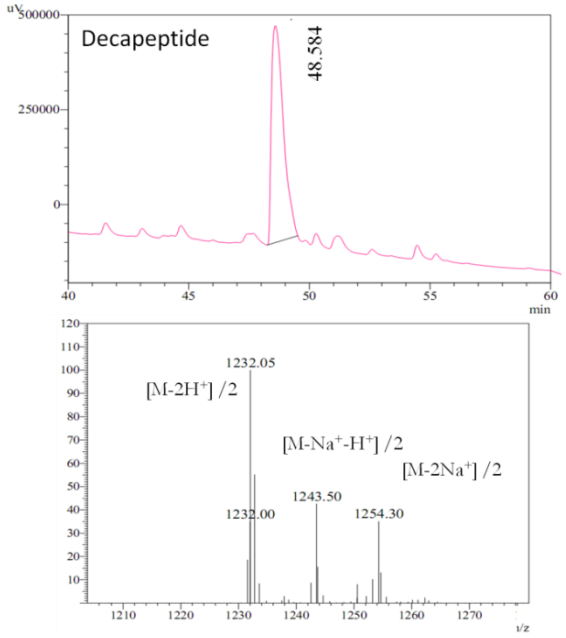
Decapeptide
48.584
uV
500000
250000
0
40
45
50
55
60
min
1232.05
[M-2H+] /2
[M-Na+-H+] /2
[M-2Na+] /2
1243.50
1232.00
1254.30
120
110
100
90
80
70
60
50
40
30
20
10
1210
1220
1230
1240
1250
1260
1270
m/z

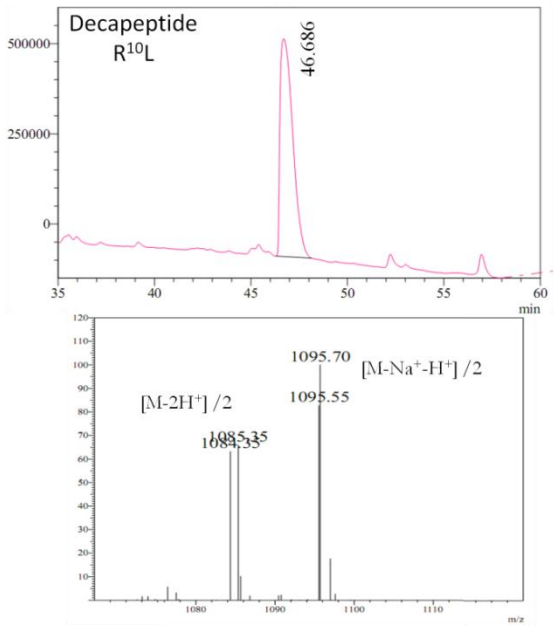
Decapeptide
R10L
46.686
500000
250000
0
35
40
45
50
55
60
min
1095.70
[M-Na+-H+] /2
[M-2H+] /2
1095.55
1085.35
1084.35
120
110
100
90
80
70
60
50
40
30
20
10
1080
1090
1100
1110
m/z

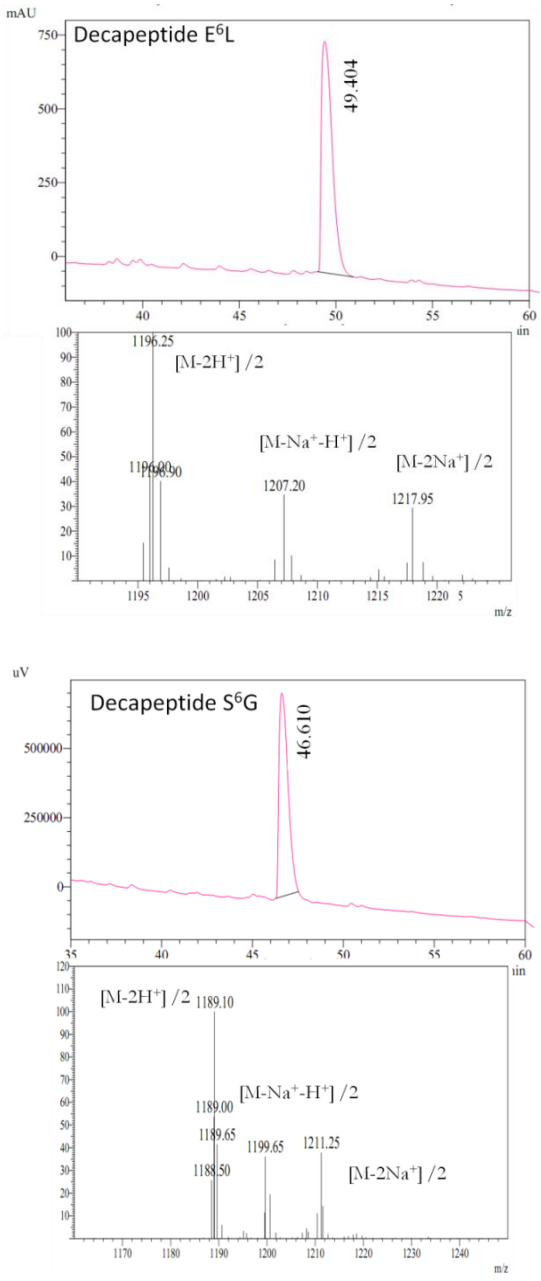

Figure 70 LCMS analysis of decapeptides deprotected of Mmt group. One single chromatographic peak (λ=210 nm) was detected and mass spectra were in agree with theoretical masses.

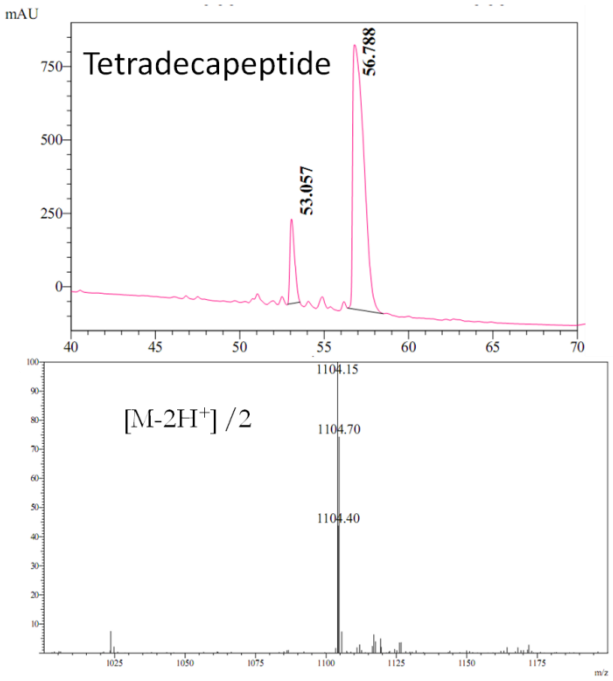
mAU
Tetradecapeptide
56.788
53.057
[M-2H+] /2
1104.15
1104.70
1104.40
m/z

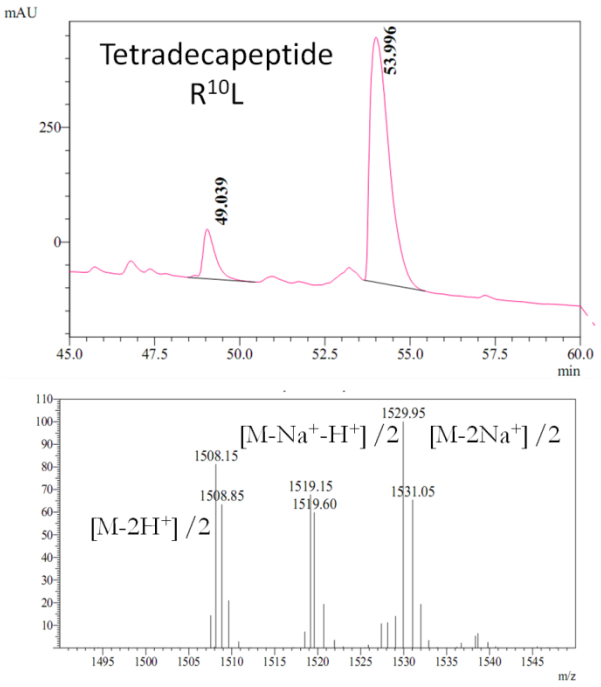
mAU
Tetradecapeptide
R10L
53.996
49.039
min
[M-Na+-H+] /2
[M-2Na+] /2
[M-2H+] /2
1529.95
1508.15
1508.85
1519.15
1519.60
1531.05
m/z

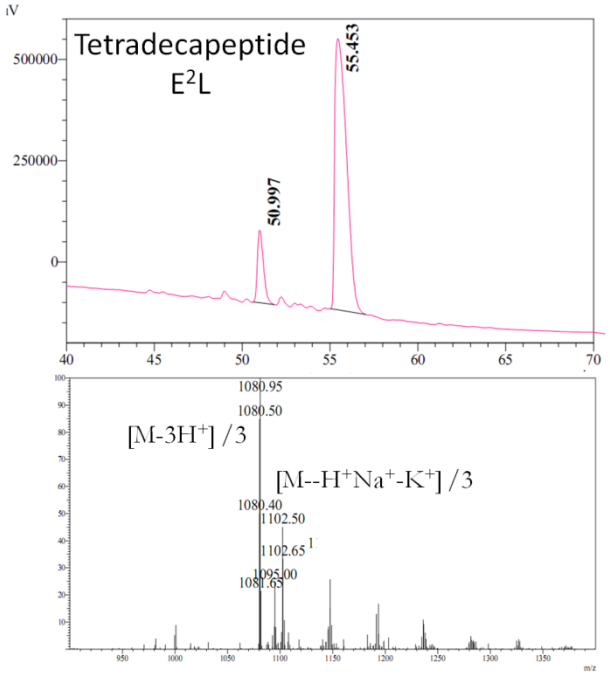

Figura 71 LCMS analysis of tetradecapeptides deprotected of Mmt group. One main chromatographic peak (λ=210 nm) was detected, whose mass spectra are in agree with theoretical masses. Mass spectrometry analysis allowed to identify the minor peak, with less retention time, as tetradecapeptides who lost a Trt protecting group. This was due to acidic elution conditions, thus confirming the good result of the synthesis.

Table 9 Analytical parameters of synthesized peptides

Peptide	t_R (min)	Theoretical mass (Da)	Measured mass (Da)
TD	56.79	3310.25±0.8	3310.22
D	48.58	2461.68±1.06	2462.11
TD R¹⁰L	53.99	3013.93±2.01	3014.85
TD E²L	55.45	3239.74±1.54	3238.15
D R¹⁰L	46.69	2167.78±1.37	2166.74
D E²L	49.40	2389.91±1.99	2390.04
TD S¹⁰G	46.61	2375.67±1.15	2375.96

6.3 Coupling strategies of peptides to deuteroporphyrin

After Mmt deprotection, peptides were coupled with the deuteronporphyrin IX (DP IX), by following the scheme in **figure 72**. Mimochrome VI Decapeptide chain (D) was coupled to deuteroporphyrin to obtain the protected D-DPIX monoadduct, which was divided in three parts. One was coupled to Mimochrome VI tetradecapeptide (TD) to obtain the parent molecule. The remaining two parts were coupled to TD (E^2L) and TD ($R^{10}L$), respectively, to obtain the corresponding analogs.

The same approach was used to construct decapeptide analogs, with the E^2L, $R^{10}L$ and S^6G substitutions, respectively. In this case the starting point was the TD-DPIX monoadduct.

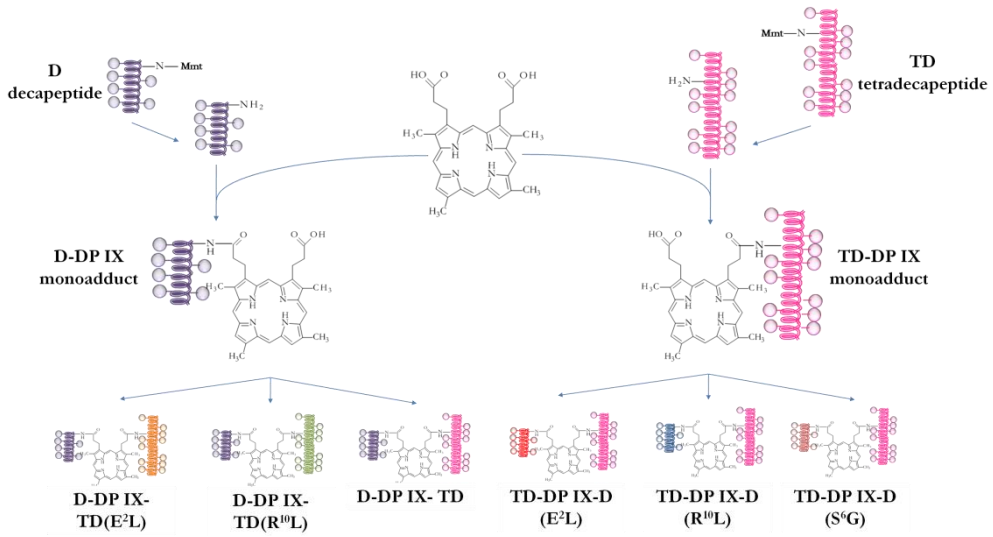

Figure 72 Synthetic strategy for Mimochrome VI and its analogs

The first peptide-deuteroporphyrin conjugation was realized on 0,16 mmol of decapeptide, or tetradecapeptide, chains (1 equivalent). This reaction was conducted in presence of DIEA (7 equivalents), HATU (1 equivalent), deuteroporphyrin IX*2HCl (1.5 equivalents). In order to avoid the formation of heterodimers, this reaction was conducted in diluted solution ($7.2 \cdot 10^{-5}$ M in DMF) and by adding drop wise the peptide to the deuteroporphyrin (30 adds every 2 minutes). The reaction mixture was stirred for 2 h at room temperature, and the pH was verified every 20 min, and adjusted with DIEA (pH ≈ 8.0), when necessary. The reaction was monitored by analytical HPLC (Vydac C8 column, using a gradient of acetonitrile in 0.1% aqueous TFA, 50% to 90% over 20 min, at a flow rate of 1.0 $mL \cdot min^{-1}$), and by TLC (eluent: chloroform/methanol 90:10, Rf = 0.52). The analytical chromatograms were recorded at λ=210 nm (amide bond) and λ=400 nm (porphyrin) and they are reported in **figures Figure** 73,Figure 74. The main peak that was detected was identified in the desired product (TD-DP IX and D-D IX monoadducts, respectively). The second peak corresponded to the diadduct product. The yield of this step reaction, evaluated on the basis of the chromatographic peaks areas, is 90% for TD-DP IX reaction and 80 % for the D-DPIX reaction.

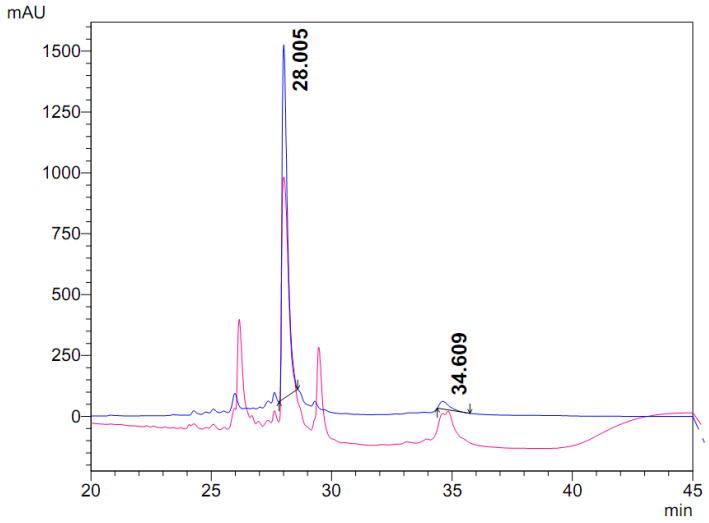

Figure 73 Analytical HPLC TD-DP IX monoadduct. The peak eluted At 28 minutes correspond to the desired products, while the one eluted at 34.6 minutes is identified as TD-DP IX-TD diadduct

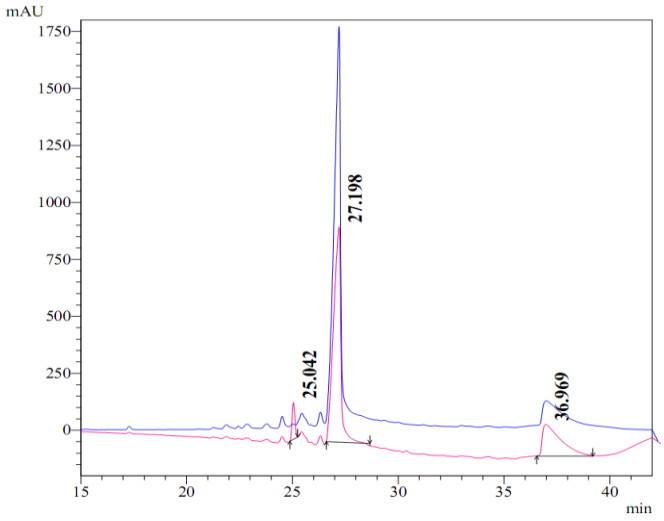

Figure 74 Analytical HPLC D-DP IX monoadduct. The peak eluted At 27.2 minutes correspond to the desired products, while the one eluted at 36.7 minutes is identified as D-DP IX-D diadduct

Once completed, the he reaction mixture was evaporated under reduced pressure and dried. The crude product was purified by Flash Chromatography, on a silica gel (230-430 mesh) column to eliminate the unreacted deuteroporphyrin (eluent: chloroform/methanol 90:10) .

Therefore, the purified mono-peptide adducts were used for the second peptide coupling. Each coupling reaction was conducted on 1/3 mono-adduct (0.045 mmol), in the presence of DIEA (6 eq) and HATU (1.2 eq). The second peptide (TDs for D-DP IX and Ds for TD-DPIX mono-adducts) was added at 10 % molar excess respect to monoadduct amount. The reaction mixture ($8.5 \cdot 10^{-3}$ M in DMF) was incubated at room temperature for a total of 2 h. The pH was checked during the reaction time an adjusted to 8, when necessary. The reaction progress was followed by TLC (eluent: chloroform/methanol 90:10, R_f = 0.65). At the end, the reaction mixture was evaporated under reduced pressure and dried.

6.4 Deprotection reactions and free base purification

Side chain deprotection was achieved by addition of the cleavage mixture (94% TFA, 2.5% EDT, 1% TIS, 2.5% H_2O v/v/v/v). The reaction was conducted under stirring, at 0 °C for 1h and at room temperature for the second hour. The final mixture was concentrated on a rotary evaporator to a volume of approximately 1-2 mL. Extraction of the scavengers and precipitation of the crude product was achieved by addition of cold diethyl ether. The mixture was centrifuged (room temperature at 3 300 g), the supernatant was removed and the precipitate was washed twice with three volumes of cold diethyl ether. The mixture was dried to remove diethyl ether, redissolved in water 0.1 % TFA and analyzed by LC-MS (Vydac C-18 column, using a gradient of acetonitrile in 0.1% aqueous TFA, 5 % to 80% over 35 min, at at 1 mL min^{-1} flow rate). The crude material was then purified by preparative RP-HPLC (Vydac 2.2 cm C18 column at 22 mL min^{-1}, using a gradient of acetonitrile in 0.1% aqueous TFA, 10% to 80% over 58.4 min); the pooled fractions containing the desired product were lyophilized, Analytical RP-HPLC and ESI-MS confirmed the expected molecular weight (data not shown).

6.5 Iron insertion and analysis of final products

Iron ion was inserted into Mimochrome VI, and its analogs, free bases according to literature procedures (Buchler, J.W.,, 1979). Iron (II) acetate (10 molar excess) was added to a solution of pure free base in 2/3 TFE/AcOH (v/v) (molar concentration=$2.0 \cdot 10^{-4}$ M), and the reaction mixture was kept at 50 °C for 2 h, refluxing under nitrogen. The reaction was monitored by analytical HPLC. The solvent was then removed under vacuum, and the product was purified to homogeneity by preparative RP-HPLC (Vydac 2.2 cm C-18 column at 22 mL min^{-1}, using a gradient of acetonitrile in 0.1% aqueous TFA, 10% to 80% over 58.5 min). Pure products were obtained as the TFA salt (yield 48 %). Reverse phase analytical HPLC coupled with ESI-MS confirmed the expected molecular weight (**figures Figure 75Figure 76**). The analytical parameters of the obtained products (purity >90%) are summarized in **table 10**.

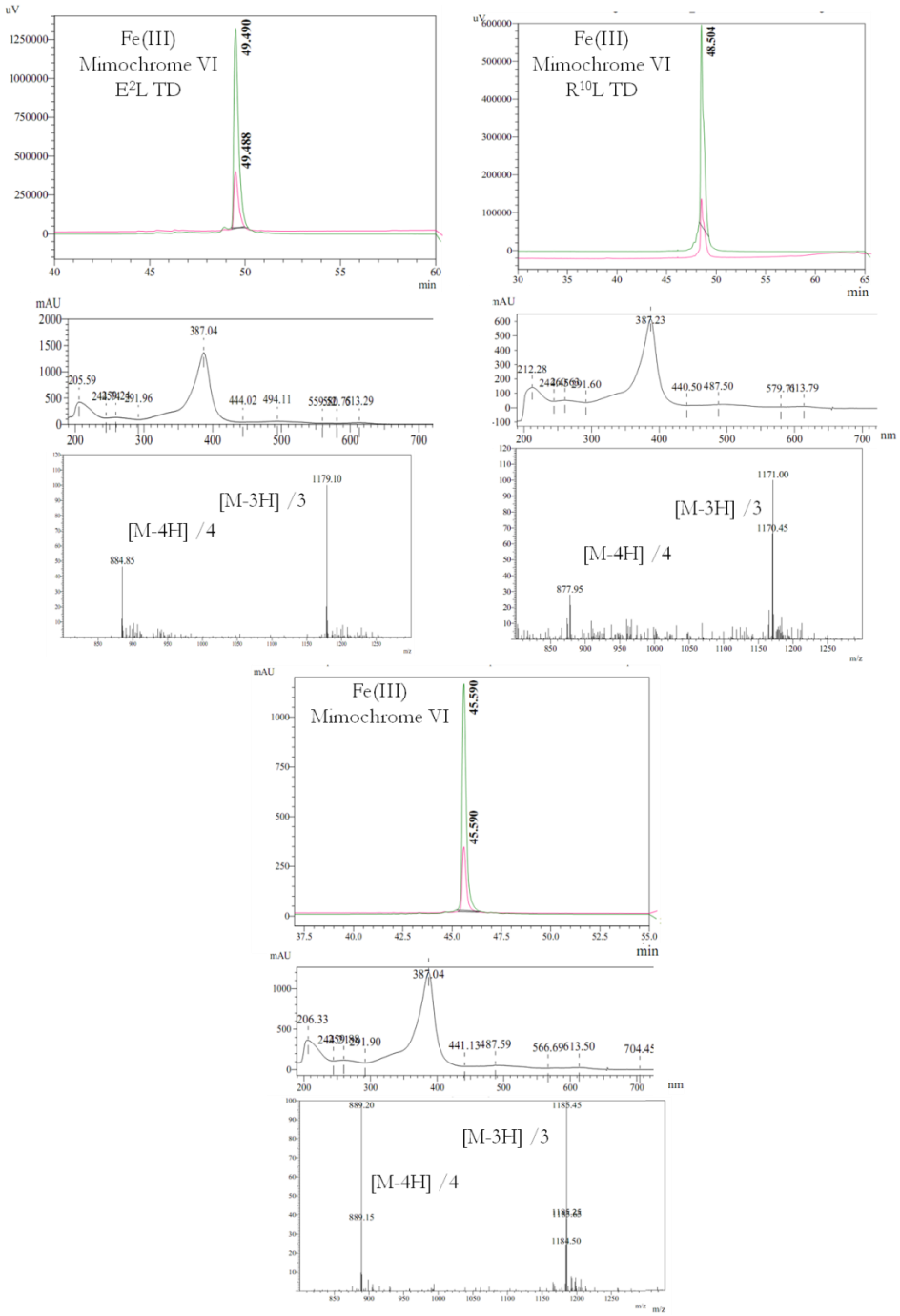

Figure 75 LCMS analysis of Mimochrome VI and E²L and R¹⁰L TD analogs

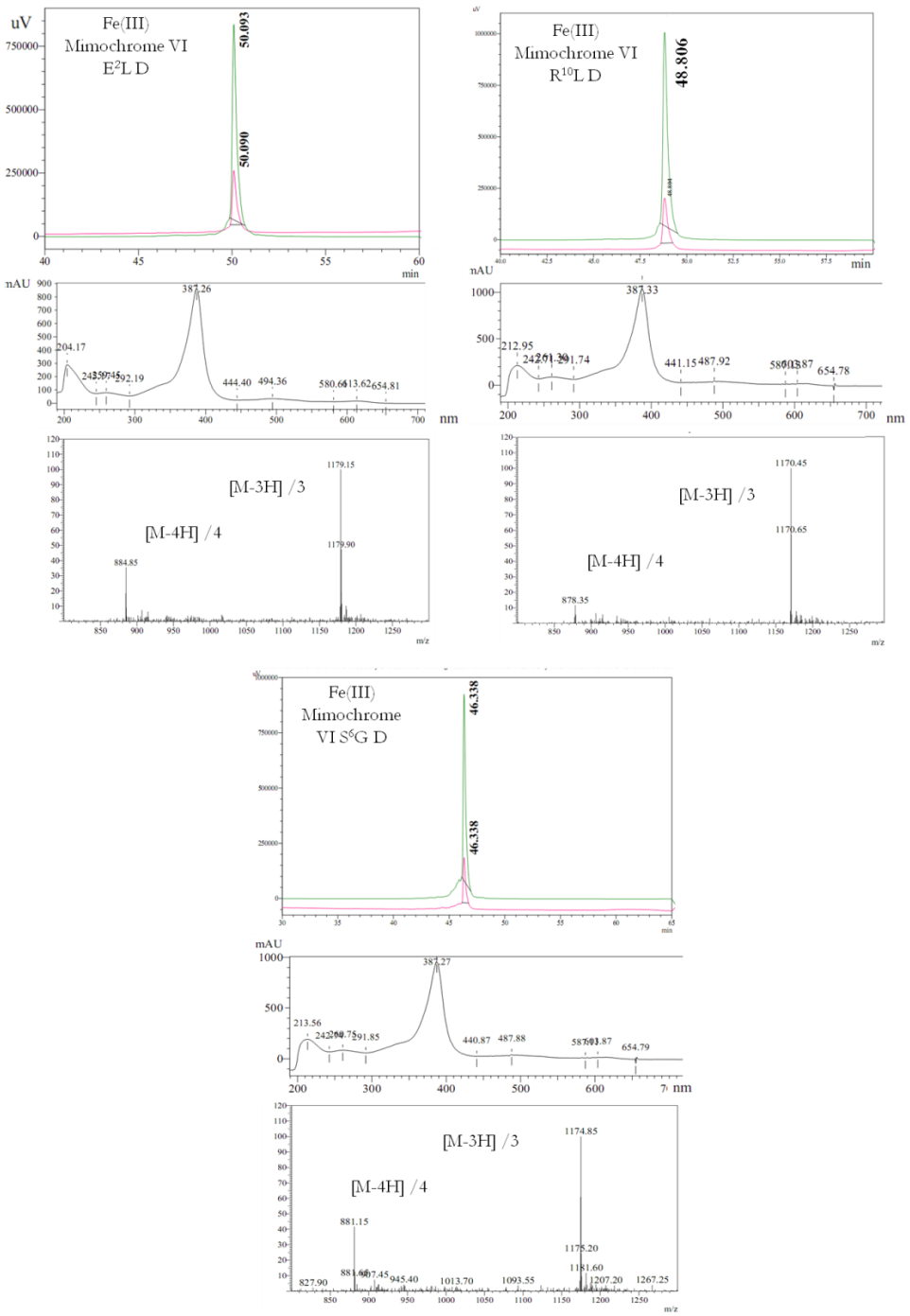

Figure 76 LCMS analysis of Mimochrome VI E²L, R¹⁰L and S⁶G TD analogs

Table 10 Analytical parameters of Fe(III) Mimochrome VI and its analogs

Fe (III) complexes	t_R (min)	Theoretical mass (Da)	Measured mass (Da)
Mimochrome VI	45.59	3553.07±0.27	3552.71
R^{10}L TD	48.50	3508.07±0.27	3509.67
E^{2}L TD	49.49	3534.85±0.55	3536.75
R^{10}L D	48.81	3534.22±0.22	3536.75
E^{2}L D	50.09	3508.87±0.52	3509.67
S^{10}G TD	46.34	3521.07±0.47	3522.67

6.6 Catalytic studies on ABTS oxidation

The catalytic experiments were followed, by measuring the appearance of the products in the reaction medium. The substrates used in the catalytic assay was ABTS. The formation of $ABTS^{\bullet+}$ cation radical was followed by spectrophotometer at 660 nm ($\varepsilon_{\lambda_{660}}$ = $1.4 \cdot 10^4$ $M^{-1}cm^{-1}$).

Kinetic parameters were determined by varying the H_2O_2 concentration by using fixed concentrations of the reducing substrates, and *vice versa*. In all catalytic experiments the reaction volume was 0.66 mL, the temperature was set at 25 °C and the reaction was followed under magnetic stirring.

In the **table 11** were reported the molar extinction coefficients used to determine the species concentrations at their λ_{max}.

Table 11 Optical parameters of regents used for catalytic experiments

Species	Solvent	λ_{max} (nm)	ε ($M^{-1}cm^{-1}$)
Enzyme	H_2O 0.1% TFA (v/v)	389	$1.10 \cdot 10^5$
H_2O_2	H_2O	240	39.4
ABTS	H_2O	340	$3.66 \cdot 10^4$
HRP	H_2O	403	$1.00 \cdot 10^5$

6.7 Spectroscopic Characterization

UV-Vis spectra were recorded at 25°C (unless otherwise specified). Quartz cuvettes with a path length of 1.0 cm were used for most measurements. Wavelength scans were performed from 200 nm to 800 nm, with a 300 nm min-1 scan speed. All data are blank subtracted.

CD spectra were collected at 25°C, from 260 to 190 nm at 0.2 nm intervals with a 20 nm min^{-1} scan speed, at 1 nm bandwidth and at 16 s response. In order to improve signal to noise ratio, spectra were averaged on 5 accumulations. Cuvette path length of 1.0 cm was used. Sample concentration was $7.0 \cdot 10^{-6}$ M, in 10mM sodium phosphate buffer, pH 6.5.

CD intensities (mdeg) are reported as molar ellipticity *per* residue (mdeg cm^2 $dmol^{-1}$). All data are blank subtracted.

6.8 Spectroelectrochemical measurements

Prior to Mimochrome VI adsorption, the ITO electrodes were carefully rinsed with acetone (15 minutes) ethanol (15 minutes) and Milli-Q. water (15 minutes) under mechanical stirring. The geometric electrode surface was delimited to 0.24 ± 0.1 cm^2, by using nail varnish. Therefore, the ITO electrode was soaked in 10 mM MES buffer solution (pH 6.5) over night at room temperature. Adsorption procedures were conducted in a 50 μM Mimochrome VI solution, 10 mM MES buffer, pH 6.5, at room temperature.

Spectroelectrochemical measurements were performed using a thermo-stated homemade three-electrode spectroelectrochemical cell. The reference electrode is an Ag/AgCl, 3 M KCl electrode (WPI) and the counter electrode is a platinum wire. Cyclic voltammetric experiments were systematically performed under ohmic drop compensation in 1.1 mL electrolyte solution (90 mM MES,10 mM KPF6, pH 6.5) at 20 °C. The spectroelectrochemical cell was carefully degassed for 1 h by argon bubbling, prior to measurements. For measurements under saturated oxygen atmosphere, the electrochemical cell was bubbled with pure oxygen gas for 30 min prior to measurements, and for a further 2 min between each measurement. The integration time for spectrometric measurements was fixed to 10 ms. Depending on the time resolution required, each data point on a CVA or DCVA can result from the averaging of 2 or 4 spectra. All potentials in the text are referred to the Ag/AgCl, 3 M KCl reference (i.e., +0.2 V vs NHE).

6.9 Resonance Raman Spectroscopic analysis

Spectra were recorded at room temperature (20 °C) with a power of 2 mW at the sample. For solution samples, the microscope was equipped with a 10× objective, resulting in an excitation power of 2 mW at the sample. The reported spectra correspond to the averaging of at least 10 scans, each recorded with a 10 s acquisition time. For the measurements on GLAD ITO electrodes, the microscope was equipped with a long-distance 100× objective and an optical filter (D1) to decrease the laser power on the sample to ca. 30 μW in order to avoid protein degradation. Reported spectra are the result of the average of typically 16 single spectra, each recorded with 5 s acquisition time. Measurements were performed from experiment to experiment on different surface areas to limit protein degradation.

6.10 Cross-linking procedures

The cross-linking procedure for Mimochrome-IgG conjugation are realized in three steps.

1. Maleimide-activation of Fe(III)-Mimochrome VI:

Fe(III)-Mimochrome VI was dissolved in 0.1 M phosphate buffer, pH 7. (2 mg of in 800 μL). Sulfo-SMCC solution is prepared immediately before use (4.3 mg in 100 μL acetonitrile, 200 μL water). Dissolved linker was added to Mimochrome VI and reaction was incubated under stirring, at room temperature for 1.5 hours. This reaction uses a 20:1 molar ratio of sulfo-SMCC to protein, even if Mimochrome VI has only one free primary amino-group. The acylation reaction to primary amines and the hydrolysis (inactivation) of these NHS-ester reagent occurs rapidly at pH ≥7. For this reason, procedures for modification with sulfo-SMCC involve addition of a molar excess of reagent. Reaction was controlled with an LC-MS. Reaction mixture was the purified from the excess of linker by desalting column (PD10 equilibrated with reaction buffer). Purified colored fractions were pooled and, if necessary, lyophilized or frozen to preserve maleimide activity. Otherwise it was immediately used for covalent binding to antibodies.

2. Sulfhydryl modification of Antibody with SATA

Antibodies were purchased in phosphate buffer (0.1 M), NaCl (0.15 M), pH 7, while the reaction of functionalization directed to lysine residues must be realized at slightly basic pH, because of Lys side chain pKa (≈10). For this reason buffer was exchanged with 0.1 M carbonate buffer, pH 9, by using

desalting column (Bio-Spin 6) and the final concentration of antibodies was 1 mg/ml. SATA solution was prepared immediately before use in acetonitrile. A 500-fold molar excess of SATA was added to antibody and the reaction was incubated at room temperature for 30 minutes, under stirring. Free amine functionalization was checked performing a Kaiser test on the antibody solution before and after modification with SATA. The Kaiser test is colorimetric test which allows to detect the presence or absence of free primary amino groups, and it can be a useful indication about the completeness of a coupling step. The test is based on the reaction of ninhydrin with primary amines, which gives a characteristic dark blue color. This test requires minimal amounts of analyte and is completed within a few minutes (Kaiser et al., 1970). Comparing the colorimetric signal, indicative of free amines, before and after SATA functionalization, it was possible to estimate the number of functionalized lysine residues (≈50). Subsequently, the deacetylation of the SATA-modified antibodies was accomplished, in order to obtain free -SH groups for the last step of the cross-linking procedure. Thiols deprotection was conducted in the presence of hydroxylamine (30-fold over SATA-antibodies). The pH was checked and adjusted with NaOH (pH 8), when necessary. Reaction mixture was then incubated for 2 hours at room temperature, under stirring. PD-10 desalting column, (equilibra-ted with 0.1 M phosphate, 25 mM EDTA, pH 5) to purify the sulfhydryl-modified antibody from the hydroxylamine. Slightly acidic pH and EDTA were used to minimize disulfide bond formation (Greg T. Hermanson, 2008).

3. Cross-linking step

Sulfhydryl-modified antibody which were purified by desalting procedure, were mixed to maleimide-activated Fe(III)-Mimochrome VI solution (molar ratio Mimochrome/antibody 50/1). Reaction mixture at room temperature for 2 hours or overnight at 4°C, on tilting plate, to avoid antibodies denaturation. Reaction progress was checked by HPLC, using a size-exclusion column (Phenomenex W-Prex 5 GP 200- 250x4.6 mm size exclusion 1000-120000 Da) and using as eluent 0.1 M phosphate buffer, 3.5 mM SDS, pH 6. The analytical HPLC is reported in **figure 77**. The first peak (t_R 3.59 minutes) is related to Mimochrome VI-conjugated IgG, as confirmed by a absorption peak at 280 nm (due to antibodies aromatic residues) and 387 nm (due to the presence of cross-linked Mimochrome VI). The second peak is related to unreacted Mimochrome VI, while and the third on is represented by the excess of linker.

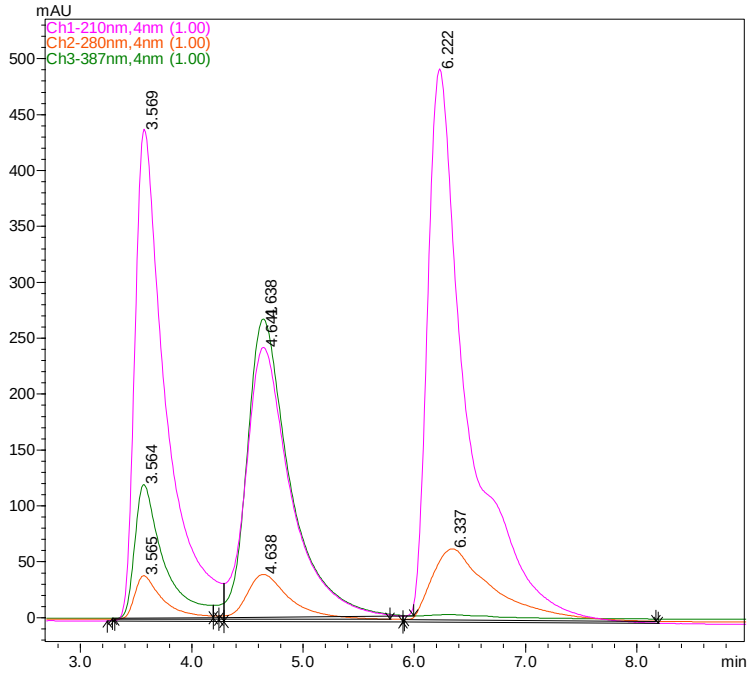

Figure 77 Analytical HPLC of the cross linking reaction mixture

At the end of the cross-linking reaction, the un-conjugated Mimochrome was removed by gel filtration chromatography, by using a Sephadex G-100 superfine resin (mesh 10-40), packed in a glass column 10x150 mm. Separation is performed in 0.1 M phosphate, pH 6.5 at a flow rate of 3 ml/h. Purified fractions were pooled and controlled by GP-HPLC as at point 3 (see results and discussion section), and then stored at 4°C.

6.11 Materials

All 9-fluorenylmethoxycarbonyl (Fmoc) protected amino acids, Nova Syn TGSieber resin and coupling reagents: N-hydroxybenzotriazole (HOBt), *O*-7-Azabenzotriazol-1-yl-N,N,N',N"-tetramethyluronium hexafluoro-phosphate (HATU) and benzotriazole-1-oxy-tris-pyrrolidino-phospho-nium hexafluorophosphate (PyBOP) were purchased fromNovaBiochem (EMD Biosciences, La Jolla, CA). Silica gel 60 (230-400 mesh) was from Merck. Precoated silica G-60 plates, F254, were used for thin-layer chromatography (tlc). All solvents used in the peptide synthesis and purification were anhydrous and HPLC grade respectively, and were supplied by Romil. Piperidine and scavengers (ethanedithiol, triisopropylsilane) were from Fluka. N,N-Diisopropylethylamine (DIPEA), trifluoroacetic acid (TFA) were supplied from Applied Biosystems. N,N-dimethylformamide (DMF), dichloromethane (DCM), pyridine, ethanol, methanol and 1-methyl-2-pyrrolidone (NMP) were supplied by Romil. Deuteroporphyrin IX was from Porphyrin Products. Iron(II) acetate waspurchased from Sigma Aldrich. TFE was supplied by Romil. All buffer solutions were made by using water with a HPLC purity degree, supplied by LabScan,

Phosphate salts (monobasic and dibasic), MES, NaCl ad SDS for the buffers preparation, were provided by Fluka.

PD10 and SP6 desalting columns were purchased by GE healthcare and BIORAD, respectively. Antibody (polyclonal human IgG) and cross-linkers were purchased by Pierce.

ITO-coated glass substrate was used as the deposition substrate (8−12 Ω/square, Delta Technologies Ltd.

6.12 Instrumentation

Protected peptides were obtained by the use of ABI 433 automatic peptide synthesizer.

HPLC and LC-MS analysis were performed with a Shimadzu LC-10ADvp equipped with an SPDM10Avp diode-array detector. ESI-MS spectra were recorded on a Shimadzu LC-MS-2010EV system with ESI interface, and Shimadzu LC-MS solution Workstation software for the data processing. A Q-array-octapole-quadrupole mass analyzer was used as the detector. The optimized MS parameters were selected as followed: CDL (curved desolvation line) temperature 250 °C; the block temperature 250 °C; the probe temperature 250 °C; detector gain 1.6kV; probe voltage +4.5kV; CDL voltage -15V. Nitrogen served as nebulizer gas (flow rate: 1.5 $L \cdot min^{-1}$).

UV-vis analysis was performed on Cary Varian 50 Probe UV Spectrophotometer, while CD analysis was realized on Jasco J-715 dichrograph.

Time-resolved UV−visible absorption spectroscopic measurements were performed on a TORUS-50 diode array spectrometer (Ocean Optics) synchronized with a potentiostat (Autolab).

Resonance Raman spectra were obtained with a Labram HR 800 microspectrometer (Jobin yvon) by excitating at 405 nm with a single frequency collimated laser module (Ondax Inc).

All the data were analyzed by using Origin Pro8 and Kaleidagraph softwares.

Acknowledgements

I want to thank all the members of The Artificial Metallo Enzyme Group of Naples. In particular, I am deeply grateful to Professor Angela Lombardi, who was my supervisor since the beginning of my studies and supported me during these years, by offering me important opportunities for my professional growth. A special thank is due to Professor Vincenzo Pavone, who daily followed my studies and research activity, sharing his knowledge and critically reviewing my experiments. I am grateful to Prof. Flavia Nastri and Dr. Ornella Maglio, for the scientific contribution to this work and the interesting discussions. I would like to thank Prof. Pompea Del Vecchio, for her interest in my research, as well as the fruitful discussions.

I want to express all my gratitude to Prof. Véronique Balland, Prof. Benoit Limoges and all the *Laboratoire d'électrochimie moléculaire* in Paris. The important contribution of our collaboration increased the scientific value of this work. In particular, I am very grateful to Véronique, because spending time with her changed my way of living Science and strengthened my desire to pursue in my research activity.

My warmest thanks are addressed to my friends and colleagues. The time we spent together was my greatest source for inspiration.

My deepest gratitude is addressed to my family and my friends, the best part of my life.

The financial support of the University of Napoli "Federico II" is gratefully acknowledged.

List of acronyms and abbreviations

ABTS2,2'-azino-bis(3-ethylbenzthiazoline-6-sulphonic acid)

Abs: Absorbance

Ac: Acetyl

Arg: Arginine

Asp : Aspartic acid

Boc: t-Butoxycarbonyl

CD: Circular dichroism

Cys: Cysteine

DCM: Dichloromethane

DOSY: Diffusion-ordered spectroscopy

DP IX: Deuteroporphyrin IX

DIEA: Diisopropylethylamine

DMF: Dimethylformamide

EDT: Ethanedithiol

ESI-MS: Electrospray ionization mass spectrometry

Fmoc: 9-Fluorenylmethoxycarbonyl

Gln: Glutamine

GluGlutamic acid

GlyGlycine

HATU: N-[(dimethylamino)-1H-1,2,3-triazolo[4,5-b]pyridin-1-yl-methylene]-N methylmethanaminium hexafluorophosphate N-oxide

His: Histidine

HOBt: N-hydroxybenzotriazole

HRP: Horseradish peroxidase

Ile: Isoleucine

Leu: Leucine

Lys: Lysine

MeOH: Methanol

Mmt: Methoxytrityl

NMP: N-Methyl-2-pyrrolidone

NMR: Nuclear magnetic resonance

Pbf: 2,2,4,6,7-Pentamethyldihydrobenzofurane-5-sulfonyl

PDB Protein Data Bank

PyBop: Benzotriazole-1-yl-oxy-tris-pyrrolidino-phosphonium hexafluorophosphate

Ser: Serine

TFA: Trifluoroacetic acid

TFE: Trifluoroethanol

TLC: Thin Layer Chromatography

Trt: Trityl

Tyr: Tyrosine

References

Al-Lazikani, B., Lesk, A.M., and Chothia, C. (1997). J. Mol. Biol. *273*, 927–948.

Akerfeldt, K.S., Kim, R.M., Camac, D., Groves, J.T., Lear, J.D., and DeGrado, W.F. (1992). Journal of the American Chemical Society *114*, 9656–9657.

Armstrong, F.A., Camba, R., Heering, H.A., Hirst, J., Jeuken, L.J., Jones, A.K., Léger, C., and McEvoy, J.P. (2000). Faraday Discuss. 191–203; discussion 257–268.

Arnold, P.A., Benson, D.R., Brink, D.J., Hendrich, M.P., Jas, G.S., Kennedy, M.L., Petasis, D.T., and Wang, M. (1997). Inorganic Chemistry *36*, 5306–5315.

Aron, J., Baldwin, D.A., Marques, H.M., Pratt, J.M., and Adams, P.A. (1986). Journal of Inorganic Biochemistry *27*, 227–243.

Arya, S.K., Solanki, P.R., Datta, M., and Malhotra, B.D. (2009). Biosensors and Bioelectronics *24*, 2810–2817.

Ashley, K., Biagini, R.E., Smith, J.P., Sammons, D.L., Mackenzie, B.A., Striley, C.A.F., Robertson, S.K., and Snawder, J.E. (2008). J Occup Environ Hyg *5*, D25–32.

Astuti, Y., Topoglidis, E., Briscoe, P.B., Fantuzzi, A., Gilardi, G., and Durrant, J.R. (2004). Journal of the American Chemical Society *126*, 8001–8009.

Astuti, Y., Topoglidis, E., Cass, A.G., and Durrant, J.R. (2009). DAnalytica Chimica Acta *648*, 2–6.

Astuti, Y., Topoglidis, E., and Durrant, J.R. (2011). Analytica Chimica Acta *686*, 126–132.

Azevedo, A.M., Martins, V.C., Prazeres, D.M.F., Vojinović, V., Cabral, J.M.S., and Fonseca, L.P. (2003). Biotechnology Annual Review, (Elsevier), pp. 199–247.

Azevedo, A.M., Prazeres, D.M.F., Cabral, J.M.S., and Fonseca, L.P. (2005). Biosensors and Bioelectronics *21*, 235–247.

Baltzer, L. (1999). In Implementation and Redesign of Catalytic Function in Biopolymers, P.D.F.P. Schmidtchen, L. Baltzer, A.R. Chamberlin, K.A. McDonnell, M. Famulok, M.A. Gilmore, B. Imperiali, A. Jenne, M. Shogren-Knaak, and L.E. Steward, eds. (Springer Berlin Heidelberg), pp. 39–76.

Baltzer, L., Nilsson, H., and Nilsson, J. (2001). Chem. Rev. *101*, 3153–3164.

Benson, D.R., Hart, B.R., Zhu, X., and Doughty, M.B. (1995). Journal of the American Chemical Society *117*, 8502–8510.

Berglund, G.I., Carlsson, G.H., Smith, A.T., Szöke, H., Henriksen, A., and Hajdu, J. (2002). Nature *417*, 463–468.

Bernad, S., Leygue, N., Korri-Youssoufi, H., and Lecomte, S. (2007). Eur. Biophys. J. *36*, 1039–1048.

Bertini, I., and Luchinat, C. (1999). Curr Opin Chem Biol *3*, 145–151.

Boehm, T. (2012). Curr. Biol. *22*, R722–732.

Bongiovanni, C., Ferri, T., Poscia, A., Varalli, M., Santucci, R., and Desideri, A. (2001). Bioelectrochemistry *54*, 17–22.

Borghesi, L., and Milcarek, C. (2006). Immunol. Res. *36*, 27–32.

Bourbonnais, R., Leech, D., and Paice, M.G. (1998). Biochimica Et Biophysica Acta (BBA) - General Subjects *1379*, 381–390.

Buchler, J.W., (1979). In The Porphyrins. In The Porphyrins, Volume 1, (NY, USA), pp. 389–483.

Bushnell, G.W., Louie, G.V., and Brayer, G.D. (1990). J. Mol. Biol. *214*, 585–595.

Cass, A.E.G., Davis, G., Francis, G.D., Hill, H.A.O., Aston, W.J., Higgins, I.J., Plotkin, E.V., Scott, L.D.L., and Turner, A.P.F. (1984). Analytical Chemistry *56*, 667–671.

Chan, M.K. (2000). Journal of Porphyrins and Phthalocyanines (JPP) *04*, 358–361.

Chan, M.K. (2001). Curr Opin Chem Biol *5*, 216–222.

Chapman, S.K., Daff, S., and Munro, A.W. (1997). In Metal Sites in Proteins and Models, H.A.O. Hill, P.J. Sadler, and A.J. Thomson, eds. (Berlin, Heidelberg: Springer Berlin Heidelberg), pp. 39–70.

Chaubey, A., and Malhotra, B.D. (2002). Biosensors and Bioelectronics *17*, 441–456.

Chen, K., Xu, W., Wilson, M., He, B., Miller, N.W., Bengtén, E., Edholm, E.-S., Santini, P.A., Rath, P., Chiu, A., et al. (2009). Nat. Immunol. *10*, 889–898.

Childs, R.E., and Bardsley, W.G. (1975). Biochem. J. *145*, 93–103.

Choma, C.T., Lear, J.D., Nelson, M.J., Dutton, P.L., Robertson, D.E., and DeGrado, W.F. (1994). Journal of the American Chemical Society *116*, 856–865.

Chunglok, W., Wuragil, D.K., Oaew, S., Somasundrum, M., and Surareungchai, W. (2011). Biosensors and Bioelectronics *26*, 3584–3589.

Collings, A.F., and Caruso, F. (1997). Reports on Progress in Physics *60*, 1397–1445.

Collman, J.P. (1997). Inorganic Chemistry *36*, 5145–5155.

Collman, J.P., Zhang, X., Lee, V.J., Uffelman, E.S., and Brauman, J.I. (1993). Science *261*, 1404–1411.

Cornish-Bowden, A. (2004). Fundamentals of enzyme kinetics (London: Portland Press).

Crane, B.R., Siegel, L.M., and Getzoff, E.D. (1995). Science *270*, 59–67.

D'Auria, G., Maglio, O., Nastri, F., Lombardi, A., Mazzeo, M., Morelli, G., Paolillo, L., Pedone, C., and Pavone, V. (1997). Chemistry - A European Journal *3*, 350–362.

DeGrado, W.F., Summa, C.M., Pavone, V., Nastri, F., and Lombardi, A. (1999). Annu. Rev. Biochem. *68*, 779–819.

Del Gatto G. (2007). Synthesis and structural characterization of artificial metalloproteins. PhD Thesis in Chemical Sciences, XX Cycle, , 2007. University of Naples "Federico II."

Dewey, R.E., Timothy, D.H., and Levings, C.S. (1987). Proc. Natl. Acad. Sci. U.S.A. *84*, 5374–5378.

Dolphin, D. (1979). The porphyrins Vol. 7, Biochemistry, Part B. (New York [etc.]: Academic Press).

Domínguez, R., Serra, B., Reviejo, A.J., and Pingarrón, J.M. (2001). Anal. Biochem. *298*, 275–282.

Dong, S., Niu, J., and Cotton, T.M. (1995). In Methods in Enzymology, (Elsevier), pp. 701–732.

Duffy, S.L., and Murphy, J.T. (2001). BioTechniques *31*, 495–496, 498, 500–501.

Duncan, R.J., Weston, P.D., and Wrigglesworth, R. (1983). Anal. Biochem. *132*, 68–73.

Fasman, G.D. (1996). Circular dichroism and the conformational analysis of biomolecules (New York: Plenum Press).

Fattakhova-Rohlfing, D., Brezesinski, T., Rathouský, J., Feldhoff, A., Oekermann, T., Wark, M., and Smarsly, B.M. (2006). Advanced Materials *18*, 2980–2983.

Geisberger, R., Lamers, M., and Achatz, G. (2006). Immunology *118*, 429–437.

Gajhede, M., Schuller, D.J., Henriksen, A., Smith, A.T., and Poulos, T.L. (1997). Nature Structural Biology *4*, 1032–1038.

Gibney, B.R., and Dutton, P.L. (1999). Protein Science *8*, 1888–1898.

Gibney, B.R., Isogai, Y., Rabanal, F., Reddy, K.S., Grosset, A.M., Moser, C.C., and Dutton, P.L. (2000) Biochemistry *39*, 11041–11049.

Goldberg, M., Dunning, S., and Bunn, H. (1988). Science *242*, 1412–1415.

Gouterman, M. (1961). Journal of Molecular Spectroscopy *6*, 138–163.

Gray, H.B., and Winkler, J.R. (1996). Annual Review of Biochemistry *65*, 537–561.

Green, A.N.M., Palomares, E., Haque, S.A., Kroon, J.M., and Durrant, J.R. (2005). The Journal of Physical Chemistry B *109*, 12525–12533.

Greg T. Hermanson (2008). Bioconjugate techniques 2nd edition.

Griffiths, D. (1993). Trends in Biotechnology *11*, 122–130.

Gündoğan-Paul, M., Çelebi, S.S., Özyörük, H., and Yıldız, A. (2002). Biosensors and Bioelectronics *17*, 875–881.

Harbury, H.A., and Loach, P.A. (1959). Proc. Natl. Acad. Sci. U.S.A. *45*, 1344–1359.

Hargrove, M.S., and Olson, J.S. (1996). Biochemistry *35*, 11310–11318.

Hargrove, M.S., Wilkinson, A.J., and Olson, J.S. (1996). Biochemistry *35*, 11300–11309.

Hashida, S., and Ishikawa, E. (1985). Analytical Letters *18*, 1143–1155.

Hellinga, H.W. (1996). Current Opinion in Biotechnology *7*, 437–441.

Hellinga, H.W. (1998). The construction of metal centers in proteins by rational design. Folding and Design *3*, R1–R8.

Hermanson, G.T. (2008). Bioconjugate techniques (Amsterdam: Academic Press).

Hildebrandt, P., and Stockburger, M. (1989). Biochemistry *28*, 6710–6721.

Howes, B.D., Schiodt, C.B., Welinder, K.G., Marzocchi, M.P., Ma, J.G., Zhang, J., Shelnutt, J.A., and

Holm, R.H., Kennepohl, P., and Solomon, E.I. (1996). Chemical Reviews *96*, 2239–2314.

Smulevich, G. (1999). Biophys. J. *77*, 478–492.

Howes, B.D., Veitch, N.C., Smith, A.T., White, C.G., and Smulevich, G. (2001). Biochem. J. *353*, 181–191.

Huang, L.E., Ho, V., Arany, Z., Krainc, D., Galson, D., Tendler, D., Livingston, D.M., and Bunn, H.F. (1997). Kidney Int. *51*, 548–552.

Huy, N.T., Xuan Trang, D.T., Uyen, D.T., Sasai, M., Harada, S., and Kamei, K. (2005). Analytical Biochemistry *344*, 289–291.

Iwaki, M., Yakovlev, G., Hirst, J., Osyczka, A., Dutton, P.L., Marshall, D., and Rich, P.R. (2005). Biochemistry *44*, 4230–4237.

Jasanoff, A., and Fersht, A.R. (1994).Biochemistry *33*, 2129–2135.

Janeway, C. (2005). Immunobiology: the immune system in health and disease (New York: Garland Science).

Iijima, M., Matsuzaki, T., Kadoya, H., Hatahira, S., Hiramatsu, S., Jung, G., Tanizawa, K., and Kuroda, S. (2010). Analytical Biochemistry *396*, 257–261.

Johannes Everse, Kathleen E. Everse, and Matthew B. Grisham (1991). Peroxidases in chemistry and biology II (Boca Raton, Fla.: CRC Pr.).

Kaiser, E., Colescott, R.L., Bossinger, C.D., and Cook, P.I. (1970). Analytical Biochemistry *34*, 595–598.

Kadish, K.M., Smith, K.M., and Guilard, R. (2000). The porphyrin handbook (San Diego: Academic Press).

Kalsbeck, W.A., Robertson, D.E., Pandey, R.K., Smith, K.M., Dutton, P.L., and Bocian, D.F. (1996). Biochemistry *35*, 3429–3438.

Kemp, G.L., Marritt, S.J., Xiaoe, L., Durrant, J.R., Cheesman, M.R., and Butt, J.N. (2009). Biochem. Soc. Trans. *37*, 368–372.

Kennedy, M.L., Silchenko, S., Houndonougbo, N., Gibney, B.R., Dutton, P.L., Rodgers, K.R., and Benson, D.R. (2001). J. Am. Chem. Soc. *123*, 4635–4636.

Khan, M.J., Qayyum, S., Alam, F., and Husain, Q. (2011). Nanotechnology *22*, 455708.

Khoa Ly, H., Sezer, M., Wisitruangsakul, N., Feng, J.-J., Kranich, A., Millo, D., Weidinger, I.M., Zebger, I., Murgida, D.H., and Hildebrandt, P. (2011). FEBS Journal *278*, 1382–1390.

Koder, R.L., and Dutton, P.L. (2006). Dalton Transactions 3045.

Koder, R.L., Valentine, K.G., Cerda, J., Noy, D., Smith, K.M., Wand, A.J., and Dutton, P.L. (2006). J. Am. Chem. Soc. *128*, 14450–14451.

Koder, R.L., Anderson, J.L.R., Solomon, L.A., Reddy, K.S., Moser, C.C., and Dutton, P.L. (2009). Nature *458*, 305–309.

Kranich, A., Naumann, H., Molina-Heredia, F.P., Moore, H.J., Lee, T.R., Lecomte, S., De la Rosa, M.A., Hildebrandt, P., and Murgida, D.H. (2009). Physical Chemistry Chemical Physics *11*, 7390.

Krause, K.M., Taschuk, M.T., Harris, K.D., Rider, D.A., Wakefield, N.G., Sit, J.C., Buriak, J.M., Thommes, M., and Brett, M.J. (2010). Langmuir *26*, 4368–4376.

Krzemiński, Ł., Ndamba, L., Canters, G.W., Aartsma, T.J., Evans, S.D., and Jeuken, L.J.C. (2011). Journal of the American Chemical Society *133*, 15085–15093.

Kuroda, N., Murasaki, N., Wada, M., and Nakashima, K. (2001). Luminescence *16*, 167–172.

Lacey, A.L., Gutiérrez-Sánchez, C., Fernández, V.M., Pacheco, I., and Pereira, I.A.C. (2008). JBIC Journal of Biological Inorganic Chemistry *13*, 1315–1320.

Léger, C., and Bertrand, P. (2008). Chem. Rev. *108*, 2379–2438.

Lemberg, R., and Falk, J.E. (1951). Biochem. J. *49*, 674–683.

Li, T., Bonkovsky, H.L., and Guo, J. (2011). BMC Struct. Biol. *11*, 13.

Litman, G.W., Rast, J.P., Shamblott, M.J., Haire, R.N., Hulst, M., Roess, W., Litman, R.T., Hinds-Frey, K.R., Zilch, A., and Amemiya, C.T. (1993). Mol. Biol. Evol. *10*, 60–72.

Liu, D., Williamson, D.A., Kennedy, M.L., Williams, T.D., Morton, M.M., and Benson, D.R. (1999a). Journal of the American Chemical Society *121*, 11798–11812.

Liu, D., Lee, K.-H., and Benson, D.R. (1999b). Chemical Communications 1205–1206.

Liu, X., Huang, Y., Shang, L., Wang, X., Xiao, H., and Li, G. (2006). Bioelectrochemistry *68*, 98–104.

Lombardi, A., Nastri, F., Sanseverino, M., Maglio, O., Pedone, C., and Pavone, V. (1998). Inorganica Chimica Acta *275-276*, 301–313.

Lombardi, A., Nastri, F., and Pavone, V. (2001). Chem. Rev. *101*, 3165–3189.

Lombardi, A., Nastri, F., Marasco, D., Maglio, O., De Sanctis, G., Sinibaldi, F., Santucci, R., Coletta, M., and Pavone, V. (2003). Chemistry - A European Journal *9*, 5643–5654.

Low, D.W., Yang, G., Winkler, J.R., and Gray, H.B. (1997). Journal of the American Chemical Society *119*, 4094–4095.

Lu, Y., and Valentine, J.S. (1997). Curr. Opin. Struct. Biol. *7*, 495–500.

Maltempo, M.M. (1976a). Biochim. Biophys. Acta *434*, 513–518.

Maltempo, M.M. (1976b). Q. Rev. Biophys. *9*, 181–215.

Mansuy, D. (1993). Coordination Chemistry Reviews *125*, 129–141.

Marritt, S.J., Van Wonderen, J.H., Cheesman, M.R., and Butt, J.N. (2006). Analytical Biochemistry *359*, 79–83.

Marshall, D., Fisher, N., Grigic, L., Zickermann, V., Brandt, U., Shannon, R.J., Hirst, J., Lawrence, R., and Rich, P.R. (2006). Biochemistry *45*, 5458–5467.Mansuy, D. (1990). Pure and Applied Chemistry *62*, 741–746.

Marques, H.M. (2007). Dalton Transactions 4371.

McInvale, A.C., Harlan, R.E., and Garcia, M.M. (2000). Brain Research Protocols *5*, 39–48.

Mello, L.D., and Kubota, L.T. (2002). Food Chemistry *77*, 237–256.

Merrifield, R. B. (1963). Journal of the American Chemical Society *85*, 2149–2154.

Meunier, B. (1992). Chemical Reviews *92*, 1411–1456.

Mikol, D.D., Ditlow, C., Usatin, D., Biswas, P., Kalbfleisch, J., Milner, A., and Calenoff, E. (2006). J. Neuroimmunol. *180*, 40–49.

Momenteau, M., and Reed, C.A. (1994). Chemical Reviews *94*, 659–698.

Monien, B.H., Drepper, F., Sommerhalter, M., Lubitz, W., and Haehnel, W. (2007).J. Mol. Biol. *371*, 739–753.

Mulchandani, A., and Rudolph, D.C. (1995). Anal. Biochem. *225*, 277–282.

Mutter, M., and Vuilleumier, S. (1989). Angewandte Chemie International Edition in English *28*, 535–554.

Nara, S., Tripathi, V., Chaube, S.K., Rangari, K., Singh, H., Kariya, K.P., and Shrivastav, T.G. (2008). Journal of Immunoassay and Immunochemistry *29*, 390–405.

Narula, J., Pandey, P., Arbustini, E., Haider, N., Narula, N., Kolodgie, F.D., Dal Bello, B., Semigran, M.J., Bielsa-Masdeu, A., Dec, G.W., et al. (1999). Proceedings of the National Academy of Sciences *96*, 8144–8149.

Nastri, F., Lombardi, A., Morelli, G., Maglio, O., D'Auria, G., Pedone, C., and Pavone, V. (1997). Chemistry - A European Journal *3*, 340–349.

Nastri, F., Lombardi, A., D'Andrea, L.D., Sanseverino, M., Maglio, O., and Pavone, V. (1998). Biopolymers *47*, 5–22.

Nastri, F., Lista, L., Ringhieri, P., Vitale, R., Faiella, M., Andreozzi, C., Travascio, P., Maglio, O., Lombardi, A., and Pavone, V. (2011). Chemistry - A European Journal *17*, 4444–4453.

North, B., Lehmann, A., and Dunbrack, R.L., Jr (2011). J. Mol. Biol. *406*, 228–256.

Nuzzo, R.G., and Allara, D.L. (1983). Journal of the American Chemical Society *105*, 4481–4483.

Paléus, S., Ehrenberg, A., Tuppy, H., and Virtanen, A.I. (1955). Acta Chemica Scandinavica *9*, 365–374.

Panicco, P., Astuti, Y., Fantuzzi, A., Durrant, J.R., and Gilardi, G. (2008). The Journal of Physical Chemistry B *112*, 14063–14068.

Park, S.-Y., Yokoyama, T., Shibayama, N., Shiro, Y., and Tame, J.R.H. (2006). Journal of Molecular Biology *360*, 690–701.

Parra, A., Casero, E., Vázquez, L., Pariente, F., and Lorenzo, E. (2006). Analytica Chimica Acta *555*, 308–315.

Peña, N., Ruiz, G., Reviejo, A.J., and Pingarrón, J.M. (2001). Analytical Chemistry *73*, 1190–1195.

Perutz, M.F., Wilkinson, A.J., Paoli, M., and Dodson, G.G. (1998). Annu Rev Biophys Biomol Struct *27*, 1–34.

Peterson, J.A., and Graham, S.E. (1998). Structure *6*, 1079–1085.

Pier, G.B., and Lyczak, J.B. (2004). Immunology, infection, and immunity (Washington, D.C: ASM Press).

Poulos, T.L., and Kraut, J. (1980). J. Biol. Chem. *255*, 8199–8205.

Privalle, C.T. (1983). Proceedings of the National Academy of Sciences *80*, 702–706.

Putnam, F.W., Liu, Y.S., and Low, T.L. (1979).. J. Biol. Chem. *254*, 2865–2874.

Rabanal, F., DeGrado, W.F., and Dutton, P.L. (1996). Journal of the American Chemical Society *118*, 473–474.

Ranieri, A., Monari, S., Sola, M., Borsari, M., Battistuzzi, G., Ringhieri, P., Nastri, F., Pavone, V., and Lombardi, A. (2010). R Langmuir *26*, 17831–17835.

Rau, H.K., and Haehnel, W. (1998). Journal of the American Chemical Society *120*, 468–476.

Rau, DeJonge, and Haehnel (2000). Angew. Chem. Int. Ed. Engl. *39*, 250–253.

Rau, H.K., DeJonge, N., and Haehnel, W. (1998). Proc. Natl. Acad. Sci. U.S.A. *95*, 11526–11531.

Reedy, C.J., and Gibney, B.R. (2004). Chemical Reviews *104*, 617–650.

Regan, L. (1995). Trends in Biochemical Sciences *20*, 280–285.

Ringhieri, P. (2010). Synthetic heme-proteins in biosensor development. PhD Thesis in Chemical Sciences, XXIII Cycle, , 2010.

Reczek, C.M., Sitter, A.J., and Terner, J. (1989). Journal of Molecular Structure *214*, 27–41.

Renault, C., Harris, K.D., Brett, M.J., Balland, V., and Limoges, B. (2011). Chemical Communications *47*, 1863.

Renault, C., Andrieux, C.P., Tucker, R.T., Brett, M.J., Balland, V., and Limoges, B. (2012). Journal of the American Chemical Society *134*, 6834–6845.

Robbie, K. (1998). Journal of Vacuum Science & Technology B: Microelectronics and Nanometer Structures *16*, 1115.

Robertson, D.E., Farid, R.S., Moser, C.C., Urbauer, J.L., Mulholland, S.E., Pidikiti, R., Lear, J.D., Wand, A.J., DeGrado, W.F., and Dutton, P.L. (1994). Nature *368*, 425–432.

Rodriguez-Lopez, J.N., Smith, A.T., and Thorneley, R.N. (1996). J. Biol. Chem. *271*, 4023–4030.

Roda, A., Simoni, P., Mirasoli, M., Baraldini, M., and Violante, S.F. (2002). Analytical and Bioanalytical Chemistry *372*, 751–758.

Salverda, J.M., Patil, A.V., Mizzon, G., Kuznetsova, S., Zauner, G., Akkilic, N., Canters, G.W., Davis, J.J., Heering, H.A., and Aartsma, T.J. (2010). Angewandte Chemie International Edition *49*, 5776–5779.

Savenkova, M.I., Kuo, J.M., and Ortiz de Montellano, P.R. (1998). Biochemistry *37*, 10828–10836.

Samanta, D., and Sarkar, A. (2011). Chem Soc Rev *40*, 2567–2592.

Sasaki, T., and Kaiser, E.T. (1989). Journal of the American Chemical Society *111*, 380–381.

Sasaki, T., and Kaiser, E.T. (1990). Biopolymers *29*, 79–88.

Schäfer, G., Purschke, W., and Schmidt, C.L. (1996). FEMS Microbiol. Rev. *18*, 173–188.

Schaming, D., Renault, C., Tucker, R.T., Lau-Truong, S., Aubard, J., Brett, M.J., Balland, V., and Limoges, B. (2012). Langmuir *28*, 14065–14072.

Serra, B., Reviejo, A.., Parrado, C., and Pingarrón, J.. (1999). Biosensors and Bioelectronics *14*, 505–513.

Shifman, J.M., Moser, C.C., Kalsbeck, W.A., Bocian, D.F., and Dutton, P.L. (1998). Biochemistry *37*, 16815–16827.

Shifman, J.M., Gibney, B.R., Sharp, R.E., and Dutton, P.L. (2000). Biochemistry *39*, 14813–14821.

Simmerman, H.K., Wang, C.C., Horwitz, E.M., Berzofsky, J.A., and Gurd, F.R. (1982). Proc. Natl. Acad. Sci. U.S.A. *79*, 7739–7743.

Smyth, D.G., Blumenfeld, O.O., and Konigsberg, W. (1964). Biochem. J. *91*, 589–595.

Somasundrum, M., Kirtikara, K., and Tanticharoen, M. (1996). Analytica Chimica Acta *319*, 59–70.

Sundaramoorthy, M., Terner, J., and Poulos, T.L. (1995). Structure *3*, 1367–1377.

Sun, M.M.C., Beam, K.S., Cerveny, C.G., Hamblett, K.J., Blackmore, R.S., Torgov, M.Y., Handley, F.G.M., Ihle, N.C., Senter, P.D., and Alley, S.C. (2005). Bioconjug. Chem. *16*, 1282–1290.

Thévenot, D.R., Toth, K., Durst, R.A., and Wilson, G.S. (1999). Pure and Applied Chemistry *71*, 2333–2348.

Thévenot, D.R., Toth, K., Durst, R.A., and Wilson, G.S. (2001). International Union of Pure and Applied Chemistry: Physical Chemistry Division, Commission I.7 (Biophysical Chemistry); Analytical Chemistry Division, Commission V.5 (Electroanalytical Chemistry).1. Biosensors and Bioelectronics *16*, 121–131.

Traylor, T.G. (1981). Accounts of Chemical Research *14*, 102–109.

Traylor, T.G., Chang, C.K., Geibel, J., Berzinis, A., Mincey, T., and Cannon, J. (1979). Journal of the American Chemical Society *101*, 6716–6731.

Tuppy, H., Paléus, S., Tuppy, H., and Virtanen, A.I. (1955). Acta Chemica Scandinavica *9*, 353–364.

Underdown, B.J., and Schiff, J.M. (1986). Annu. Rev. Immunol. *4*, 389–417.

Vainshtein, B.K., Melik-Adamyan, W.R., Barynin, V.V., Vagin, A.A., Grebenko, A.I., Borisov, V.V., Bartels, K.S., Fita, I., and Rossmann, M.G. (1986). T J. Mol. Biol. *188*, 49–61.

Veitch, N.C. (2004). Phytochemistry *65*, 249–259.

Veitch, N.C., and Smith, A.T. (2000). In Advances in Inorganic Chemistry, (Elsevier), pp. 107–162.

Venturi, M. (2012). In The Exploration of Supramolecular Systems and Nanostructures by Photochemical Techniques, P. Ceroni, ed. (Dordrecht: Springer Netherlands), pp. 209–225.

Vermeersch, P., Geboes, K., Mariën, G., Hoffman, I., Hiele, M., and Bossuyt, X. (2012). Clinica Chimica Acta *413*, 1761–1767.

Vuilleumier, S., and Mutter, M. (1993). Biopolymers *33*, 389–400.

Wang, Y., Brezesinski, T., Antonietti, M., and Smarsly, B. (2009). ACS Nano *3*, 1373–1378.

Wang, Y., and Hasebe, Y. (2011). Electroanalysis *23*, 1631–1637.

Wang, M., Kennedy, M.L., Hart, B.R., and Benson, D.R. (1997). Chemical Communications 883–884.

Weiss, R., Gold, A., and Terner, J. (2006). Chemical Reviews *106*, 2550–2579.

Welinder, K.G. (1976). FEBS Letters *72*, 19–23.

Williamson, D.A., and Benson, D.R. (1998). Chemical Communications 961–962.

Whitehouse, C.J.C., Bell, S.G., Yang, W., Yorke, J.A., Blanford, C.F., Strong, A.J.F., Morse, E.J., Bartlam, M., Rao, Z., and Wong, L.-L. (2009).Chembiochem *10*, 1654–1656.

Wu, S., Bellei, M., Mansy, S.S., Battistuzzi, G., Sola, M., and Cowan, J.A. (2011). Journal of Inorganic Biochemistry *105*, 806–811.

Yabuki, S., Mizutani, F., and Hirata, Y. (2001). Electroanalysis *13*, 380–383.

Yang, B.Y., Gray, J.S.S., and Montgomery, R. (1996). Carbohydrate Research *287*, 203–212.

Yavo, B., Brunetti, I.L., Da Fonseca, L.M., Catalani, L.H., and Campa, A. (2001). Luminescence *16*, 299–304.

Yoshikawa, S. (2002) Adv. Protein Chem. *60*, 341–395.

Zhang, Y., He, P., and Hu, N. (2004). Electrochimica Acta *49*, 1981–1988.

Zhou, Y., Tian, X.-L., Li, Y.-S., Pan, F.-G., Zhang, Y.-Y., Zhang, J.-H., Yang, L., Wang, X.-R., Ren, H.-L., Lu, S.-Y., et al. (2011). Biosensors and Bioelectronics *26*, 3700–3704.

F. Nastri, L. Lista, P. Ringhieri, **R. Vitale**, M. Faiella, C. Andreozzi, P. Travascio, O. Maglio, A. Lombardi, V. Pavone

Chemistry - A european journal (2011) 17(16):4444-53

Title. *A heme-peptide metalloenzyme mimetic with natural peroxidase-like activity*

Abstract. Mimicking enzymes with alternative molecules represents an important objective in synthetic biology, aimed to obtain new chemical entities for specific applications. This objective is hampered by the large size and complexity of enzymes. The manipulation of their structures often leads to a reduction of enzyme activity. Here, we describe the spectroscopic and functional characterization of FeIII-Mimochrome VI, a 3.5 kDa synthetic heme-protein model, which displays a peroxidase-like catalytic activity. By the use of hydrogen peroxide, it efficiently catalyzes the oxidation of several substrates, with a typical Michaelis-Menten mechanism and with several multiple turnovers. The catalytic efficiency of FeIII-Mimochrome VI in the oxidation of ABTS and guaiacol (kcat/Km = 4417 and 870 $mM^{-1} \cdot s^{-1}$, respectively) is comparable to that of native HRP (kcat/Km = 5125 and 500 mM-1 s^{-1}, respectively). These results demonstrate that small synthetic peptide can impart high enzyme activities to metal cofactors, and anticipate the possibility of constructing new biocatalysts tailored to specific functions.

***

Staiano M, Baldassarre M, Esposito M, Apicella E, **Vitale R**, Aurilia V, D'Auria S

Environmental technology (2010) 8-9: 935-42

Title. *New trends in bio/nanotechnology: stable proteins as advanced molecular tools for health and environment*

Abstract. In this work the thermophilic trehalose/maltose-binding protein from Thermococcus litoralis is presented as a probe for the design of a high stable fluorescence biosensor for glucose. In particular, we show the possibility of modulating the protein specificity by changing temperature. In addition to glucose sensing, we also report on the possibility of utilizing odorant-binding proteins as a

probe for the development of optical sensors for analytes of environmental interests.

***

This project was proposed in "InKidia" business idea and received one of the Start Cup Campania 2012 prizes, for the foundation of new Start Up Companies.